ISOLATION AND CHARACTERIZATION OF RECOMBINANT U24, A MEMBRANE PROTEIN FROM HUMAN HERPESVIRUS TYPE 6

by

ANDREW ROBERT TAIT

M.Sc., Concordia University, 2004
B.Sc., Concordia University, 2001

A THESIS SUBMITTED IN PARTIAL FULFILLMENT OF THE REQUIREMENTS FOR THE DEGREE OF

DOCTOR OF PHILOSOPHY

in

THE FACULTY OF GRADUATE STUDIES
(Chemistry)

THE UNIVERSITY OF BRITISH COLUMBIA
(Vancouver)

July 2011

Abstract

This thesis describes the isolation and characterization of the U24 membrane protein encoded by Human Herpesvirus type-6 (HHV-6), obtained from an *E. coli* recombinant expression system. HHV-6 infection has been previously associated with the disease multiple sclerosis (MS), and the U24 protein is of interest because it has a seven amino-acid sequence (PRTPPPS) identical to myelin basic protein (MyBP), a candidate auto-antigen in MS.

In the first part of this thesis, I describe the methods that were developed to enable milligram quantities of U24 to be isolated and purified from litre cultures of *E. coli*. Levels of U24 expressed with a maltose binding protein-hexahistidine fusion tag were particularly enhanced by combinations of low temperature, oxidizing conditions, and/or use of minimal media culture. The significance of these results may be considered useful in application to other difficult-to-obtain membrane proteins.

Subsequent chapters of this thesis describe testing the recombinant U24 for potential mimicry of MyBP structure and function. Since the polyproline region in MyBP is now being recognized for its potential in cell-signalling roles that relate to myelin sheath development and structural integrity, I hypothesized that U24 may retain some of the same attributes as MyBP on the basis of identical sequence. Results here suggest that U24 can adopt a polyproline type II helix much like MyBP, which is a structural feature important for engaging in protein-protein interactions. Furthermore, the region is also found to represent a PX(T/S)P MAPK phosphorylation motif and PXXP-based Fyn tyrosine kinase SH3 binding domain. These observations are of particular relevance since phosphorylated MyBP is particularly decreased in MS patients, and Fyn is critical to myelin development. Like MyBP, results suggest that U24 can

be phosphorylated at the equivalent threonine and is also able to bind to the Fyn-SH3 domain. These results support the possibility that U24 interferes with essential myelin regulation pathways on the basis of its sequence shared with MyBP, thereby contributing to a pathological process.

I conclude with a presentation of preliminary NMR structural data for U24, as well as review results from a study of U24 in an animal model system. Future directions are also discussed.

Preface

The work presented in this dissertation is the result of collaborations with other scientists. Their contributions are summarized here, as follows.

My supervisor, Dr. Suzana K. Straus (S.K.S), identified U24 protein as a novel target of study. All areas of research described in this thesis were conceived through discussion between us. Chapter 2 has was prepared as manuscript and accepted for publication as "Tait, A.R., Straus, S.K., Overexpression and purification of U24 from Human Herpesvirus Type-6 in E. coli: unconventional use of oxidizing environments with a maltose binding protein-hexahistine dual tag to enhance membrane protein yield. *Microbial Cell Factories* 2011, 10:51". Chapter 3 was published as "Tait, A.R., Straus, S.K., Phosphorylation of U24 from Human Herpes Virus type 6 (HHV-6) and its potential role in mimicking myelin basic protein (MBP) in multiple sclerosis. *FEBS Lett* 2008**,** 582, 2685-2688." For these chapters, I designed and carried out all experimental work. I analyzed the data and wrote the manuscript, which S.K.S. edited. Work for Chapter 4 was carried out by several individuals. I conceived of all the experimental work, and carried out a significant portion, with some notable exceptions. Mr. Prashant Kumar synthesized and purified the synthetic $U24_{1\text{-}15}$ peptide. The NMR experiments were performed by S.K.S. and myself. S.K.S. and Dr. W.R.P. Scott analyzed the NMR data and provided sequence assignment, corresponding chemical shift perturbation data, and molecular model structures. A manuscript is currently being prepared by S.K.S. In Chapter 5, I conceived of and carried out all experimental work, with the exception of the NMR spectroscopy of U24; the samples were prepared by me, and run on the spectrometer by Dr. Mark Okon. The animal protocol was prepared by me, and its ethics approved by the UBC Animal Care Committee (Animal Care cert#A07-0663).

Table of Contents

List of Tables

List of Figures

List of Abbreviations

6xHis	hexahistidine
ATP	adenosine triphosphate
BBB	blood brain barrier
BCA	bicinchoninic acid
CD	circular dichroism
CD[*number*]	cluster of differentiation protein
CHAPS	3-[(3-cholamidopropyl)dimethylammonio]-1-propanesulfonate
CI-HHV6	chromosomally-integrated human herpesvirus type 6
CMC	critical micelle concentration
CMV	Cytomegalovirus
CNS	central nervous system
Da	Daltons
DHPC	dihexanoylphosphocholine
DNA	deoxyribonucleic acid
DPC	dodecylphosphocholine
DRMS	detergent-resistant microdomains
DTT	dithiothreitol
EAE	experimental autoimmune encephalitis
EBV	Epstein-Barr Virus
EDTA	ethylenediaminetetraacetic acid
EGFP	enhanced green fluorescent protein
ENaC	epithelial sodium channel
ER	endoplasmic reticulum
Erk	extracellular signal-regulated kinase
GLB	Glascow lysis buffer
Golli	genes of oligodendrocyte lineage
GPCR	G-protein coupled receptor
GST	glutathione-S-transferease
GTPase	guanosine triphosphate hydrolase
HHV	Human Herpesvirus
HLA	human leukocyte antigen
HPLC	high-performance liquid chromatography
HSQC	heteronuclear single quantum coherence
HSV	Herpes Simplex Virus
HVS	Herpesvirus Saimiri
IPTG	isopropylthiogalactoside
IUP	intrinsically unstructured protein

LB	Luria Bertani
LDAO	N, N-Dimethyldodecylamine-N-oxide
LPPG	1-palmitoyl-2-hydroxy-*sn*-glycero-3-[phospho-RAC-(1-glycerol)]
MAG	myelin-associated glycoprotein
MALDI-TOF MS	matrix-assisted laser desorption ionization time of flight mass spectrometry
MAPK	mitogen-activated protein kinase
MBP[†]	maltose binding protein
MES	2-(N-morpholino)ethanesulfonic acid
MHC	Major Histocompatibility Complex
MOG	myelin oligodendrocyte glycoprotein
MOPS	3-(N-morpholino)propanesulfonic acid
MRI	magnetic resonance imaging
mRNA	messenger ribonucleic acid
MS	multiple sclerosis
MWCO	molecular weight cut-off
MyBP[†]	myelin basic protein
Nedd4	neuronal precursor cell-expressed developmentally downregulated 4
NEM	N-ethylmaleimide
NMR	nuclear magnetic resonance
NTR	neurotensin receptor
OD	optical density
ORF	open reading frame
PAD	peptidylarginine deiminase
PAGE	polyacrylamide gel electrophoresis
PBS	phosphate-buffered saline
PCR	polymerase chain reaction
PLP	proteolipid protein
PNS	peripheral nervous system
PPI	polyproline type I
PPII	polyproline type II
PTM	post-translational modification
r.p.m.	revolutions per minute
RNA	ribonucleic acid
SDS	sodium dodecyl sulfate
SH[*number*]	src homology
SNP	single nucleotide polymorphism

[†] The acronym ‘MBP’ commonly refers to both myelin basic protein and maltose binding protein in scientific literature. To avoid ambiguity, this thesis uses ‘MyBP’ to describe myelin basic protein, and ‘MBP’ for maltose binding protein.

src	sarcoma
TA	tail-anchor
TCA	trichloroacetic acid
TCEP	tris(2-carboxyethyl)phosphine
TCR	T-cell receptor
TLC	thin layer chromatography
TM	transmembrane
TMEV	Theiler's murine encephalomyelitis virus
TRC	transmembrane recognition complex
Tris	tris(hydroxymethyl)aminomethane
UV	ultraviolet
VZV	Varicella-Zoster Virus

Acknowledgements

I would not be where I am today without the kind support from many, many individuals. I am truly blessed to have known each and every one of them.

Firstly, I would like to thank my supervisor, Professor Suzana Straus, for not only presenting me with an extremely interesting project, but allowing me the privilege to pursue my own scientific curiosity to its fullest extent. Under her gentle guidance, I have been able to explore many different incredibly fascinating directions in research, and ultimately, she has helped me grow into a truly independent scientist who also values the opportunity for new collaboration. I must also mention my sincere gratitude for the mentorship and inspiration provided my Professors M.J. Kornblatt and Justin Powlowski; in many respects, they helped me build the solid foundation on which my academic research career is based.

I express my appreciation to Professor Lawrence McIntosh, as member of my supervisory committee and for being the reader on this thesis.

Members of the Straus Lab will always be fondly remembered for their help and companionship: Paresh Dave, Jinhe Pan, John Cheng, Htet Bo and Yurou Sang. Our transient but intelligent and helpful research assistants should also be mentioned: Dustin Bleile, Andrew Thamboo, Joseph Lee, Francis Lin, Cian Zybutz, Eun-Jun Kim, Ricardo Bortolon, Winnie Chan, and especially Prashant Kumar for making the U24 peptide for me. Others in the Chemistry Department who have offered their support and friendship over the years include John Wright, Adrian Weber, Grant Bare, Ben Hui, John Freeman, Bronwyn Gillon, Josh Bates, Paul Siu, Yasmin Mawani, Maria Telpoukhovskaia, Paloma Salas, Christoph Herrmann, Doralyn Dalisay, and too many others to mention.

An extra special thank-you is for Jacqueline Cawthray, who generously provided hours of editing and insightful comments to help bring this thesis into tip-top shape.

The staff of Bioservices, Elena Polishchuk, Candace Martens, and Jessie Chen must be acknowledged for their hard work in overseeing that fermenters were fermenting, autoclaves were autoclaving, centrifuges were centrifuging, and generally ensuring that biological work could be efficiently done inside of the Chemistry Department.

I would now like to thank my parents, whose love, support and encouragement have fired my enthusiastic belief that I could pursue whatever career path my heart desired. Like a third parent to me is Norma Carruthers, who, in addition to love, has given me years of financial support to help pay for my tuition.

Being of no help whatsoever in the completion of this thesis, rather, to help me forget thesis-related work for a time and remember what is like to be human, are my long-time friends: Jason Walters, Erik Hansen, Mathieu Bilodeau, Darren Butler, Jason Hossein, Francis Dubuc, Mathew and Liz Perrin, Stavros Spetsieris, Julie Bonvin, Zack Papachristou, Jason Wraight, and Chad Cook.

Last, but certainly not least, I thank my wife, Natalie, for her unending love and support over the last decade. Never having been to Vancouver, she trusted me when I said she'd like it here, and she moved across the country for me. Her perpetual patience and encouragement are admirable, and I can honestly say she has helped me become a better man for knowing her.

Oh, and God always deserves a shout out too.

For Natalie,

"You believed in me,

Against all odds,

You knew I could do it,

You knew I could prevail,

And girl, that's why I love you,

Forever and a day. . . yeah"

Chapter 1: Introduction

This thesis describes the purification and characterization of recombinant U24, a membrane protein encoded by Human Herpesvirus Type-6 (HHV-6). U24 has been previously implicated in the pathogenesis of multiple sclerosis (MS) based on its polyproline region that is identical to myelin basic protein (MyBP), a candidate autoantigen in MS. Chapter 1 lays the foundation on which the research presented herein is based, beginning with a general overview of MS: epidemiology, symptoms, pathological characterization; then focuses on the molecular characterization of potential biochemical triggers of the disease. It is within this framework of hypothetical disease initiators that the study of U24 is rationalized. Chapter 2 describes the methodology that was developed for obtaining pure recombinant U24 from an *E. coli* expression system, thus representing a first report on how to obtain this membrane protein. The chapter further deals with describing optimization of the protein expression yields and also provides new insights into membrane protein expression in general, techniques that can be applied to membrane proteins that are difficult to express. Finally, the chapter describes some preliminary findings relating to the immunogenicity of U24 in an animal system. In Chapter 3, the possibility that U24 may have a cell-signal interference role in myelin sheath maintenance is examined, recognizing that its polyproline region is a potential phosphorylation target of Erk2 MAPK. Chapter 4 further explores the potential ability that U24 has in interacting with other signalling proteins directly related to myelin health, based on the possible affinity U24 has in binding to the SH3 domain of Fyn tyrosine kinase. In Chapter 5, preliminary but significant results are presented from two separate branches of study: tests of immunogenicity of U24 in an animal model, and the progress in structural studies of U24 by NMR. Chapter 6 concludes the thesis with a general review of the experimental results and the impact they have on elucidating

the signal-interference mechanisms of U24 in 1) either triggering or sustaining disease in MS and 2) providing a potent immune evasion mechanism for the HHV-6. Future directions of the research are also discussed.

1.1. Overview of Multiple Sclerosis

MS is recognized as a debilitating neurological disease for which there is currently no known cure (see [1] for a review). The disease is an inflammatory, autoimmune disorder pathologically characterized by diffuse demyelinated regions and axonal damage within regions of the central nervous system (CNS), i.e.: the brain, spinal cord, and optic nerves. The results of the disease can be devastating. Cognitive and physical deficits are evidenced by seizures, dementia, severe pain, loss of sight, sexual dysfunction, lack of coordination, and eventual difficulty walking; later-stages can involve quadriplegia, and sometimes, death.

Symptoms of MS are usually acquired in young adulthood, at about 30 years of age [2], and the disease progresses over several decades, so that health care costs can be considerably high[3]. Canada has some of the highest rates of MS in the world[4] (Figure 1.1), ranging between 55-240 [5] individuals per 100,000 for a total of nearly 75,000 Canadians [3]. Regional differences in incidence are observed, with the Prairie Provinces and Atlantic regions at the highest rates [5, 6]. Women appear to be harder hit by the disease than men [7]; the ratio of women to men who are afflicted has been increasing over time, now reaching 3.2:1.

Extensive study has been done on assessing the complex interplay between genetics and environment that gives rise to the disease [8, 9], with greater incidence in familial associations [10], although specific heritable factors have not been firmly established. Genome-wide analysis of populations around the globe suggest that single nucleotide polymorphisms (SNPs) in the HLA-

DRB1 genetic locus on chromosome 6p21 have the greatest association with MS susceptibility [11], but only account for less than 50 % of MS cases. There are many other candidate non-HLA SNP associations that are currently under investigation [12, 13].

Viruses and retroviruses are also being explored as possible causative factors in multiple sclerosis [14], including Epstein Barr Virus [15], Human Endogenous Retrovirus type W [16], and Human Herpesvirus Type 6 [17].

1.1.1 History, Epidemiology and Types of MS

Jean-Martin Charcot is credited as the first to describe the symptoms of the disease and subsequently give it a name, "*sclérose en plaques disseminées*", in 1868 [18], although Charcot himself acknowledged that the disease had been described by others long before [19, 20]. Many had already observed the characteristic hallmarks of MS, which Charcot summarized as progressive instability, together with the pathological description as disseminated grey plaques found throughout the central nervous system (CNS). By the turn of the 20th century, MS cases would be the leading cause for patient admittance to a neurological ward [21].

Based on clinical symptoms, there are four main classifications of MS [22]: relapse remitting (RR-MS), primary progressive (PP-MS), secondary progressive (SP-MS) and progressive relapsing (PR-MS). RR-MS, which accounts for 80% of MS cases [1], is characterized by episodes of weakness, inflammation and demyelination which can last days,

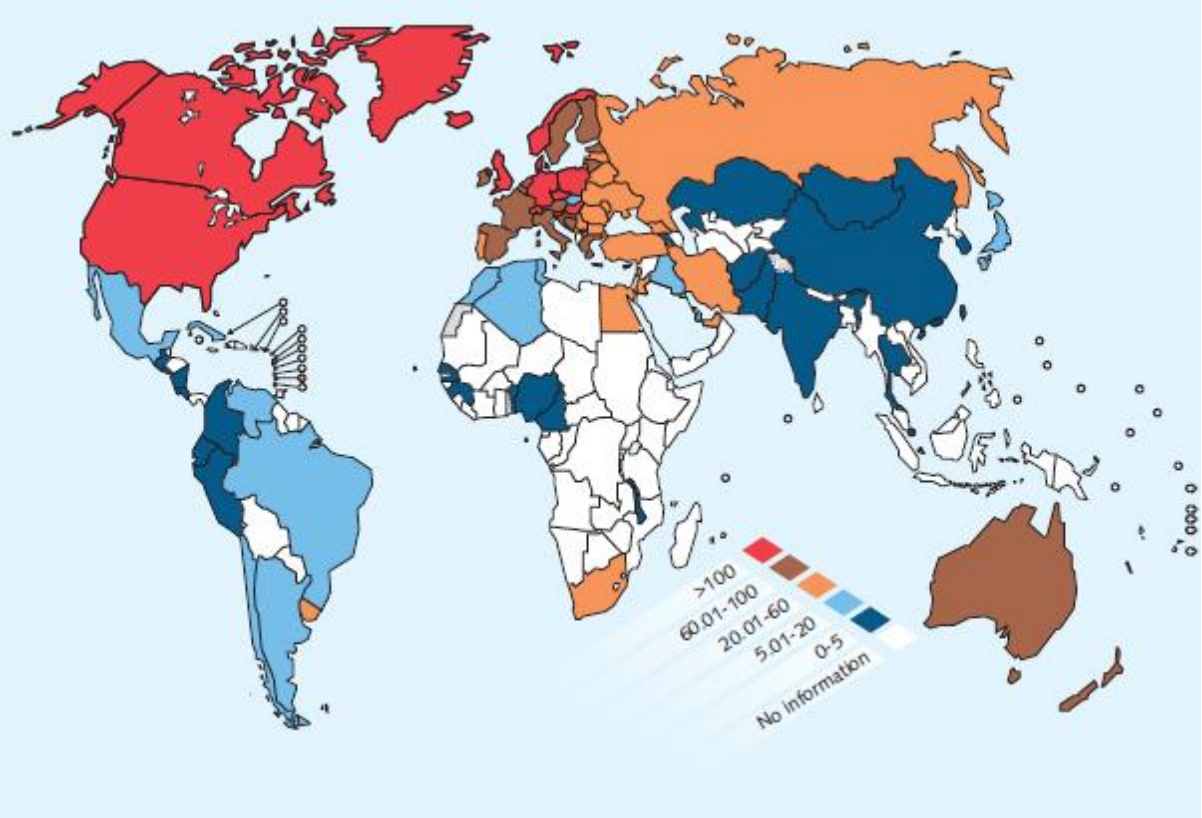

Figure 1.1 Global incidence of MS per 100,000 of the population. (Source: World Health Organization)

weeks or months, followed by periods of remission, in which partial to almost complete recovery occurs. Subsequent negative episodes usually return in the form of relapses, although disease symptoms typically worsen and the degree of recovery is less pronounced. In PP-MS, the disease symptoms generally steadily worsen over time and may include plateaus or only very minor, temporary improvements. A patient with SP-MS may start with a course of disease similar to the path taken by RR-MS, only to later have the disease steadily progress, and may or may not have plateaus or periods of remission. With PR-MS, which is the rarest[23] of all forms of MS, the disease takes on an initial progressive course of symptoms, yet there are some periods of symptom flare-up, followed by slight improvement.

Other diseases[24] which exhibit symptoms similar to MS are often cause for mistaken MS diagnosis [25]. A non-exhaustive list of these diseases include: Lyme disease, Hepatitis C, HIV/AIDS, Brucellosis, Whipple's disease, Syphilis, Mycoplasma, Creutzfeld-Jacob disease, Lupus, Sjorgen syndrome, amongst many others. It is only within the last several decades in which clinicians have begun to agree on sets of criteria [26, 27] with which to accurately give a diagnosis of MS. In addition to symptom analysis, positive diagnosis is usually done by combination of magnetic resonance imaging (MRI) to observe for lesions and cerebral spinal fluid (CSF) examination for autoimmune reactivity.

1.2 Molecular Characterization of MS

Myelin is the protective, lipid-rich insulating sheath which wraps around the nerve axons of the CNS (brain and spinal cord) and PNS (peripheral nervous system – in muscles, skin, etc.); in the CNS of MS patients, the myelin is broken down (Figure 1.2). The purpose of myelin is to increase electrochemical signal conduction velocity along the axons of nerves in vertebrates [28]. The CNS is made up of long bundled nerve fibers, which have a cell body and long axon. Electrochemical signal is propagated along the nerve axon to transmit messages to and from the brain, in order to control breathing, muscular movement, etc. The velocity is 1 m/sec in unmyelinated nerve compared to 50-100 m/sec in the myelinated nerve. Myelin is believed to have first appeared 475 million years ago in placoderms, the first fish with hinged jaws [29], and the hypothesis is that myelination evolved as a necessity for rapid tracking movement of the eye to fulfill the requirements of chasing moving prey.

There are plenty of observable traits in pathology that enable differentiation between normal and MS CNS tissues, at both the macroscopic and microscopic levels. Starting from a

more coarse-grain perspective, MRI of MS brains reveal tell-tale signs of the disease in the way of small spots, which are the lesions (Figure 1.2). In 95% of clinically definite cases of MS, lesions can by observed by MRI [30]. There are several different methods by which to make an MS diagnosis by MRI which rely on observing the size, number, and location of lesions within the brain architecture [31]. For example, Fazekas' criteria [32] rely on observing ≥3 lesions with at least two of the following properties: i) a lesion in the infratentorial region of the brain, ii) a lesion in the perventricular region of the brain, and/or iii) lesions > 6 millimeters. MRI observables such as these are used to convert suspected MS cases to clinically definite ones.

Figure 1.2 MRI of the brain of a patient with MS, with lesion areas indicated by arrows. Image was courteously provided by Prof. Alex MacKay (Department of Physics and Astronomy, University of British Columbia).

Besides imaging of lesions, MRI can be used to demonstrate that overall brain volume decreases in MS patients [33]. Also, N-acetyl-aspartate, a neuronal marker that can be quantified by MRI, has a lower concentration in the lesion area than in surrounding brain tissue[34].

The molecular pathology of early lesions is poorly understood, since the lesions are rarely fatal and they generally do not give rise to symptoms. The autopsies done on the brains of new MS patients who died suddenly from MS demonstrated significant oligodendrocyte (cells which make up myelin) death in the area of the lesion, but there was no infiltration of immune system cells into the brain [35]. This finding is somewhat in contrast to the commonly-held belief that MS is primarily a T-cell-mediated autoimmune disease [36] indicating that there may be a small but relevant subgroup of MS patients that signify that demyelination can occur in the absence of inflammatory infiltrates. A high degree of CNS infiltration of T- and B-cells in chronic MS patients generally appears to correlate well with the level of inflammation and neurodegeneration [37]. Ultimately, it is evident from these contrasted experimental findings that MS is pathologically a highly heterogeneous disease [38-40]. It is clear that nerve axons are highly damaged in actively demyelinating lesions, regardless of whether the demyelination is directly related to inflammation and autoimmunity. Trapp *et al.* [34] found an average of 11,236 transected axons per mm^3 in active lesions of MS patients but less than one in the normal-appearing white matter of the control, non-MS patients. It should be noted that demyelination can be reversed as there is continual break-down and build-up of myelin [41]. Unfortunately, demyelinated axons themselves are subject to transection and the resulting damage is usually considered irreversible [34].

Evaluation of the autoimmune component of new potential MS cases was proposed by Berger *et al.* to be useful in precisely predicting clinical conversion to definite MS [42]. Serum detection of antibodies directed against myelin basic protein (MyBP) and myelin oligodendrocyte protein (MOG), two proteins found abundantly in myelin, indicated certain relapse in 95% percent of patients tested, but absence of these antibodies predicted that 77% of

these patients were likely to remain symptom-free for several years. Interestingly, however, Kuhle *et al.* could not reproduce these findings, claiming that there is no prognostic ability for disease progression by measurement of anti-MyBP and anti-MOG antibodies [43].

Autoimmunity may be related to the increase in permeability of the blood brain barrier (BBB) observed in MS patients. Increased expression of proteases such as matrix-metalloproteinases [44] may degrade the BBB enough to allow infiltration of T- and B- cells. Once inside the BBB, these immune cells can encounter cellular debris from initial apoptotic oligodendrocytes, and thus be presented with protein epitopes from myelin proteins. By definition, an *epitope* is the part of an antigen that is recognized by the immune system, specifically by T-cells, B-cells and antibodies; a particular stretch of amino acid sequence from a protein is an example. After an epitope stimulates the immune system activation (in MS), resulting inflammation may be driven by CD4+ Th1 proinflammatory cells, and CD8+ cells are found extensively in chronic brain lesions. However, it is under intense debate what role these infiltrating T-cell subpopulations actually play in the pathogenesis of the disease [45], the observed demyelination and concomitant destruction of the axon.

1.3 Advancing our Knowledge of MS with Animal Models

Biopsied CNS material from living human subjects is not readily obtainable, thus animal models of MS [46] have been invaluable in making progress in understanding the molecular complexities of the disease in humans. While much has been learned from these animal models, there are still many differences between human and animal pathologies, likely arising from the differences in our basic physiologies. For example, many models rely on creating inflammatory allergic response in the animal, which leads to demyelination, but this disease course only

mimics chronic MS conditions, not the early non-allergic demyelinating events that take place in some humans. No one animal model can mimic all aspects of human MS because of interspecies physiological differences, as well as the inherent and the heterogeneous nature of MS itself.

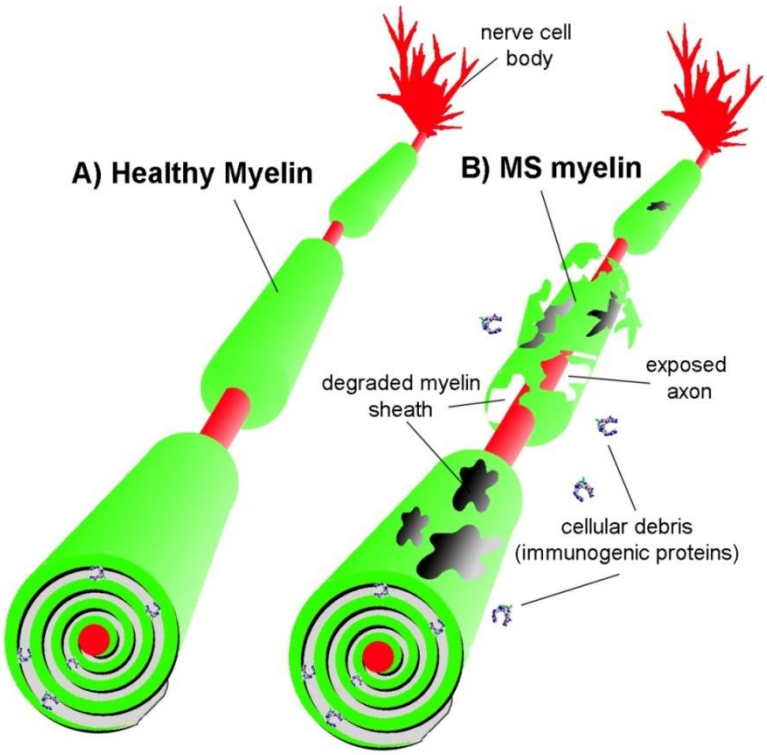

Figure 1.3 Cartoon depiction of A) healthy myelin sheath insulating nerve axons and B) damaged myelin observed in MS, with exposed axon and immunogenic cellular debris present.

Knocking out or mutating genes in animals [47-50] has also provided insight into the genetic complexity of MS, allowing the study of specific gene functions and evaluation of their relationship to the interplaying mechanisms of degradation and repair.

1.3.1 Experimental Autoimmune Encephalitis

Experimental autoimmune encephalitis (EAE) is a blanket term to describe a variety of different animal MS models that have been established, mostly in rodents and primates.

Immunization with homogenates of CNS tissue (i.e.: spinal cord) or purified proteins (i.e.: MyBP, MOG or PLP) sensitizes the immune system against epitopes of these proteins [51]. The primed animal host then mounts an attack on self-proteins of the CNS, the result of which is akin to the inflammatory T-cell response and demyelinating events observed in chronic MS patients. Adoptive-transfer EAE (AT-EAE) can be triggered in healthy animals injected with auto-reactive immune cells (activated neuroantigen/neuroepitope-specific CD4+ T-cells[52]) from another animal that has already developed EAE[53, 54], or from *in vitro* cell culture. Another type of EAE is virally induced such that animals injected with certain viruses [55-57], can also develop demyelination.

1.3.1.1 MyBP, PLP, MOG, and MAG Induction of EAE

MyBP is the second most abundant protein component (30-40%) in myelin after proteolipid protein (PLP) [58]. It is able to induce acute EAE in rodents after immunization with the full-length protein mixed with adjuvant; the disease follows a monophasic course where the animal becomes partially paralyzed and then fully recovers. Once having experienced EAE induced by MyBP, the animal is resistant to reinduction of the EAE[59]. Because animals do not normally relapse, this model has its limitations in comparison to MS, where relapsing is common. Induction of EAE has been mapped to several MyBP epitopes, and short peptides containing these epitopes are also capable of inducing EAE. There are also shifts in which epitopes are primarily recognized depending on the phase of the disease[60]. The immunodominant epitope, amino acid sequence 87-99 in MyBP, whose sequence is V^{87}HFFKNIVTPRTP^{99}, is also recognized by T-cells from lesion area of diseased brains [61] and will be discussed later.

Myelin oligodendrocyte glycoprotein (MOG) is only present in minor amounts in myelin but can initiate a strong paralytic and demyelinating response in rodents, and can either be relapsing or non-relapsing depending on the species [62]. The major epitopic region appears to be the amino acid sequence between residues 35-55. In humans with MS, T-cell responses were found to be much stronger to MOG than either MyBP or PLP.

Myelin associated oligodendrocyte glycoprotein (MAG) is yet another minor myelin component with the ability to produce EAE symptoms in rodents [63], although the symptoms are mild. The characterized major T-cell epitope is the amino acid region sequence of 97-112.

Proteolipid protein is the major protein component of myelin (50%) [58], and contains many encephalitogenic epitopes, the major one being region amino acid sequence 139-151. The course of PLP-induced EAE is very similar to chronic relapsing MS [64] and T-cells recognizing PLP epitopes are clearly elevated in MS patients.

1.3.2 Viral Animal Models of Multiple Sclerosis

Virus-induced demyelination in animals represents an attractive MS model because of the possibility that viruses do play a role in humans with MS, either acting as a trigger of disease, or acting as opportunistic pathogens which exacerbate the existing disease state. In addition to those discussed below, there are other animal viruses emerging in the literature which are being studied, such as the JHM virus (coronavirus) and Semliki Forest Virus [14].

1.3.2.1 Theiler's Murine Encephalomyelitis Virus

Theiler's murine encephalomyelitis virus (TMEV) [56, 65] was isolated from the intestinal cavity of mice and was found to be quite ubiquitously widespread, yet only rarely caused

problems in the CNS. While the virus normally resides benignly in the gut, it was surmised that genetic predisposition combined with certain pathological events allow the virus to gain CNS access. After CNS infection, a chronic relapsing disease progression occurs, with varying levels of paralysis observed: some animals have minor paralysis in the hind section, whereas with others the paralysis is so severe that death is the result. Much like in human MS, remission can occur for almost complete recovery, yet for those animals that were severely paralyzed, some disability remains.

Molecular characterization of immune components in animals undergoing TMEV induced demyelination showed that there is differential reactivity to various CNS components, depending on the stage of the disease. For example, T-cells activated by exposure to TMEV can trigger reactivity towards $PLP_{139-151}$, a major EAE epitope discussed earlier [66]. However, it is believed that it is not necessarily actual TMEV epitopes which prime autoreactivity towards CNS antigens like PLP (that is, molecular mimicry) rather a TMEV attack can initiate exposure of CNS epitopes, and subsequent T-cell populations arise where more and more CNS epitopes are being recognized (that is, epitope spreading). Concepts of epitope spreading and molecular mimicry are focal points to be discussed further.

1.3.2.2 Human Herpesvirus type-6-Induced MS in Primates and Rodents

The HHV-6 primate model of MS in macaques does not yet appear in peer reviewed literature, but a US patent exists [67] describing how macaques can develop MS symptoms if injected with live HHV-6A virus. Claude Genain also presented these results in 2008 at the *World Congress on on Treatment and Research in Multiple Sclerosis* conference [68].

The common marmoset, *Callithrix jacchus,* represents an appropriate model for studying the relationship between HHV-6 and MS in humans because of high genetic-similarity between humans and marmosets. For example, marmosets express a CD46 homologue, the cellular receptor required for HHV-6 particles to bind with for infection of human cells [69, 70]. This CD46 receptor is of interest in multiple sclerosis [71], particularly because its expression appears to be upregulated in 80% of MS patients [72].

Several key findings from this work on marmosets were: 1) animals appear to need two separate exposures to the virus (injections at intervals separated by days/weeks); 2) it is the HHV-6A strain, not HHV-6B strain which initiates disease symptoms; 3) the autoimmune component of the disease appears several weeks after initial disease symptoms occur. Taken together, this means that repeated exposure to HHV-6A can result in MS-like symptoms in macaques, long before autoimmunity, such as anti-MOG antibody appearance, occurs. Interestingly, there is actually a brief immunosuppressive period where there is actually *less* autoreactivity than normal right before T-cell increase in reactivity towards self-proteins, MyBP and MOG (Figure 1.4).

Findings that HHV-6A is capable of causing neurological impairment in marmosets were recently confirmed by separate investigators [73]; their data were presented at the *7th International Conference on HHV-6 & 7*.

A rodent model of HHV-6-induced MS is also currently in development, a breakthrough that would facilitate research compared to using the marmoset model. Results were recently presented at the 7th International Conference on HHV-6 & 7 [74]. Since the CD46 receptor is required for HHV-6 entry into human cells, a transgenic mouse was created that expresses Cyt1

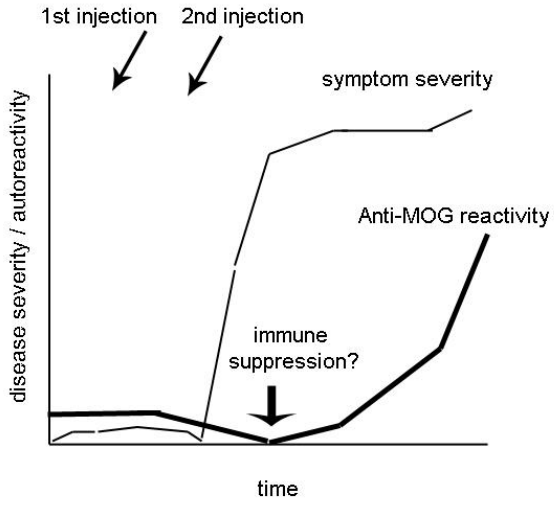

Figure 1.4 General interpretation of results obtained with macaques injected with HHV-6A; correlation of disease severity and anti-MOG reactivity over time. For clarity, symptom severity is portrayed above as monophasic, whereas the symptoms actually vary in intensity over time (relapsing), but they do not appear to be proportional to levels of autoreactivity (interpretation of data presented in [67]).

and/or Cyt2 isoforms of CD46. Primary mouse brain cell cultures expressing CD46 and infected with HHV-6A and –6B strains showed signs of active HHV-6A infection for up to two months, but HHV-6B DNA levels rapidly dropped shortly after infection. Live mice infected with HHV-6A did not display overt disease symptoms, but there was histological evidence of demyelination and cell infiltration into the brain. In addition, these mice exhibited a more severe form of disease when EAE (Section 1.3.1) was induced. These results corroborate a role for HHV-6A (but not -6B) in the pathogenesis of human MS.

1.3.3 Cuprizone Model

Cuprizone (bis-cyclohexanone-oxaldihyrazone), a copper chelator [75] (Figure 1.5), has found use in spectroscopic determination of copper because the complex absorbs at 595 nm and

yields an intense blue colour. Feeding of cuprizone to young adult mice results in a synchronous, consistent demyelination event [76]. Its mechanism of action is unknown, but it is presumed that cuprizone exposure results in a copper/zinc dismetabolism that results in severe toxicity to myelin [77]. Recent results show that cuprizone is not capable of absorbing through the intestinal cell wall and also does not accumulate in the brain, so it is most likely that the toxic effects are from the molecule's chelation properties only [78].

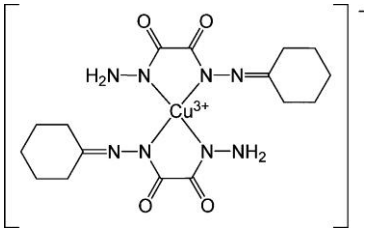

Figure 1.5 Chemical structure of hypothetical copper-cuprizone complex [75].

The cuprizone model provides a contrast to the inflammatory (EAE) animal models of MS because there is no concomitant inflammation and activation of reactive T-cells [79]. There is evidence to support that cuprizone actually suppresses EAE through inhibition of T-cell activation [80]. Without the complication of inflammatory infiltrates, use of cuprizone has allowed the study of mechanisms which control demyelination and remyelination. Both demyelinating and remyelinating events appear to be occurring simultaneously, and cessation of administration of cuprizone results in virtually complete remyelination.

Genetic knockout mouse models used in conjunction with cuprizone have allowed determination of certain proteins which either enhance or attenuate susceptibility to cuprizone-induced demyelination. For example -/- CXCR2 chemokine receptor knockout mice are insensitive to cuprizone[81]. Also, mice that had a double knockout of FcRγ and Fyn tyrosine

kinase were resistant to cuprizone-induced demyelination as well [49], a finding which will be discussed in the context of the experimental work described later in this thesis.

1.4 Epitope Spreading

A typical immune response involves recognition of one or two epitopes of a self or foreign protein, termed dominant epitopes [51]. Over time, T-cells may respond to an expanded repertoire of epitopes within the protein, and these are called cryptic epitopes. For example, EAE induced in mice with dominant epitope $PLP_{139-151}$ will later demonstrate reactivity towards $PLP_{178-191}$. This would be a case of intramolecular epitope spreading, that is, new epitopes emerging within the same protein. Later, these same animals will begin to display reactivity towards the epitope $MyBP_{84-104}$ (containing the sequence mentioned in Section 1.3.1.1), as a form of intermolecular epitope spreading between two different proteins. Epitope spreading in this example appears in a consistent hierarchical manner: $PLP_{139-151} > PLP_{178-191} > MyBP_{84-104}$ [64]. The process of epitope spreading rooted from PLP has been observed in humans with MS, where normal control subjects lack autoreactivity [82].

TMEV is capable of initiating epitope spreading leading to autoimmunity in mice [56]. After infection by TMEV, autoreactivity towards self-epitopes, such as $PLP_{139-151}$, is observed. A study was carried out on candidate viral protein sequences with homology to self-antigens of PLP, MOG and MyBP, yet none of the candidate viral peptides were able to initiate cross reactivity with these proteins[56]. It was concluded that TMEV assault initiates the release of CNS proteins which normally have their dominant epitopes sequestered from immune system detection, thus triggering a cascade of autoreactivty and epitope spreading among self, non-viral peptides only. There is the possibility that viral and bacterial T-cell epitopes with structural

similarity to self-protein epitopes can induce an autoagressive T-cell response [83, 84]. MyBP is a candidate autoantigen where $MyBP_{85-99}$ is the immunodominant region and a small subset of T-cells is activated by this peptide.

1.5 Molecular Mimicry

The concept of molecular mimicry was first tested in an experimental animal model with a hepatitis B virus polymerase peptide in which six amino acids were identical to the encephalitogenic region of rabbit myelin basic protein ($MyBP_{85-99}$) [85]. T cell reactivity to MyBP was observed following immunization of rabbits with this viral peptide, and four out of eleven animals showed histological signs of EAE progression. A hypothesis was postulated that foreign bacterial and viral proteins with regions structurally similar to this MyBP epitope at the same key residue positions would be sufficient to bind to T-cells receptors and stimulate T-cell activation. In a study of 129 peptides from viral and bacterial sources that fit the structural criteria, seven viral and one bacterial peptide could stimulate T-cell reactivity towards MyBP. Structural similarity, not sequence identity, was deemed the most important factor, as only one peptide of these peptides was closely related to $MyBP_{85-99}$ by sequence (Figure 1.6). Because many different sequences from varied sources are able to stimulate MyBP-specific T-cell clones, it may be difficult to pinpoint any one particular foreign pathogen as a cause of MS; rather, it could be that simultaneous infections and presentation of several stimulatory foreign epitopes are what shift the balance from healthy to disease states.

Based on sequence and structural similarity between foreign proteins and CNS self-proteins, the list of foreign epitopes with the potential of stimulating T-cell clone expansion towards CNS proteins is expanding. A JC-virus peptide, for example [86], which has significant

sequence identity to MyBP, was shown to trigger EAE symptoms and neural T-cell infiltration in rats.

$MyBP_{85-99}$	**ENPVVHFFKNIVTPR**
Herpes simplex UL15 protein	**FRQLVHFVRDFAQLL**
Adenovirus type 12, ORF	**DFEVVTFLKDVLPEF**
Pseudomonas, phosphomannomutase	**DRLLMLFAKDVVSRN**
Human Papillomavirus type 7, L2 protein	**IGGRVHFFKDISPIA**
EBV DNA polymerase	**TGGVYHFVKKHVHES**
Influenza type A, hemagglutinin	**YRNLVWFIKKNTRYP**
Reovirus type 3, sigma 2 protein	**MARAAFLFKTVGFGG**

Figure 1.6 Peptides able to stimulate MyBP-T-cell-specific clones [84]. Only the Human Papillomavirus type 7 L2 protein has significant sequence homology to dominant epitope $MyBP_{85-99}$.

1.5.1 A Case for Human Herpesvirus type-6 and Molecular Mimicry in MS

There is extensive literature that suggests that a correlation between HHV-6 and MS exists [87]. With the molecular mimicry hypothesis circulating as a possible explanation for the pathogenesis of MS, Tejada-Simon *et al.* [88] found a connection to HHV-6. The group had previously found that HHV-6 DNA was more frequently detected in MS patients compared to controls, and that reactivity towards the 101-kDa virion protein was altered in MS patients [89]. It was realized that U24, a protein from HHV-6 of unknown function at the time of their study, has a seven amino acid stretch identical with MyBP [88] (Figure 1.7). This sequence is PRTPPPS, and is present in U24 from HHV-6A, -6B and -7. Using 13-mer synthetic peptides corresponding to $MyBP_{93-105}$ and HHV6- $U24_{1-13}$ it was found that 50% of T cells recognizing $MyBP_{93-105}$ cross-reacted with and could be activated by $U24_{1-13}$ in MS patients, and the frequency of these cross reactive cells was significantly higher in MS patients.

It is worth noting that the HHV-6 U24 peptide used in the aforementioned study was the sequence from the HHV-6B version of the U24 protein, whereas there is increasing evidence

indicating that it is the HHV-6A [67, 68, 72, 73, 90-93] strain specifically that is associated with MS. Within the peptide that was studied, U24 differs by only one amino acid, at position 3: there is a proline in the HHV-6A U24 and an arginine in HHV-6B U24. Nevertheless, even a small change such as this may elicit a very different immunological response, so it would therefore be of interest to see how data for HHV-6A U24 compares to that which was obtained for HHV-6B U24.

Figure 1.7 MyBP and U24 peptide sequences used to examine T-cell activation and cross-reactivity in MS patients [88]. Identical sequences are indicated by grey shading.

1.6 Structure/Function of Myelin Basic Protein

The sequence identity between U24 and MyBP (PRTPPPS) has provided the basis of the molecular mimicry study that was carried out by Tejada-Simon *et al.* [88] as described in the previous section. While U24 protein may be able to trigger an adverse immunologic cross-reactivity towards MyBP, an autoantigen in MS, we must consider additional effects that the presence of this identical sequence in U24 may have on the structure and function of MyBP. Reports are emerging that suggest that the polyproline region in MyBP may have important implications in both the intricate structural and signalling roles of MyBP [94], underlying mechanisms important for the rebuilding of damaged myelin.

This section of the thesis provides background about the MyBP protein molecule, with a special focus on the significance of the polyproline region. Essentially, the possibility that U24

may either destabilize and/or interfere with the signalling of MyBP as a mechanism for pathologic myelin dysfunction is explored.

1.6.1 The MyBP Molecule

Myelin is made up of multilamellar lipid-rich sheets which wrap around the nerve axon for insulation. In Section 1.3.1.1, it was mentioned that MyBP is a major protein component of myelin, the other major protein being PLP. The MyBP found in myelin is termed "classic" MyBP, and is from a larger gene complex called Golli (Genes of OLigodendrocyte Lineage) [94, 95]. Differential splicing of a single mRNA transcript gives rise to the four forms of classic MyBP in humans which are: 21.5, 20.2, 18.5, and 17.2 kDa. The 18.5 kDa form is the most abundant one in human CNS myelin. To underline the importance of MyBP to myelin health, partial deletion of the MyBP gene in *shiverer* mice [96] results in severe hypomyelination. However, upon transplantation of normal MBP-producing cells, myelination can be rescued [97].

The 18.5 kDa form of MyBP can take on a number of postranslational modifications (PTMs) such as phosphorylation of Ser/Thr residues and deimination, the conversion of arginine to citrulline. PTMs give rise to a number of charge variants: C1, C2, C3, C4, C6 and C8. C1 is the most positively charged being +19 at neutral pH, and each increment isomer represents a charge loss of 1 [94]. In other words, C8 is the least positively charged.

1.6.2 Tertiary Structure and Dynamics

All forms of classic MyBP are considered intrinsically unstructured proteins (IUPs), regardless of the splice variant, number or type of PTMs that are on the molecule [98]. Interestingly, MyBP can adopt different structures depending on its environment, as

demonstrated with circular dichroism (CD) spectroscopy[99]. In simple salt buffer solution, MyBP attains a random coil structure, but in the presence of membrane mimetic additives such as dodecylphosphocholine or trifluoroethanol, MyBP becomes highly α-helical [100]. MyBP's unstructured nature may have to do with its ability to interact with a wide range of partners, such as metal ions [101], other proteins [94], and especially, lipid membranes [94, 95].

The disordered nature of MyBP has precluded any successful attempts at solving a high resolution X-ray crystal structure of the molecule. However, reconstitution of bovine C1 charge isomer of MyBP on a lipid monolayer allowed for electron microscopy analysis and the development of a model of the molecule to a low resolution of 2.8 nm [102]. As seen in Figure 1.8, MyBP adopts an overall "C" shape.

1.6.3 Post-Translational Modifications on MyBP: Relationship to MS

There is long list of post-translational modifications that have been observed on MyBP [98], most of which their significance is unknown. But of the major modifications, such as citrullination, methylation and phosphorylation, they are either measurably increased or decreased in MS.

1.6.3.1 Citrullination

Deimination of arginine to citrulline is catalyzed by peptidylarginine deiminase (PAD) [103] (Figure 1.9), and it is normal for a few citrullinated arginines to be present out of the 18 arginines in MyBP. Hypercitrullination, on the other hand, leads to an inability of MyBP to organize myelin [104]. A mutant mouse model overexpressing the PAD2 enzyme experienced

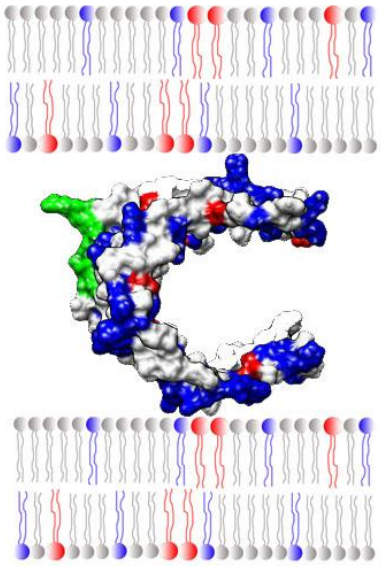

Figure 1.8 Model of myelin basic protein (1qcl.pdb from the Protein Data Bank) and its potential interaction with two leaflets of the lipid bilayers of myelin. Positively-charged residues/lipids are in blue, and negatively-charged residues/lipids in red. The identical sequence shared with U24 protein, PRTPPPS, is in green.

increased citrullination on MyBP and demyelination was observed [105]. MS patients experience 3-fold higher levels of MyBP citrullination, and in Marburg's disease (an extremely rapidly-progressing form of MS), virtually all of the arginines in MyBP have been deiminated [104]. The presence of citrullines on MyBP also renders MyBP more susceptible to proteolytic cleavage, presumably because the citrullinated protein molecule has a more open conformation. Cathepsin D, a myelin-associated metalloproteinase, was able to digest a hexa-citrullinated form of MyBP four-fold faster than uncitrullinated MyBP. It was also found that 18 citrullinated residues increased the rate of digestion by 35-fold [106]. Consequently, greater citrullination of MyBP leads to the generation of greater amounts of the immunodominant peptide of MyBP (see Section 1.3.1.1)

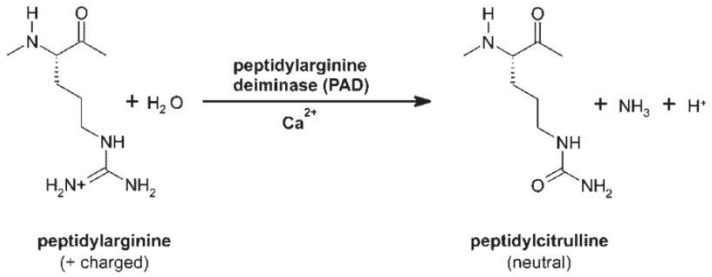

Figure 1.9 Citrullination (deimination) of peptidylarginine by PAD. The guanidino group of arginine is hydrolyzed yielding a ureido group and ammonia.

1.6.3.2 Methylation

MyBP can be mono- or di-methylated on arginine 107 by a specific methyltransferase, whose activity is upregulated during active myelination [107]. Methylation is thought to stabilize MyBP; in cultured cerebral cells from embryonic mice, inhibition of methyltransferase resulted in demyelination [108]. Mono- or di-methylation of arginine 107 is likely to induce a more compact structure of MyBP, as increasing methylation at this site decreased the rate of deimination [107].

1.6.3.3 Phosphorylation

Phosphorylation of MyBP is readily reversible, unlike methylation and deimination, and therefore is likely to be useful for dynamic changes in protein structure and related signalling events. Phosphorylation of MyBP can occur on many different Ser/Thr residues, but perhaps the most important is the phosphorylation of threonines 95/98 (of the sequence $\underline{T}^{95}PPR\underline{T}^{98}PPPS$) because these are both *in vivo* and *in vitro* recognition sites for MAPK- related kinases[109]. (Note that bovine numbering is Thr94 and Thr97, and human numbering refers to Thr95 and Thr98; the two conventions will be used interchangeably throughout the thesis). Phosphorylation of Thr98

is particularly decreased in MS [50]. MAPKs are important intermediates in signal transduction pathways that are initiated by many types of cell surface receptors [110]. MAPK-targeting of this region is believed to have many downstream effects that stabilize myelin perhaps by signalling for rapid remyelination after a demyelinating event. The FcRγ–pathway signalling recruits Fyn tyrosine kinase and uses p38 MAPK downstream to increase phosphorylation on the 21.5 kDa isoform of MyBP, initiating remyelination in the cuprizone mouse model [49] (Section 1.3.3). Phosphorylation may also control local structure around the phosphorylation site, as it was shown that the nearby major epitope insertion into the lipid bilayer is decreased because of electrostatic charge repulsion [98].

1.6.3.3.1 Lipid Raft Partitioning

Lipid rafts are are small (10–200 nm), heterogeneous, highly dynamic, sterol- and sphingolipid-enriched domains that compartmentalize cellular processes [111]. Considered a form of signalling hub to bring together substrates for carrying out essential protein-protein or protein-lipid interactions within the cell, lipid rafts are believed to play a critical signalling role in myelin development [112]. Lipid rafts are also referred to as detergent-resistant microdomains (DRMS), for their inability to be solubilized by detergents. Figure 1.10 illustrates the temporal and spatial partitioning of components of myelin. Early myelin is enriched with Src kinases Fyn and Lyn, which are important for PNS and CNS myelin formation [113]. Only the mature form of myelin has rafts enriched with phosphorylated MyBP, and both citrullinated and methylated forms of MyBP are excluded from these lipid domains.

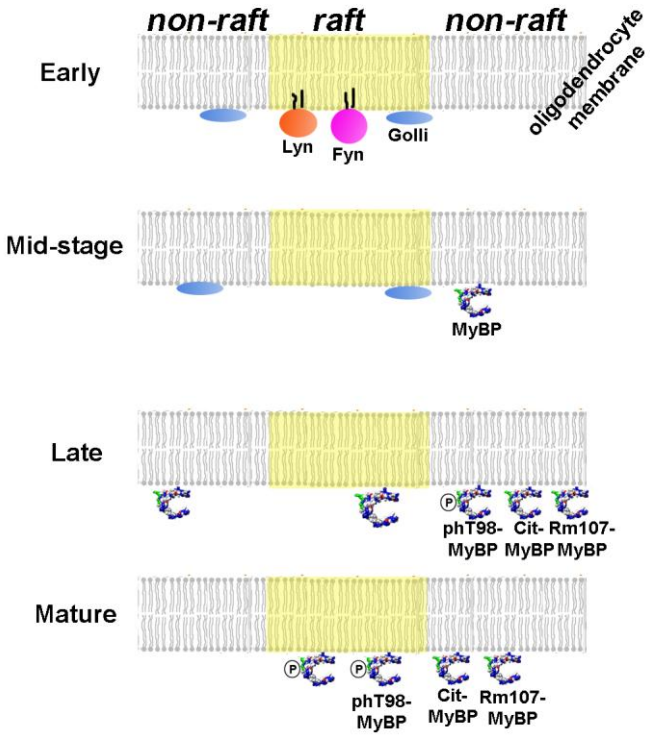

Figure 1.10 Temporal and spatial partitioning of myelin components (adapted from [112]). In the early stages of myelin development, Fyn and Lyn tyrosine kinases colocalize with Golli isoform of MyBP in lipid rafts. Classic MyBP enters into lipid rafts in later stages and lipid rafts become enriched with phosphorylated MyBP (phT98-MyBP) in mature myelin. Citrullinated MyBP (Cit-MyBP) and methylated MyBP (Rm107-MyBP) are excluded from rafts. Other major membrane protein components (i.e.: MOG, MAG, PLP) are not shown here for clarity.

1.6.3.3.2 Cytoskeleton Interactions

MyBP is able to bind actin filaments then attach them to a negatively- charged lipid membrane[114]. Such an association of MyBP with a main cytoskeletal component like actin is likely to have important ramifications on the dynamic processes of myelination. Phosphorylation of MyBP has been shown to dramatically reduce the affinity the MyBP/actin complex has for negatively charged lipid bilayers, without affecting the affinity MyBP has for actin. The transient process of phosphorylation may allow MBP/actin to rapidly grapple to different parts of

the developing membrane to provide cytoskeletal stability and signal transduction where and when it is required.

MyBP can also bind to and polymerize microtubules [115], another component of the cytoskeleton. Evidence suggests that actin, tubulin and MyBP all colocalize to enable dynamic myelination processes. Furthermore, MyBP can also tether microtubules to the lipid membrane, and bind lipid vesicles to microtubules. Unlike actin, however, phosphorylation generally has very little effect on the MyBP/microtubule interactions.

1.6.4 Polyproline Region of MyBP

The PRTPPPS sequence is not only important for presenting the requisite PX(T/S)P motif for MAPK recognition, but there is indication that the polyproline segment is able to impart both structural rigidity and to favour protein-protein interactions.

1.6.4.1 Polyproline Type II Helix

Amino acids primarily adopt a *trans* configuration about the peptide bond and proline is the only amino acid likely to be found in a *cis* configuration. The *cis/trans* isomeration can be catalyzed by prolyl isomerases, and proline isomeration can have a profound impact on the function of many key proteins involved in diverse cellular processes, including cell growth regulation, genotoxic and other stress responses, immune response, germ cell development and neuronal differentiation and survival [116]. The polyproline regions of proteins can adopt local secondary structure in the form of two kinds of helices: polyproline type I (PPI) helix and polyproline type II (PPII) helix[117] (Figure 1.11). PPI helices are right handed, unfavourable in solution, and arise from *cis*-prolines where the dihedral angles are $\Phi = -75^{\circ}$ and $\Psi = +160^{\circ}$. PPII

helices are formed from *trans*-prolines ($\Phi = -75^{\circ}$ and $\Psi = +145^{\circ}$) and are more extended than PPI helices. PPII helices are important for mediating protein-protein interactions with protein scaffold domains including those of the SH3 and WW type [118]. The polyproline region of MyBP that is shared with U24 was demonstrated by CD spectroscopy to form a PPII helix[119].

1.6.4.2 SH3 Interactions with MyBP

The Src homology 3 (SH3) domain is a small (~60 amino acids) domain that recognizes proline-rich protein regions of approximately 10 amino acids in length. The affinity of SH3 domains for proline-rich peptides is usually in the range of 5-100 μM [120]. While the minimal core SH3 binding motif is usually based around the minimal PXXP motif, non-PXXP exceptions have been reported [121]. The SH3 domains are found in tyrosine kinase signalling proteins, but also in cytoskeletal arrangement proteins, among others. There are more than 500 SH3 domains encoded by the human genome [122].

In a binding study in which a host of SH3 domains were screened, it was found that the SH3 domain of Fyn tyrosine kinase could bind to MyBP [119]. It was then shown that MyBP can tether the Fyn-SH3 domain to a negatively-charged lipid membrane [123]. Modelling the interaction between MyBP and Fyn-SH3 predicted low affinity in the micromolar range, but the interaction appears to be biologically relevant nonetheless. Early in myelin development, Fyn is localized to lipid rafts (Figure 1.10), through dual lipidation (palmitoylation and myristoylation) at its C-terminus. Fyn itself has been shown to be essential for the initial signalling events of myelination in several respects, and not strictly as a result of its interaction with MyBP [49, 124, 125]. The Fyn-SH3 domain can bind to Tau protein and α- and β-tubulin subunits to organize microtubules at the membrane, and this interaction is critical for efficient myelination [126, 127].

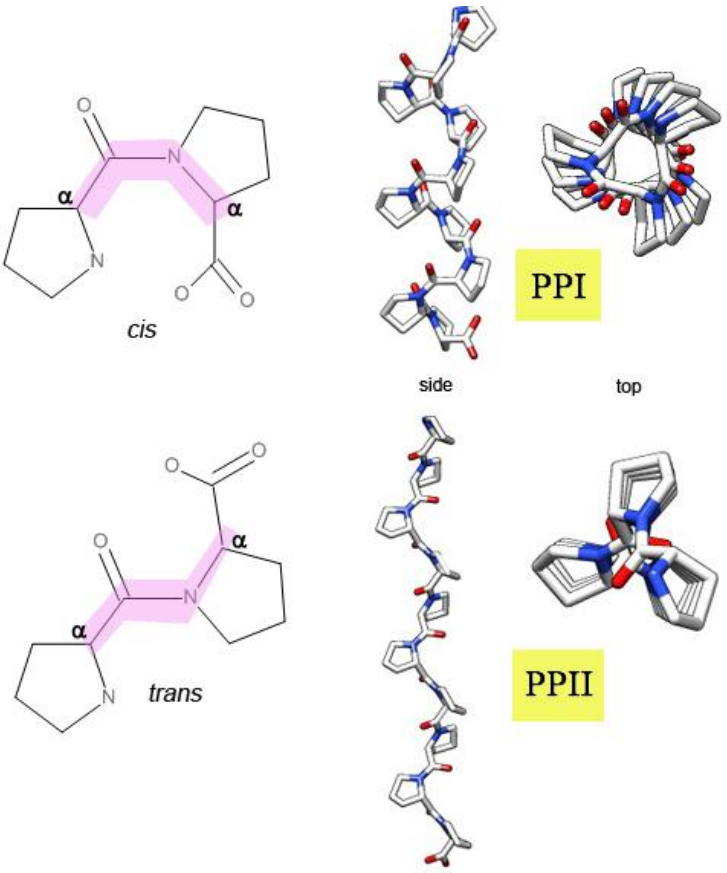

Figure 1.11 Illustration of *cis/trans* diproline peptides (left) configurations that give rise to PPI and PPII configurations (right). PDB coordinates to model the helices are from [128]. The model was generated using Chimera [129]

Interestingly, Fyn kinase activity is important for production of MyBP by increasing its mRNA transport to the membrane [130] and concomitant transcription levels [130, 131]. From the connection between MyBP, Fyn and the microtubules/actin filaments of the cytoskeleton, it can be speculated that their interaction permits: 1) dynamic membrane remodelling of oligodendrocyte membranes that leads to effective myelination of the nerve axon and 2) the transmission of signals from the myelin membrane down through the cytoplasm to the nucleus, where the transcription of myelin development-related genes can be controlled.

1.6.5 Relationship between MyBP and U24

The presence of U24 in myelin, with its identical region to MyBP, PRTPPPS, may understandably interfere with MyBP functioning and/or stability on the basis of this similarity. Myelination is a spatially and temporally sensitive process of events dependent on MyBP, so U24 interference with posttranslational modifications on MyBP such as phosphorylation and protein-protein interactions with Fyn tyrosine kinase via its SH3 domain may significantly hinder the myelination process. Figure 1.12 is a theoretical model of U24 protein based on primary sequence, and experimental evidence of its behaviour as a membrane protein[132].

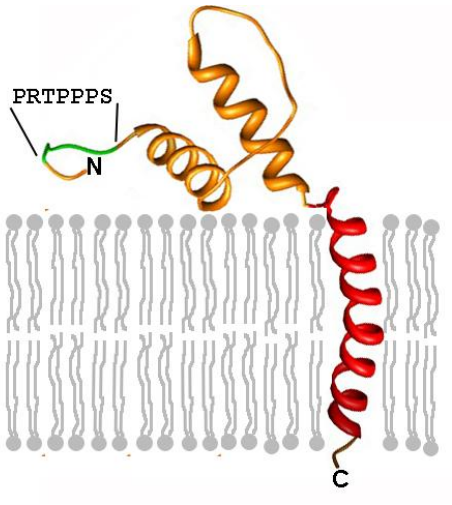

Figure 1.12 Theoretical model of U24 embedded in a membrane generated using I-TASSER[133] and visualized using Chimera[129]. Illustrated in green is the putative polyproline signaling region / region shared with MyBP. In red is the transmembrane helix domain (residues 57-79) [132].

Together with knowledge of how U24 functions *in vivo*, and what we know about the polyproline domain it shares with MyBP, we may also develop a better understanding about not only how U24 relates to MS but also how U24 contributes to the fitness of the HHV-6 virus from which it is expressed.

1.7 Human Herpesvirus type-6

Human Herpesvirus type-6 was first isolated from AIDS patients and reported in 1986[134]. There are eight known types of herpesvirus which infect human hosts, and HHV-6 has two closely related but distinct types, HHV-6A and HHV-6B, which are part of the β-herpesviridae subfamily (Figure 1.14). There is 90% nucleotide sequence homology between the two strains [135]. The strains can further be subcategorized [136]: the A strain has U1102 and GS variants, and B strain has Z29 and HST variants. As for protein coding, the genes are very tightly packed with very little non-coding DNA [137]; HHV-6A has 110 open reading frames (ORFs) while HHV-6B has 97 unique genes and a total of 119 ORFs [138]. Over 95% of humans test positive for either HHV-6 strain above the age of two [139]. CD4+ T lymphocytes are preferentially infected, and several diverse cell types (e.g., endothelial cells, epithelial cells, astrocytes, B cells and oligodendrocytes) can also harbor the virus [140]. Complications from HHV-6 are normally only expected in patients who are already chronically immunosuppressed, such as AIDS patients or organ transplant recipients, but that is not always the case. For example, both immunocompetent and immunosuppressed patients have been reported as developing HHV-6-induced encephalitis (inflammation of the brain), confirmed by an excess of HHV-6 DNA detected in the cerebral spinal fluid and acute abnormalities detected by MRI [141].

Since their discovery, HHV-6 strains have been controversially associated [142] with a number of diseases, although concrete evidence to support definitive roles in disease pathology is lacking. HHV-6 early and late transcripts are more highly detected in MS brain lesions [143] compared to normal control patients' brains, and the virus itself is detected in blood of MS patients more frequently than any of the other herpesviruses [141] (Figure 1.13).

Unfortunately, because HHV-6A and -6B are so ubiquitous, it has been difficult to determine whether they are actually the cause of the disease, or just that they are activated after some sort of other deleterious event, by the "bystander effect"[144]. Another confounding element is that much of the literature describes "HHV-6" without differentiating between A&B strains.

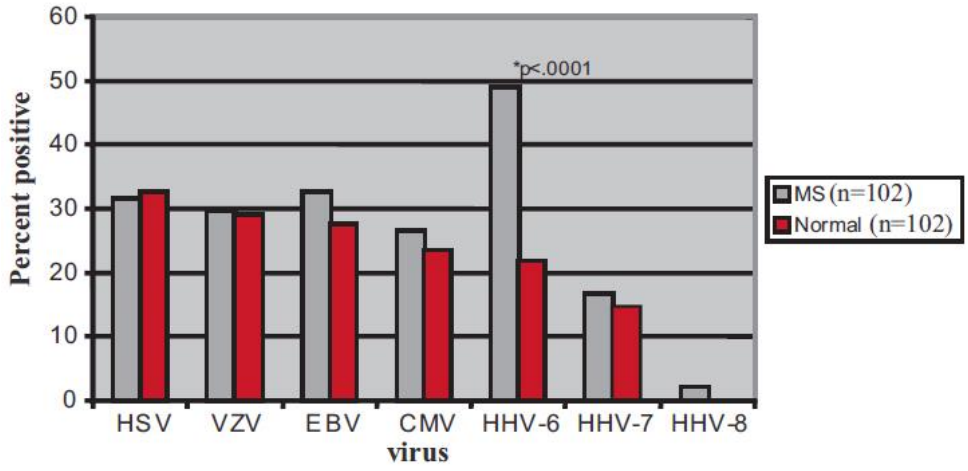

Figure 1.13 Prevalence of herpesvirus DNA in peripheral blood mononuclear cells (from [141]). HSV: Herpes Simplex Virus; VZV: Varicella Zoster Virus; EBV: Epstein-Barr Virus; CMV: Cytomegalovirus; HHV: Human Herpesvirus. The presence of HHV-6 DNA is more than double in MS patients compared to normal individuals

The primary mode of transmission of HHV-6 strains is believed to be through saliva, but approximately 1 % of transmission in the United States occurs vertically, directly from parent to child in the form of chromosomal integration (CI-HHV6) [140]. HHV-6A was found to specifically integrate into host chromosome telomere regions in both *in vitro* and *in vivo* tests [145]. Because CI-HHV6 is ubiquitously found in every cell of the body, a high level of HHV-6

found in the blood may erroneously suggest active infection, even though the virus is actually in a latent state[146].

While there is no antiviral medication approved for treatment of HHV-6 infection, certain drugs used for treatment of Human Cytomegalovirus (CMV) have been somewhat effective in treating HHV-6-related complications in immunocompromised patients [147].

1.7.1 HHV-6A

HHV-6A is considered more neurotropic than HHV-6B. While no disease is currently associated with HHV-6A, there have been strong suggestions that this strain of HHV-6 may act at least as an accessory to trigger or exacerbate certain diseases. For example, HHV-6A was suggested to act in cooperation with HIV to accelerate the progression of AIDS[146]. Recently active HHV-6A (not -6B) was suggested to be the cause of syncytial giant-cell hepatitis that developed in a liver-transplant recipient[148].

HHV-6A virus particles could be purified from 10 % of MS patients[149]. HHV-6A is highly associated with host ligands such as CD46. CD46 is required for virus entry into the cell [70], and CD46 expression is upregulated in 80% of MS patients. HHV-6A (but not -6B) [90] displays an active infection in *in vitro* culture of oligodendrocytes, the cells that make up myelin. Both HHV-6A and -6B exposure can indirectly lead to oligodendrocyte death, with HHV-6A being the more cytotoxic of the two [150].

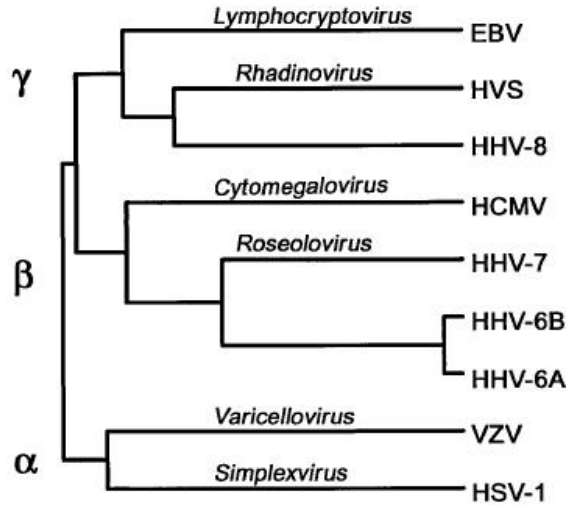

Figure 1.14 Phylogenetic tree of the eight human herpesvirus. HHV-6A, -6B and -7 are all part of the Roseolovirus genus [139]. HVS: Herpesvirus Saimiri; see Figure 1.13 for definition of other abbreviations.

1.7.1.1 MHC2TA link between HHV-6A and MS

Analysis of seemingly benign genetic polymorphisms and correlation to disease is uncovering new associations. For example a -168A to G polymorphism in the type III promoter of the Major Histocompatibility Complex type II transactivator (MHC2TA) is associated with increased susceptibility to rheumatoid arthritis, myocardial infarction and multiple sclerosis [151]. The MHC2TA gene contains over 200 single nucleotide polymorphisms, and the r4774G to C polymorphism, changing a alanine to a glycine, showed a strong correlation in MS patients with HHV-6A [152]. These results were confirmed later when a much larger patient group was studied, and it was noticed that these patients with the r4774G to C polymorphism also had a different clinical behaviour than other MS patients [92].

1.7.2 HHV-6B

HHV-6B is the cause of the childhood illness, *Exanthem Subitum,* also known as *Infantum Roseola* or "sixth disease"[139, 153]. Children normally present with symptoms of a fever and rash, which then usually subside without complication. The virus enters into a latent state, usually only reactivating in chronically immune suppressed individuals, like organ transplant recipients [154]. There are recent studies to suggest that HHV-6B is specifically involved in mesial temporal lobe epilepsy [155, 156].

1.7.3 Immunomodulation Strategies Employed by HHV-6

Many of the proteins encoded by HHV-6 strains are under investigation to elucidate their functional roles in virus structure, replication mechanisms, cell-hijacking machinery and immunomodulatory strategies. The virus has adopted several sophisticated mechanisms by which to evade detection [140] and eradication by the human immune system. HHV-6 encodes an interesting array of different proteins for this purpose, such as U12, U21, U24, U51, U83, and IE1, whose modes of action are all quite different [157-163]. Only U24 will be discussed here.

1.8 Characterization of U24

This section is intended to give an overview about what is known about the U24 protein. When experimental work had begun for this thesis, there was no experimental work reported in peer-reviewed literature about U24 protein, except the report by Tejada-Simon *et al.* indicating that it was potentially immunogenic [88] (Section 1.5.1). Reports soon emerged showing mRNA for U24 could be detected [154, 164], suggesting that the protein was actually being expressed from the ORF in the HHV-6 genome. Microarray experiments performed by Yao *et al.* [164]showed

that U24 mRNA from HHV-6A is expressed after 8 h of a lytic infection in a CD4+ T-cell culture. In a separate report, Yao *et al.* [154] presented data showing that U24 mRNA from HHV-6B was the second most abundant HHV-6 transcript detected in post-mortem brain tissue from a bone-marrow transplant recipient.

U24 protein was introduced in Section 1.5.1 as a molecular mimic of MyBP, possibly triggering an immune response in MS patients on the basis of sequence identity. Ironically, the *in vivo* function of U24, when expressed by CD4+ T-cells was quite the opposite of immunostimulatory: U24 expression was found to be highly immunosuppressive [165]. CD3 (part of the T-cell receptor (TCR) complex) is normally internalized, passing through early to late endosomes. When normally encountering an antigen, the internalized CD3/TCR stimulates activation/proliferation mechanisms inside the cell, before being recycled back to the cell surface. Expression of U24 prevents recycling of CD3 by trapping CD3 in early endosomes and preventing it from entering into late endosomes. T-cells cannot then be properly activated, presumably reducing the level of cytokines released and the ability of the immune system to be locally activated around the infection site. HHV-6A, -6B, and -7 encode functionally similar versions of U24 [132].

1.8.1 U24 Affects Endosomal Recycling

In a screen of candidate genes U4, U21, U24, U61, U78 from the location of the HHV-6A genome [137] coding for host-cell interactions, U24 was identified as being capable of blocking CD3 from recycling back to the cell surface in T-cells [165]. In the presence of expressed U24, CD3ε (a subunit of CD3 receptor) was analyzed for its co-localization with Rab proteins, which are small GTPases used to differentiate between early, mid, late, recycling and sorting

endosomes [166]. Endosomes are lipid vesicles important for intracellular transport of many types of cargo (proteins, mRNA, lipids, etc.). Fluorescence studies of EGFP-U24 fusions showed that U24 caused CD3 to be trapped in Rab4- and Rab5-containing endosomes, where Rab4 and Rab5 are markers of sorting endosomes and early endosomes, respectively[165]. CD3 was not found to be in Rab9 late endosomes or Rab11 recycling endosomes. Unlike U21, which physically binds to MHC I in order to block its endosomal recycling[161], U24 does not appear to colocalize with CD3 [132]. It was confirmed that U24 from HHV-6A, -6B and 7 all exerted the same ability in being able to block endosomal recycling (Figure 1.16), and that U24 also does not appear to affect the recycling of other immune-related receptors that were tested, such as MHC I and CD1d.

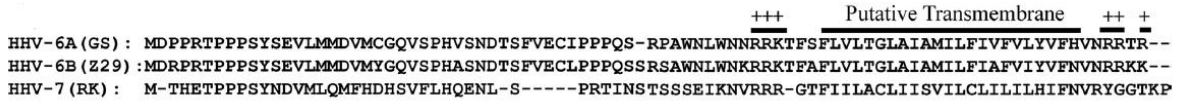

Figure 1.15 Sequences of U24 from HHV-6A (GS Strain), HHV-6B (Z29) strain, and HHV-7 (RK strain). The transmembrane domain is indicated, along with flanking positively- charged residues [132].

Transferrin receptor (TfR) has been extensively studied as a marker of endosomal transport and recycling [167]. To further demonstrate that the activity of U24 interfered with the endosomal recycling pathway, confocal microscopy was done and results showed that U24 expression also prevented TfR from recycling back to the cell surface [132]. The consequence of U24 blockade of CD3/TCR recycling is the time-dependent reduction of CD3/TCR at the cell surface [165]. Ultimately, the lack of the CD3/TCR complexes at the cell surface severely hinders the T-cell's ability to be activated in the presence of an antigen. Using the superantigen, Staphylococcal enterotoxin (SEE), an activator of T-cells, it was shown that cells expressing U24

had a much lower level of CD69, a marker of T-cell activation, compared to control, non-U24 expressing cells [165].

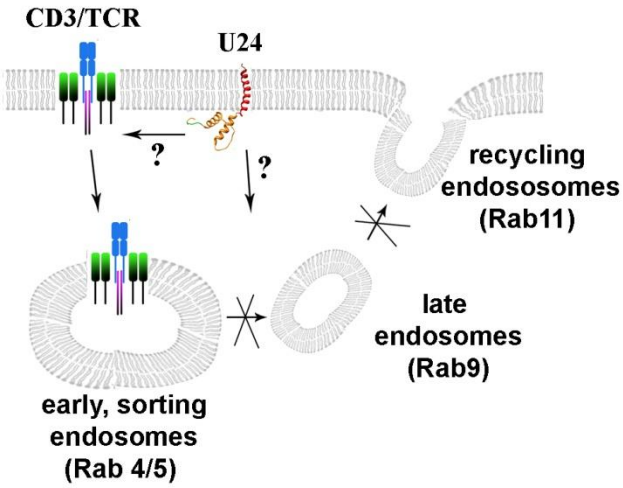

Figure 1.16: Effect of U24 expression on CD3/TCR recycling. U24 causes CD3 to be sequestered to early (Rab5) and sorting (Rab4) and preventing the CD3/TCR from being recycled back to the cell surface [165].

These results agree with previous findings, for example, where Lusso *et al.* reported that patients with HHV-6 infection had less CD3 expressed at the surface of actively infected T-cells[168]. In addition, CD3 subunit transcripts were found to be downregulated in cells infected by HHV-6 [169]. CD3-deficiency is apparently a common feature of HHV-6 infected cells [170, 171].

While the U24 protein appears to be unique to HHV-6A, -6B and -7, other herpesviruses have the ability to modulate immune receptor signalling. The LMP2A protein from Epstein-Barr virus (HHV-4) blocks B-cell receptor signalling by blocking downstream tyrosine kinases [172]. Karposi's sarcoma-associated herpesvirus (HHV-8) can also block B-cell receptor signalling by

expression of K1 protein, which specifically inhibits the transport of the receptor to the cell surface [173]. Also, Herpesvirus saimiri, a gammaherpesvirus of New World monkeys, encodes Tip, a protein that downregulates TCR and CD4 coreceptor signalling through targeting of Lck tyrosine kinase into lysosomes for degradation [174].

1.8.2 Posttranslational Potential of U24

The U24 from HHV-6A is 87 amino acids, -6B is 88 amino acids and -7 is 82 amino acids for a predicted MW of ~ 9-10 kDa each (Figure 1.15). Despite U24 having only a predicted mass of ~10 kDa as judged from its primary sequence, U24 from HHV-6A was observed as a doublet at around 20 and 23 kDa on SDS-PAGE when expressed in T-cells. These results suggest that U24 is potentially heavily modified by post-translational modification[132]. N-glycosylation may be one contributing factor to the mass increase, as U24 from HHV-6A & -6B have a single characteristic N-glycosylation motif[175]: NX(T/S); U24 from HHV-7 has two sites. Doubling in mass may also be an indication that the protein forms detergent-resistant dimers. In a screen to determine residues critical to the activity of U24, it was noticed that while certain mutations had no effect on activity, they had an effect on the amounts of each of the doublet bands that were detected in SDS-PAGE [132]. No *in vivo* post-translational modifications have yet been confirmed, but there is the possibility of phosphorylation by MAPK; phosphorylation may also retard the movement of the protein through the gel. In Section 1.8.4.2, the possibility of U24 interacting with a ubiquitin ligase is discussed, and therefore U24 may also be ubiquitinated (~8.5 kDa per ubiquitin molecule).

1.8.3 Evidence of U24 as a Transmembrane Protein

TMHMM v2.0 software analysis [176] of U24 from HHV-6A predicts that the protein has a transmembrane helix domain between residues 57 and 79. To confirm that this hydrophobic patch was indeed a transmembrane segment, alkaline carbonate extraction was used to verify that U24 expressed in T-cells is membrane-embedded [165].

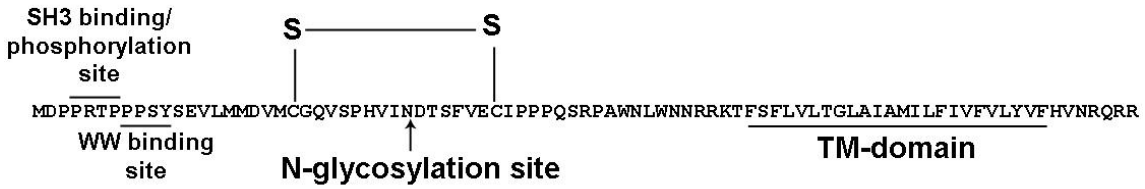

Figure 1.17 Primary sequence of U24 from HHV-6A (U1102 strain), with several potential features indicated: transmembrane (TM) domain, N-glycosylation motif (NX(T/S)), intramolecular disulfide bond, SH3 binding site motif (PXXP), phosphorylation motif (PX(S/T)P), and WW binding site motif (PPXY).

1.8.4 Features Critical to U24 Activity

The amino acid sequence of U24 from HHV-6A is 84% identical to its counterpart in HHV-6B, and only shares 28% identity with U24 from HHV-7, yet all three proteins exhibit the same type of activity in blocking endosomal recycling[132]. In an effort to determine common features of U24 that are critical to the protein's mode of action, mutational analysis was systematically carried out.

1.8.4.1 Basic Residues Flanking the Transmembrane Domain of U24

U24 has its transmembrane domain located close to its C-terminus, classifying U24 as a tail-anchor (TA) protein[177]. A unique feature of TA-proteins is that their transmembrane

domains are usually flanked by stretches of basic residues (lysine/arginine) [178]. These positively-charged amino acids help guide the TA-protein to insert into the membrane of its preferred cellular destination, such as endoplasmic reticulum, peroxisomes, or mitochondrial outer membrane. The TM domain of U24 from HHV-6A is flanked by three positively-charged residues on either side (Figure 1.15). While removal of the three positively-charged residues at the carboxy-side had no effect on the activity of U24, mutation of the three at the amino side abolished all of U24's ability to downregulate CD3 [132].

1.8.4.2 PPXY Domain

At the N-terminus of U24 there is a proline-rich region, and this is the same region shared with MyBP (Figure 1.7, Section 1.5). Two main domains classes known to bind to polyproline regions are SH3 domains and WW domains [118]. SH3 domains primarily bind a PXXP consensus sequence (where X is any amino acid) while WW domains bind a PPXY sequence. Both MyBP and U24 share an identical potential SH3 binding site [119], yet U24 has a putative WW binding site directly C-terminal to the SH3 binding site, and the sequence is PPSY (Figure 1.18). PPXY motifs recruit WW domain-containing proteins such as E3 ubiquitin ligases for a diverse array of cellular processes, such as facilitation of viral budding [179], sodium channel ENaC stability [180] and TGF-β signalling [181]. Post-translational addition of ubiquitin to proteins normally signals a protein for transport to lysosomes, where the ubiquitinated protein is then degraded.

Mutation of either of the two prolines or the tyrosine to alanine within the PPSY motif of U24 abolished the activity of U24, suggesting that U24 requires recruitment of a WW domain containing protein for proper functioning[132]. Sullivan and Coscoy alluded to having carried out

a screen for potential WW domain binding partners for U24 and found that U24 is quite promiscuous in binding several WW domains [132], but a specific WW domain-containing protein required for U24 activity has not yet been identified.

The polyproline region of U24 has a high sequence identity to the β- and γ-subunits of the epithelial sodium channel, ENaC. Through these polyproline domains, ENaC activity is regulated by binding to WW domains of Nedd4 ubiquitin ligase [182]. In Liddle's Syndrome, mutational removal of WW binding domains in ENaC prevents proper Nedd4 (an E3 ubiquitin ligase) binding and results in hypertension. It was found that Erk2 MAPK binds to and phosphorylates the serine/threonine directly preceding the PPXY domain in ENaC subunits (Figure 1.18). This phosphorylation enhances the ENaC binding strength to Nedd4 by several fold [183]. Since U24 has this positional threonine, and its identical counterpart in MyBP is a known *in vivo* and *in vitro* MAPK target [184], it is reasonable to consider that U24 may also undergo a similar phosphorylation event [185] in order to modulate its binding affinity to WW domains.

$U24_{4-11}$	PRTPPPSY
MBP_{96-102}	PRTPPPSQ
Human ENaC$\gamma_{621-628}$	PGTPPPKY
Frog ENaC$\gamma_{621-628}$	PRTPPPKY

Figure 1.18 Protein fragments of similar sequence that can be phosphorylated by Erk2 MAPK (phospho-threonine site underlined). U24 and ENaC segments have the PPXY motif for binding WW domain proteins such as Nedd4 ubiquitin ligase; ENaC binding to Nedd4 is enhanced by phosphorylation.

1.8.5 U24 as Part of a Newly Discovered Membrane Protein Translocation System (TRC40/ASNA-1)

TA-proteins have a hydrophobic single transmembrane pass segment near their C-terminus, which causes a tendency for the newly synthesized proteins to aggregate. To cope with this problem, eukaryotic cells have evolved mechanisms by which to avoid TA-protein aggregation and to efficiently insert the TA-proteins into their target membranes [178, 186]. A unique pathway by which a subset of TA-proteins is inserted into membranes was recently discovered in mammalian cells, which requires the ATPase Asna-1, also known as the Transmembrane Recognition Complex (TRC) 40 [187, 188]. U24 was also found to require Asna-1/TRC40 for U24's proper functioning[132], although it is still unclear if Asna-1/TRC40 acts directly on U24 or on some other yet unknown protein essential to U24 activity.

As the cytosol of the mammalian cell is a crowded place, the Bat3 protein complex helps guide newly synthesized TA-protein to Asna-1/TRC40[189]. Asna-1/TRC40 appears to be an essential cofactor for membrane insertion of some TA-proteins such as RAMP4 and Sec61β, but not a requirement for others, such as cytochrome b5[187]. RAMP4 has been used as a primary model to investigate Asna-1/TRC40 function. RAMP4 forms large complexes with Asna-1/TRC40 (~400 and 700 kDa) and requires ATP hydrolysis in order for the cargo to be delivered [187, 188]. The mechanism of insertion also appears to be redox sensitive, as N-ethylmaleimide (NEM), a modifier of free-thiols, was able to block insertion [187]. Also, there appears to be some yet-unknown protein factor at the membrane that is trypsin-sensitive, which is essential for extricating the TA-protein from its complex and inserting it into the lipid bilayer of the membrane. Get3 is a yeast homolog of Asna-1, and requires Get1 and Get2 proteins for inserting some TA-proteins into the endoplasmic reticulum membrane [190]. Since the crystal

structure of Get3 is known [191], structure/function studies [192] are thus permitting a greater understanding of TA-proteins which are utilizing the Get3- or Ansa-1/TRC40-dependent insertion mechanisms.

Exploitation of the tail-insertion properties of Ansa-1/TRC40 in connection with immune signalling may be a common feature in Herpesviruses and other viruses as well. Cytotoxic T-cells play an important role in protecting against viral infection, and recognize viral peptides that have been internally processed and are presented at the cell surface by Human Leukocyte Antigen (HLA) Class I molecules. Viral peptides are processed in the cytoplasm and are transported to the endoplasmic reticulum by TAP protein, where they are loaded onto HLA Class I complexes. BNLF2a is a small, 60 amino acid TA-protein encoded by the Epstein-Barr virus (HHV-4) and expression of BNLF2a inhibits TAP[193]. TAP inhibition hampers the loading of viral peptides onto the HLA complex, and cells expressing BNLF2a consequently avoid recognition by cytotoxic T-cells. BNLF2a, like U24, requires Asna-1/TRC40 for activity, and a better understanding of Asna-1/TRC40 may in turn help in combatting these virally-encoded immunoevasive proteins.

1.8.6 U24 and Endosomal Recycling: a Hypothetical Mechanism for MS

U24 expression-induced blockade of endosomal trafficking has been shown to occur in two different cell types tested, T-cells and endothelial cells [132]. It is yet unknown in what other cell types U24 may exert its effects. HHV-6 has been shown to infect oligodendrocytes which make up the myelin sheath [90], and myelin proteins in oligodendrocytes have been shown to recycle in a manner similar to transferrin [194] (recall that TfR recycling is blocked by U24). This recycling is important for myelin remodelling. Therefore, it is plausible that U24 may

block endosomal recycling in oligodendrocytes, ultimately resulting in a dysfunction in myelin dynamics - as one observes in MS pathology.

Recently, it was shown how mutations in the SH3TC2 gene block endosomal recycling and give rise to PNS demyelination as a form of Charcot-Marie-Tooth disease [195, 196]. This would appear to be the first reported link between endosomal recycling and a demyelinating disease. SH3TC2 is an effector of Rab11 through an uncharacterized binding site. Blocking this protein-protein interaction in turn blocks endosomal transport and leads to subsequent demyelination. Transcription of genes that are involved with the initiation and progression of myelination are also downregulated.

The possibility of endosomal transport dysfunction as an underlying cause of demyelination in the PNS and CNS is currently being explored. While not suggesting that U24 and SH3TC2 interact with each other, it is nevertheless tempting to consider that U24 may interact directly or indirectly with an unknown effector of Rab proteins as a way to block endosomal trafficking. SH3TC2 has two SH3 domains and its binding partners have not yet been identified, and it is unknown what role these SH3 domains play. U24 has a putative SH3-binding domain whose identical sequence in myelin basic protein has been shown to bind a number of SH3 domains [119], such as Fyn tyrosine kinase, a kinase involved in myelin maintenance. While this SH3-binding segment does not appear to be essential to U24 activity [132], it is intriguing to consider the possible signalling role that SH3-mediated interactions might have in this context.

1.9 Aim of the Dissertation

There are many examples in the literature of membrane proteins of biological interest being isolated in sufficient yields for biophysical study. However, obtaining a high quantity and quality of each new protein represents a great technical challenge. The motivation for developing methods to obtain pure U24 is fuelled by the desire to understand its function and ultimately block activity if it so relates to a devastating disease such as MS. With protein in hand, U24 can be comparatively studied on the basis of its polyproline region identical to MyBP – a region now being recognized for its diverse cellular-signalling roles. Figure 1.19 is a conceptualized cartoon scheme of how U24 may interrupt the normal functioning of MyBP.

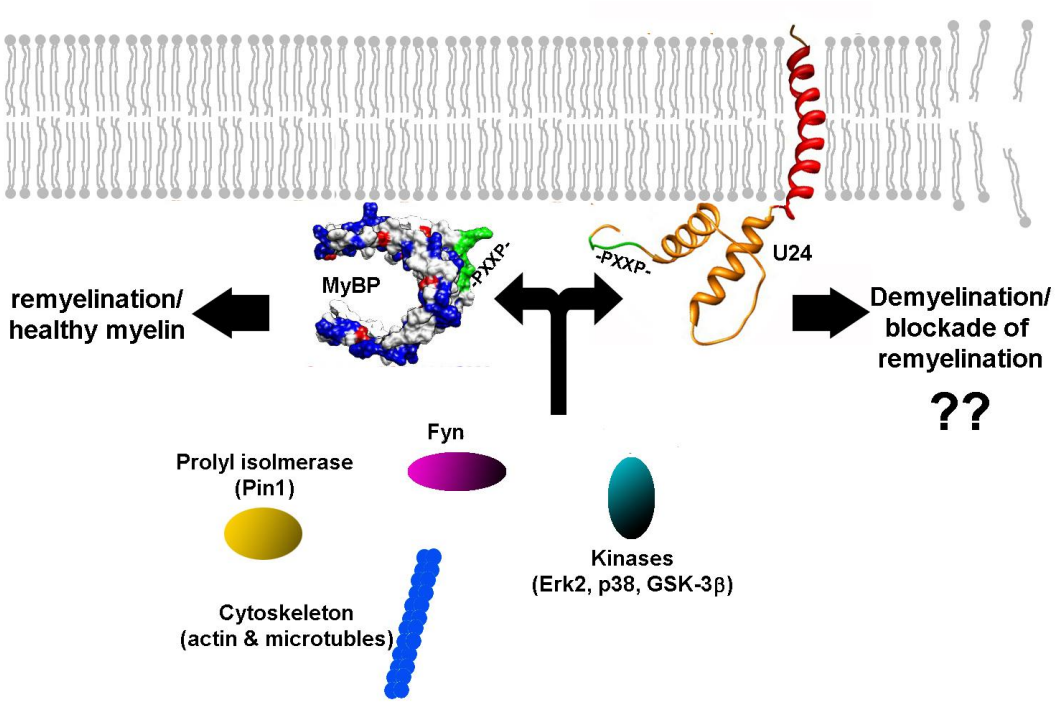

Figure 1.19 Scheme of U24 involvement in the myelin sheath maintenance: a possible binding competition for PXXP domains (PRTPPPS in MyBP and U24), involving essential interactions with kinases (e.g., Erk2, p38 MAPK, GSK-3β), Fyn, and cytoskeleton (e.g., microtubules and actin filaments) and possibly, prolyl isomerases (e.g., Pin1).

Through the work presented in this thesis, I have set out to accomplish two main goals:

1) Develop methods to obtain milligram quantities of high-quality U24 protein
2) Determine how U24 can act as both a functional and structural mimic of MyBP on the basis of:
    a. Being a phosphorylation target of MAPK
    b. Binding to the SH3 domain of Fyn tyrosine kinase
    c. Immunogenicity (ability to cause disease in animals)
    d. Specific structural motifs (PPII helix, secondary/tertiary structure determined by CD, NMR, etc.)

While my work focuses on probing the possible relationship between U24 and MS, it should be noted that by making U24 available, it opens up the potential for many more studies on the protein than could have been done here. The polyproline region of U24 was recently shown by others to be essential for U24`s ability in modulating immunodetection [132, 165]. The work presented here and elsewhere in the future will further define the role that the protein plays in viral infection and/or multiple sclerosis certainly by highlighting the importance of this polyproline domain.

Chapter 2: Method Development for Obtaining Recombinant U24[†]

2.1 Introduction

Chapter 1 provided the rationale for studying the U24 protein within the context of multiple sclerosis. Structure/function studies of membranes proteins of biological interest such as U24 however has historically been a difficult task, primarily because of the limited amount of material available [197]. Proteins extracted from natural sources can also have a backdrop of post-translational modifications such as glycosylation, phosphorylation, etc., thereby precluding any meaningful structural study of the heterogeneous pool of protein. It was demonstrated that U24 appeared to have extensive post-translational modifications if expressed in human cells, consistently giving molecular weights of 20 and 23 kDa by SDS-PAGE [198], which is more than double the mass predicted by the primary sequence. Heterologous expression of U24 in a prokaryotic system such as *E. coli* therefore represents a cost-effective and relatively easy way to obtain large yields of homogeneous membrane proteins where post-translational modifications can be added subsequently in a controlled manner.

Protein fusion tags have a direct bearing on expression levels, solubility and/or can make purification more efficient. Typical fusion tags used include glutathione-S-transferase (GST) [199], maltose binding protein (MBP) [200] and hexahistidine (6×His) [201], tags amongst many others. Since no single bacterial strain or fusion tag has been shown to work in all cases for membrane proteins, the trial-and-error task of discovering which selection will work to produce enough pure protein for study can be quite daunting [202].

[†] A version of this chapter has been published: "Tait, A.R., Straus, S.K., Overexpression and purification of U24 from Human Herpesvirus Type-6 in E. coli: unconventional use of oxidizing environments with a maltose binding protein-hexahistine dual tag to enhance membrane protein yield. *Microbial Cell Factories* 2011, 10:51".

Combining the solubility-enhancing chaperone ability of MBP [200, 203] with the high affinity of a polyhistidine tag (≥ 6 consecutive histidines) for efficient protein expression and purification is not a recent development [204], but has seen a recent revival in the context of high-throughput protein production [205]. Even so, the combinatorial use of MBP and 6×His tags is only beginning to be extensively explored with membrane proteins. For instance, Korepanova *et al.* demonstrated that this system could enable a 70% success rate in expressing 16 of 22 integral membrane proteins from *Mycobacterium tuberculosis* in the cytoplasm of *E. coli,* proteins which would otherwise be unobtainable due to poor or undetectable expression levels [206].

MBP contains a signal sequence and thus naturally resides in the periplasm of *E. coli*, yet if the signal sequence is deleted, MBP remains in the cytoplasm. Consequently, an added benefit of using MBP as a fusion tag is that one can generally choose the location within the *E. coli* where the expressed protein resides: either in the cytoplasm or periplasm [205]. While the most common approach is to express fusion proteins in the cytoplasm [205], because the yield is generally higher than those expressed in the periplasm, there may still be valid reasons why the expression of a protein of interest should be directed to the periplasm. For instance, the guinea pig sigma-1 receptor, when engineered as a fusion to the MBP-6×His dual tag, could only be expressed as a periplasmic-directed fusion protein [207]. In this case, it was hypothesized that the receptor portion becomes stably embedded in the *E. coli* membrane as a result of the periplasmic transport process. This hypothesis is consistent with what was observed for the expression of the aquaporin Z membrane protein as a periplasmic MBP fusion, where 200 mg/L of protein were obtained, but was not found to be secreted out into the periplasmic space [208].

If there are cysteines in the primary sequence of protein and their oxidation state is unknown, as is the case with U24, it can be beneficial to express the protein in the oxidizing

environment of the periplasm [209] or use an oxidizing strain of *E. coli* [210]. It is generally accepted that disulfide bonds cannot be formed in the cytoplasm of *E. coli* unless strains such as Origami (Novagen), which are defective in reductases (*(Δtrx/Δgor)* are used. More recently however, it was shown that disruption of reducing pathways in *E. coli* was not absolutely essential to obtain disulfide bonded protein in the cytoplasm [211, 212]. Introduction of the sulfhydryl oxidase Erv1p into a native reducing cytoplasm was used to achieve greater yields of disulfide bonded protein than with reductase-deficient strains alone.

Interestingly, MBP may help promote correct disulfide bond formation in fused proteins. Planson *et al.* [213] showed that C-terminal fragment of *Plasmodium falciparum* merozoite surface protein 1 was misfolded and formed disulfide linked polymers when expressed untagged in the periplasm, but was a correctly folded monomer with six intramolecular disulfides when expressed fused to MBP. This result clearly demonstrates the potential that MBP has for introducing correct disulfide bonding into globular proteins, a property which would be important in membrane proteins as well.

2.2 Results

2.2.1 Cloning and Expression

Oligonucleotide fragments representing the U24 gene (Table 2.1) were synthesized and the full-length gene was obtained by overlap PCR, before being cloned into three expression vectors: pMAL-c2x, pMAL-p2x and pGEX-4T3 (Figure 2.1). Vectors pMAL-c2x and pMAL-p2x direct the MBP-6×His-U24 fusion protein to the *E. coli* cytoplasm and periplasm, respectively. The pGEX vector encodes a GST-U24 fusion to be expressed in the cytoplasm.

Table 2.1 Synthetic primer and oligonucleotide sequences used to construct plasmids expressing MBP-6×His-U24 (pMAL-p2x and pMAL-c2x) and GST-U24 (pGEX-U24). Primer sequences used for amplifying or sequencing the cloned insert are also listed.

Vector Target	Primers 5'→3'	Oligonucleotides 5'→3'
pMAL-c2x or pMAL-p2x	**1ThU24-P1** GAATTCGGATCCCATCATC **Primer 2** GTTCCACGCCGGACGGGACTG **Primer 3** CAGTCCCGTCCGGCGTGGAAC **4ThU24-P4** GTGCCAAGCTTGCGACTAACG **pMal-seq (sequencing)** GGTCGTCAGACTGTCGATGAAGCC **pMal-seqrv (sequencing)** CGCCAGGGTTTTCCCAGTCACGAC	**1ThU24-O1** GAATTCGGATCCCATCATCATCATCATCACAGCAGCGGCCTGGTGCCGCGCGGCAGCATGGACCCGCCGCGTACCCCGCCACCGTCTTACTCCGAAGTTCTGATGATGGACGTTATGTGCGG **Oligo 2** GTTCCACGCCGGACGGGACTGCGGTGGCGGGATACATTCAACGAAGGAGGTGTCGTTGATAACGTGCGGGGAAACCTGACCGCACATAACGTCCATCATC **Oligo 3** CAGTCCCGTCCGGCGTGGAACCTGTGGAACAACCGTCGCAAAACCTTCTCCTTCCTGGTTCTGACTGGTCTGGCTATCGCTATGATCC **4ThU24-O1** GTGCCAAGCTTGCGACTAACGACGCTGGCGGTTAACGTGGAAAACGTACAGAACGAAAACGATGAACAGGATCATAGCGATAGCCAG
pGEX-4T3	**GSTU24-P1** CCGCGTGGATCCATGGACC **Primer 2** (SEE ABOVE) **Primer 3** (SEE ABOVE) **GSTU24-P4** GGCCGCTCGAGCTAACGACG **pGEX 3' (sequencing)** CCGGGAGTGCATGTGTCAGAGG **pGEX 5' (sequencing)** GGGCTGGCAAGCCACGTTTGGTG	**GSTU24-O1** CCGCGTGGATCCATGGACCCGCCGCGTACCCCGCCACCGTCTTACTCCGAAGTTCTGATGATGGACGTTATGTGCGG **Oligo 2** **(**SEE ABOVE**)** **Oligo 3** (SEE ABOVE) **GSTU24-O4** GGCCGCTCGAGCTAACGACGCTGGCGGTTAACGTGGAAAACGTACAGAACGAAAACGATGAACAGGATCATAGCGATAGCCAG

A)

BamHI

```
gaattcggatcccatcatcatcatcatcacagcagcggcctggtgccgcgcggcagcatg
 E  F  G  S  H  H  H  H  H  H  S  S  G  L  V  P  R↑G  S  M
                                                Thrombin

gacccgccgcgtaccccgccaccgtcttactccgaagttctgatgatggacgttatgtgc
 D  P  P  R  T  P  P  P  S  Y  S  E  V  L  M  M  D  V  M  C

ggtcaggtttccccgcacgttatcaacgacacctccttcgttgaatgtatcccgccaccg
 G  Q  V  S  P  H  V  I  N  D  T  S  F  V  E  C  I  P  P  P

cagtcccgtccggcgtggaacctgtggaacaaccgtcgcaaaaccttctccttcctggtt
 Q  S  R  P  A  W  N  L  W  N  N  R  R  K  T  F  S  F  L  V

ctgactggtctggctatcgctatgatcctgttcatcgttttcgttctgtacgttttccac
 L  T  G  L  A  I  A  M  I  L  F  I  V  F  V  L  Y  V  F  H
                              HindIII
gttaaccgccagcgtcgttagtcgcaagcttggcac
 V  N  R  Q  R  R stop
```

B)

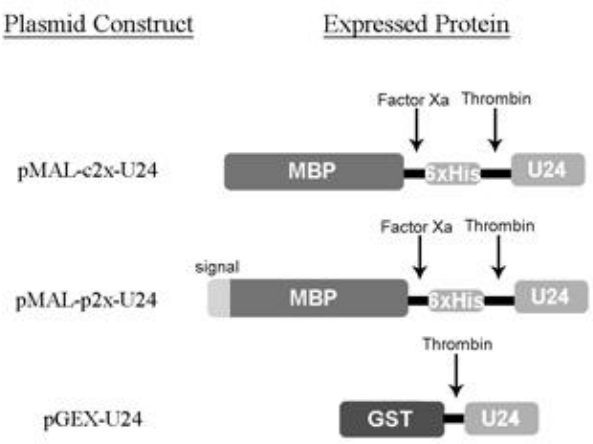

Figure 2.1 U24 codon-optimized gene, amino acid sequence and graphical representation of expressed protein constructs. A) *Bam*HI/*Hin*dIII cut sites are indicated and used to clone the PCR-amplified duplex DNA into the corresponding sites of pMAL-p2x and pMAL-c2x vectors, from which the MBP-6×His-U24 fusion protein is expressed. The U24 gene was designed to be preceded by a hexahistidine tag (6×His) and LVPRGS thrombin cleavage site (indicated by an arrow). The pGEX construct sequence is not shown, but save for the flanking regions that include *Bam*HI/*Xho*I restriction site, the U24 gene sequence itself is essentially identical; note that there is no 6×His tag and the thrombin cutsite is vector-encoded in pGEX. For all three vectors, final thrombin-cleaved and purified U24 protein should leave an additional two amino acids (Gly-Ser) at the N-terminus. B) Cartoon representation of expressed protein. There is signal sequence at the N-terminus of the protein expressed by pMAL-p2x-U24, directing expression to the periplasm. The Factor Xa cleavage site is vector-encoded in the pMAL systems.

The commercially available *E. coli* cell strains that were chosen for expression were XL1-Blue (Stratagene), BL21(DE3) (Stratagene), C41(DE3) (Lucigen), Origami 2 (Novagen), SHuffle (New England Biolabs). Expression of pGEX-U24 was only attempted in the latter three strains. The C41(DE3) strain [214] is a derivative of the commonly used BL21(DE3) strain which allows high expression yields of membrane proteins by reducing their toxicity to the host [215]. Origami 2 is deficient in the glutathione and thioredoxin reductases (Δ*trx*/Δ*gor*) and therefore provides an oxidizing environment conducive to disulfide bond formation. SHuffle is deficient in the same reductases, but expresses a signal-truncated disulfide bond isomerase (DsbC) in the cytoplasm. Normally found in the periplasm, DsbC rearranges incorrect disulfide bonds [216] and can also act as a chaperone to assist in the proper folding of proteins that do not require disulfide bonds [209].

The GST-U24 fusion protein was very poorly expressed in any of the three cell strains attempted, at either high or low temperature (Figure 2.2). Comparing pre- and post- induced cells by SDS-PAGE and Coomassie Blue staining, one expects a highly prominent band to appear in the post-induction samples, to indicate overexpression of the desired protein. Only a faint band presumed to be that of GST-U24 was observed. While many parameters could be adjusted, further attempts to enhance expression of GST-U24 were abandoned in favor of the more promising MBP system.

Initial attempts to express MBP-6×His-U24 in the cytoplasm of various cell lines at 37°C yielded high amounts of the target protein that had been truncated (Figure 2.3 C&D, indicated by lower arrow). This truncation product could be purified by Ni^{2+} affinity chromatography, indicating that the truncation likely occurs C-terminus to the 6×His; MALDI-ToF confirmed that

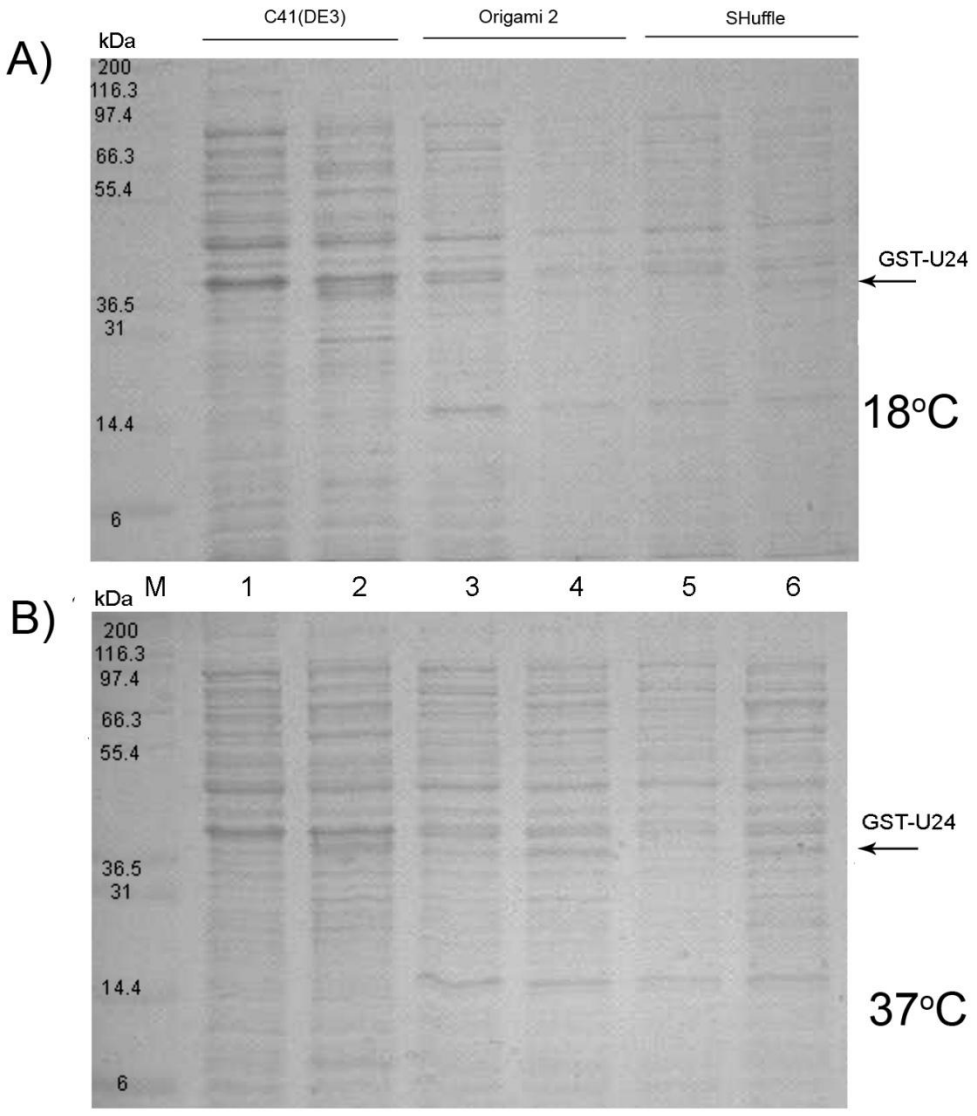

Figure 2.2 Expression of GST-U24 in C41(DE3), Origami 2 and SHuffle *E. coli*. Pre-induction samples are in the even-numbered lanes, post-induction in the odd-numbered. Faint banding may indicate some GST-U24 protein is expressed (arrow), but lack of a singular prominent band suggests that expression is poor.

the mass of the isolated protein was ~9 kDa less than expected for full-length MBP-6×His-U24 (55 kDa) (see Appendix A). Of the numerous parameters tested, lowering the induction temperature to 18°C appeared to have the greatest effect on alleviating the problem of protein

truncation, yet the expression of full-length protein was still poor (Figure 2.3 A&B, indicated by arrow). When expression of MBP-6×His- U24 was directed to the periplasm, low levels of full-length protein could be observed at either 18°C or 37°C, but a substantial increase in yield of the full-length protein was observed for C41(DE3), especially over either the XL1 Blue or BL21(DE3) strains. It is unclear why C41(DE3) should fare any better than its parent strain

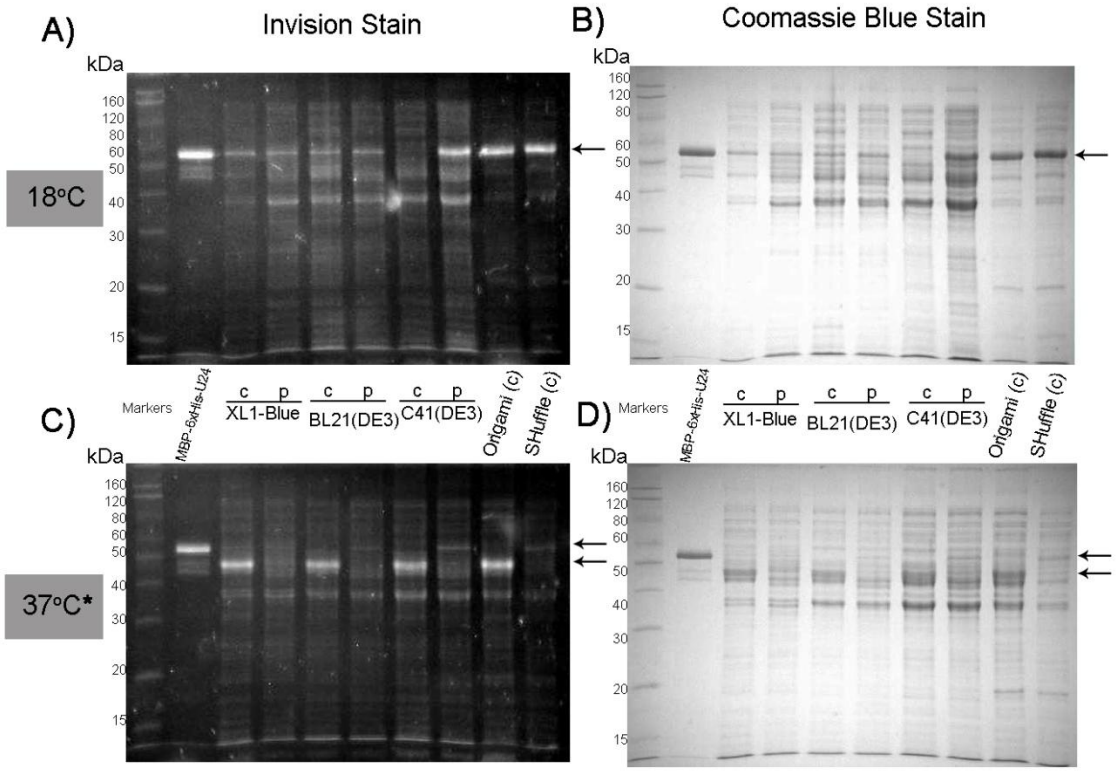

Figure 2.3 Comparison of MBP-6×His-U24 expression in various *E. coli* strains, at low (18°C) and high temperature (37°C*). Cultures induced at 18°C (A&B) and 37°C* (C&D) and visualized with His-tag-specific Invision stain (A&C) and Coomassie Blue stain (B&D). Cytoplasmic and periplasmic expressions are denoted by c and p, respectively. While at high temperature (C&D) MBP-6×His-U24 appears degraded (c lanes) or poorly expressed (p lanes), optimal expression conditions are observed at low temperature especially in the periplasm of C41(DE3), and cytoplasm of Origami 2 and SHuffle. (*)SHuffle was grown at 30°C, as per vendor's recommendations, perhaps explaining why at this lower temperature some trace full length MBP-6×His-U24 is observed. Position of full-length MBP-6×His-U24 (right of the marker lane) is denoted by arrows in A&B, upper arrow in C&D (lower arrows point to truncated/degraded protein).

BL21(DE3), since C41(DE3) is presumed to only enhance protein production from a T7-based promoter [215]; here a P_{tac} promoter was used.

We were prompted to question whether it was specifically an oxidizing environment like the periplasm that had a positive effect on expression levels. When MBP-6×His-U24 was expressed in the oxidizing cytoplasm of Origami 2 and SHuffle, higher expression was observed in these strains over the reducing cytoplasm of the other strains tested. Low temperature was still critical for the generation of full-length protein. The presence of DsbC in the SHuffle strain did not enhance the apparent protein yield over Origami 2 cells. Since MBP has no cysteines, these findings suggest that the oxidation state of the cysteines in U24 may have an effect on expression levels. The chaperone-like qualities of the MBP moiety may help protect the U24 passenger protein against proteolysis under oxidative conditions and low temperature, enabling optimal conditions for folding and possible disulfide-formation. An alternative factor for increased yields is that degrading proteases are either inactive or absent under the oxidizing, low-temperature expression conditions that were tested.

2.2.2 Purification and Isolation of U24

The MBP-6×His-U24 fusion protein expressed in the C41(DE3) periplasm, Origami 2 and SHuffle cytoplasm at low temperature were extracted in soluble form and purified by Ni^{2+}-affinity (Histrap) chromatography. Fractional analysis by SDS-PAGE for C41(DE3) and Origami 2 purifications are shown in Figure 2.4. Optimization of imidazole concentration to 45 mM in the intermediate wash step was found to be necessary to remove impurities that otherwise would remain through the subsequent steps of the purification. After dialysis and digestion by thrombin, U24 was liberated from MBP-6×His and further purified to homogeneity by applying

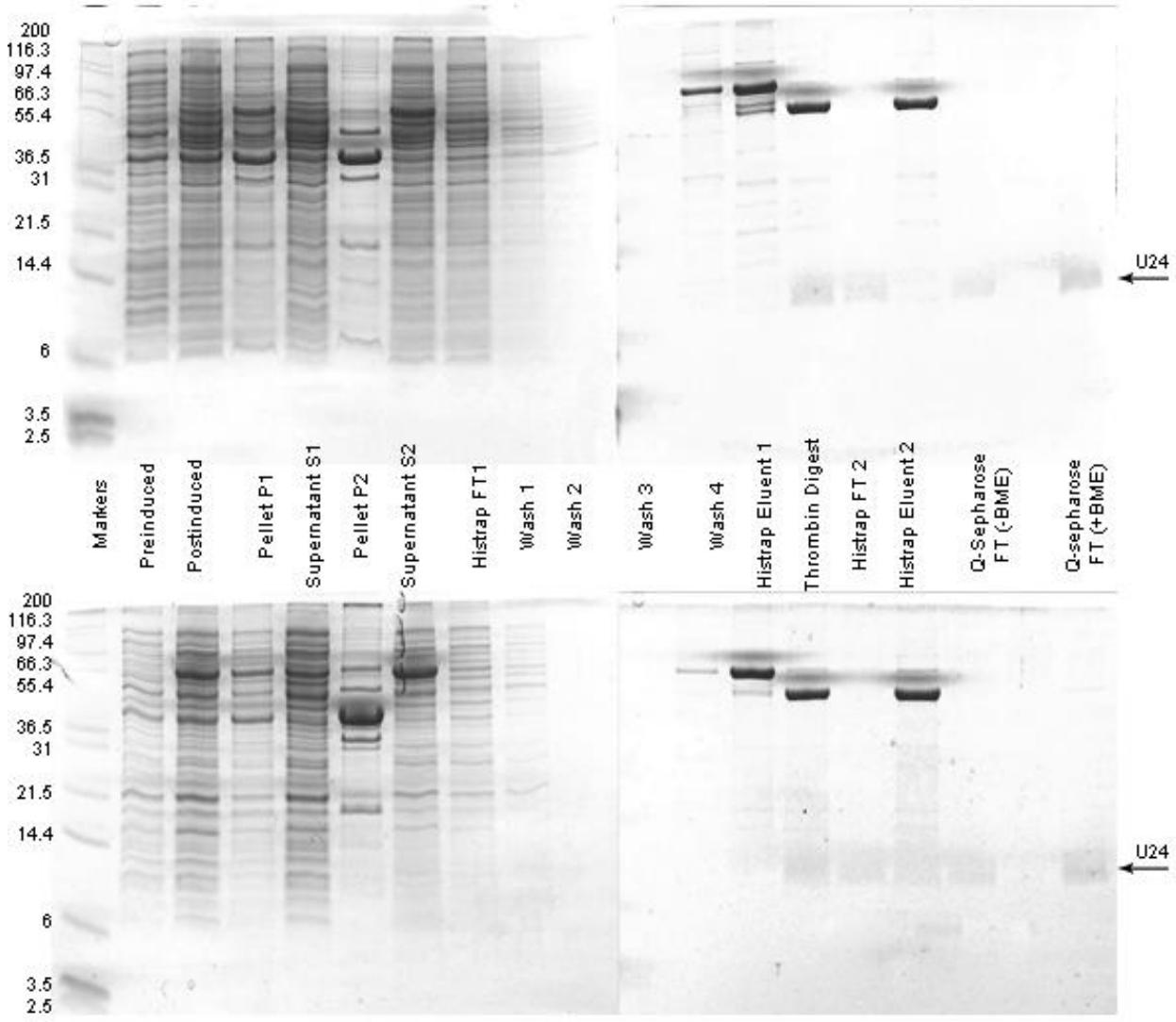

Figure 2.4 SDS-PAGE of fractions collected during the course of U24 purification from C41(DE3) cells (top) and Origami 2 cells (bottom). Preinduced: preinduced cell pellet; Postinduced: cell pellet after induction with IPTG; Pellet P1: pellet collected after lysis and centrigation; Supernatant S1: supernatant collect after lysis and centrifugation; Pellet P2: pellet collected after buffer containing 1% Triton X-100 added, mixed and centrifuged; Supernatant S2: the corresponding supernatant; Histrap FT1: flowthrough from the Ni^{2+} affinity column; Wash 1-3: samples from 50 mL of column wash; Wash 4: column wash sample containing 45 mM imidazole; Histrap Eluent 1: eluted MBP-6×His-U24 from Ni^{2+} affinity column; Thrombin digest: dialyzed MBP-6×His-U24 treated with thrombin protease; Histrap FT2: Column flowthrough from digested protein reapplied to Ni^{2+} affinity column; Histrap Eluent 2: eluted MBP-6×His from column; Q-sepharose FT – BME): U24 isolated from Q-sepharose anion-exchange, without β-mercaptoethanol added; Q-sepharose FT + BME): same as previous with β-mercaptoethanol added.

Table 2.2 Expression summary and purification yields for cultures grown at 18°C. Results are based on the intensity of expected bands observed by SDS-PAGE and by the BCA assay. U24 was purified as described from the indicated strains grown in 4 × 1L of LB (or M9), induced at 18°C. N/A: Not applicable. Concentration is the mean ± s.d. of n = 4-6 independent assay measurements.

Vector	Expressed protein	Cellular location	C41(DE3) *E. coli* isolated U24 (mg /L)	Origami 2 *E. coli* isolated U24 (mg /L)	Shuffle *E. coli* isolated U24 (mg /L)
pMAL-c2x	MBP-6×His-U24	Cytoplasm	N/A	1.84 ± 0.31	1.60 ± 0.24
pMAL-p2x	MBP-6×His-U24	Periplasm	0.46 ± 0.27 2.81 ± 0.32 (M9)	N/A	N/A

the digest mixture to tandem Histrap and Q-sepharose columns, and collecting U24 in the flowthrough. Because of the high theoretical isoelectric point of U24 (pI = 9.38), use of the Q-sepharose at neutral pH acted as a final polishing step to capture residual impurities while allowing U24 to be isolated in the flowthrough. The U24 protein that had been purified from the three *E. coli* strains ran as a monomer under both reducing and non-reducing conditions, indicating that U24 does not form significant amounts of disulfide-linked polymers (Figure 2.8), although some trace amounts of what is presumed to be a U24 dimer was observed under some conditions. The dimer disappears upon addition of reducing agent. Since our recombinant form of U24 runs at ~10 kDa by SDS-PAGE, we conclude that we have avoided the unknown post-translational modifications which cause U24 to run as a doublet of 20 and 23 kDa when expressed from human cells. Highest yields of U24 were from C41(DE3) grown in M9 minimal

media. Pryor *et al.* [204] suggested that use of minimal media reduces the levels of endogenous *E. coli* proteases which cleave the sensitive region between the MBP-6×His tag and protein of interest.

2.2.3 Secondary Structure Analysis of Purified U24 by CD Spectroscopy

In order to determine whether the strains used have an impact on secondary structure of the purified protein, we investigated the structure of the purified U24 obtained above in the presence of membrane-mimetic SDS detergent, using circular dichroism (CD) (

Figure 2.7). U24 was found to be highly α-helical under all conditions tested (Table 2.3). The relative proportions of secondary structure components (α-helix, β-sheet, etc.), as determined by fitting the spectra in

Figure 2.7 using the programs CONTILL, SELCON3, and CDSSTR [217] remain highly similar in the presence and absence of tris(2-carboxyethyl)phosphine (TCEP) reducing agent.

2.2.4 Disulfide Analysis

MALDI-TOF MS was used to analyze purified U24 obtained from the three *E. coli* strains representing the highest overexpressed proteins levels, confirming that U24 existed in a monomeric form of expected molecular mass (experimental = 10,235 Da ± 0.2% [218]). When the cysteine modifying reageant N-ethylmaleimide (NEM) (Figure 2.5) was added alone, no increase in mass was observed. NEM cannot directly react with disulfide-bonded cysteines. If a reducing agent is added such as TCEP, the cysteine disulfide in U24 is broken, and then the mass shift attributed to both cysteine thiols being modified by NEM could be observed (+250 m/z) (Figure 2.9 A&C). These results are the same for U24 samples obtained from all strains tested. To

further confirm the presence of the disulfide between Cys21-Cys37, a sample of U24 from SHuffle was subjected to GluC protease digestion in the presence and absence of reducing agents, and the resulting peptide fragments were analyzed by MALDI-TOF MS and SDS-PAGE (Figure 2.9 B&C).

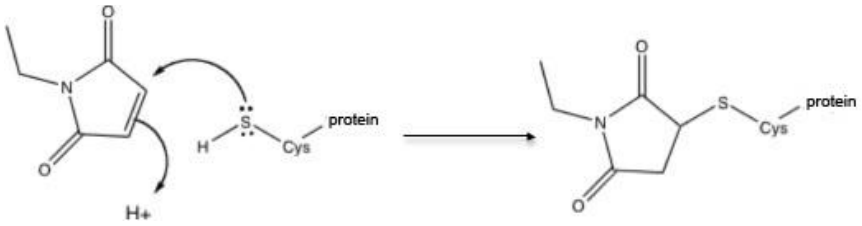

Figure 2.5 Mechanism of NEM modification of protein free-thiol groups of cysteine.

2.2.5 Analysis of Cys-free U24 to Determine the Effects of the Disulfide on Protein Expression

After confirming that our recombinant U24 forms an intramolecular disulfide bond, another objective was to see if formation of this bond directly contributed to the stability of the expressed full-length MBP-6×His-U24. When Cys-free C21SC37S mutant U24 plasmids were expressed under ideal periplasmic and cytoplasmic conditions (pMAL-p2x-U24 in C41(DE3) and pMAL-c2x-U24 in Origami 2) in LB media, we observed a similar trend in expression as compared to wild-type by SDS-PAGE (Figure 2.10). Removal of the disulfide bond had no apparent effect on the ability to produce full-length MBP-6×His-U24, neither promoting degradation at low-temperature nor enhancing yield of full-length fusion protein at high temperature.

2.2.6 Comparison of Cellular Mass Yields

We observed a trend in the amount of protein-expressing cells from large scale preparations of U24, where pMAL-p2x-U24 is expressed in C41(DE3) and pMAL-c2x-U24 in Origami 2. Despite C41(DE3) being grown in nutrient-limiting M9 media, these cells regularly accumulated to a much higher final mass than Origami 2, which were grown in nutrient-rich LB media. In our hands, Origami 2 cells expressing MBP-6×His-U24 grew so slowly in M9 media that further attempts with this combination were not attempted. It is clear that Origami 2 cells experience extreme metabolic strain compared to other strains like C41(DE3). However, with high yields of U24 protein isolated Origami 2 (Table 2.2) with low background of other endogenous *E. coli* proteins (Figure 2.3 A&B), we hypothesize that the unique metabolism of oxidizing strains like Origami 2 may favor production of recombinant protein while minimizing expression of proteases and other factors which lower the expression of full-length protein.

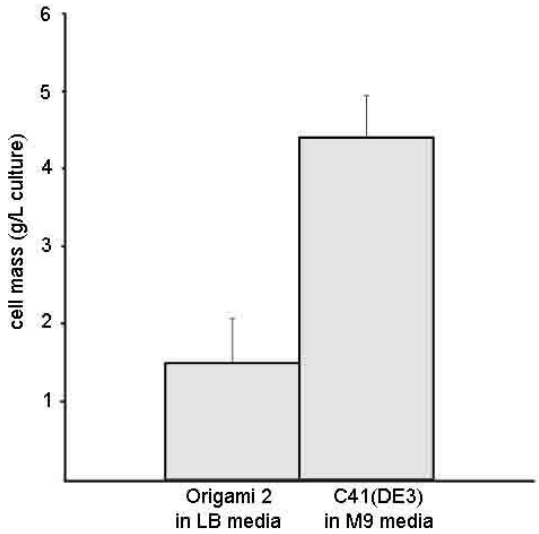

Figure 2.6 Mass of isolated cells expressing MBP-6×His-U24. Cell masses which correspond to highest yields of protein are notably different between the cell types; although grown in rich LB media, Origami 2 cells (pMAL-c2x-U24) are consistently ~3× lower in mass than C41(DE3) (pMAL-p2x-U24), which is grown in M9 minimal media. Data is based on mean ± s.d. for n=4-5 batches of cells isolated from 4×1L of culture, expressed 18°C overnight.

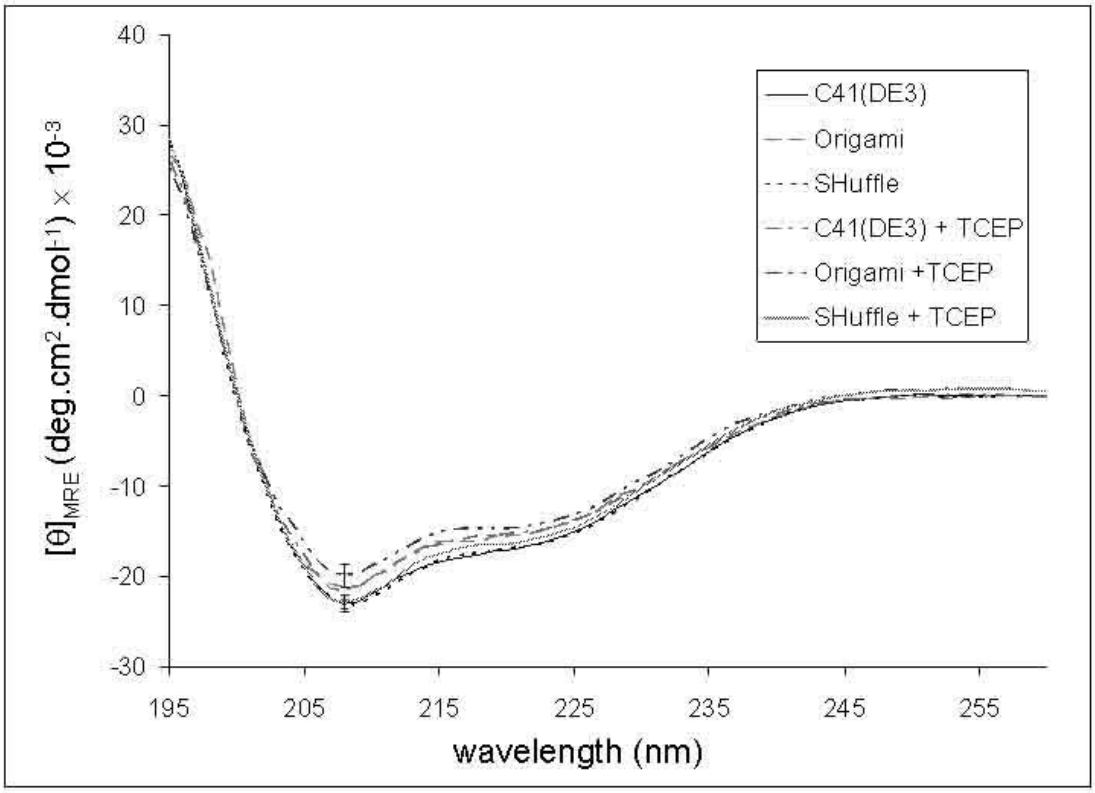

Figure 2.7 Far-UV CD spectra of U24 obtained from the different cell strains used in this study. U24 protein that had been isolated from various *E. coli* cell strains was reconstituted in 10 mM Tris·HCl, 10 mM NaCl, 10 mM SDS, pH 7.5 and far-UV CD was run in the presence and absence of TCEP reducing agent. Concentration of protein in the samples were determined by BCA assay to be $[U24]_{C41(DE3)} = 0.106 \pm 0.004$ mg/mL, $[U24]_{Origami} = 0.093 \pm 0.006$ mg/mL, and $[U24]_{SHuffle} = 0.118 \pm 0.004$ mg/mL, where the standard deviation is based on four independent assay measurements.

Table 2.3 Secondary structure analysis of purified U24 by CD spectroscopy. [a]U24 protein that had been isolated from various *E. coli* cell strains was reconstituted in 10 mM Tris·HCl, 10 mM NaCl, 10 mM SDS, pH 7.5 and far-UV CD was run (260-195 nm) in the presence and absence of TCEP reducing agent. [b]Fractions of secondary structure were determined by combining the software analysis results of the CONTIN/LL, SELCON3 and CDSSTR software [217] using the SMP56 reference data set. Structural classes are given as: α_R, regular α-helix; α_D, distorted α-helix; β_R, regular β-strand; β_D, distorted β-strand; T, turns; U, unordered. [c]Normalized Root-Mean-Square Deviation. NRMSD is defined as $\Sigma[(\theta_{exp} - \theta_{cal})^2/(\theta_{exp})^2]^{½}$, summed over all wavelengths, and where θ_{exp} and θ_{cal} are, respectively, the experimental ellipticities and ellipticities of the back-calculated spectra for the derived structure[217, 219]. It is generally accepted[220] that experimental and calculated spectra are in good agreement if NRMSD <0.1, are similar if 0.1 < NMRSD < 0.2, and are in poor agreement if NRMSD > 0.2.

U24 sample[a]	Secondary Structure Fraction[b]						NRMSD[c]
	α_R	α_D	β_R	β_D	T	U	
C41(DE3)	0.412	0.208	0.006	0.032	0.113	0.234	0.150
C41(DE3) + TCEP	0.367	0.212	0.018	0.035	0.127	0.243	0.143
Origami	0.379	0.223	0.023	0.032	0.120	0.222	0.130
Origami + TCEP	0.341	0.201	0.021	0.041	0.134	0.256	0.130
SHuffle	0.411	0.204	0.003	0.03	0.117	0.231	0.156
SHuffle + TCEP	0.401	0.212	0.013	0.032	0.112	0.239	0.147

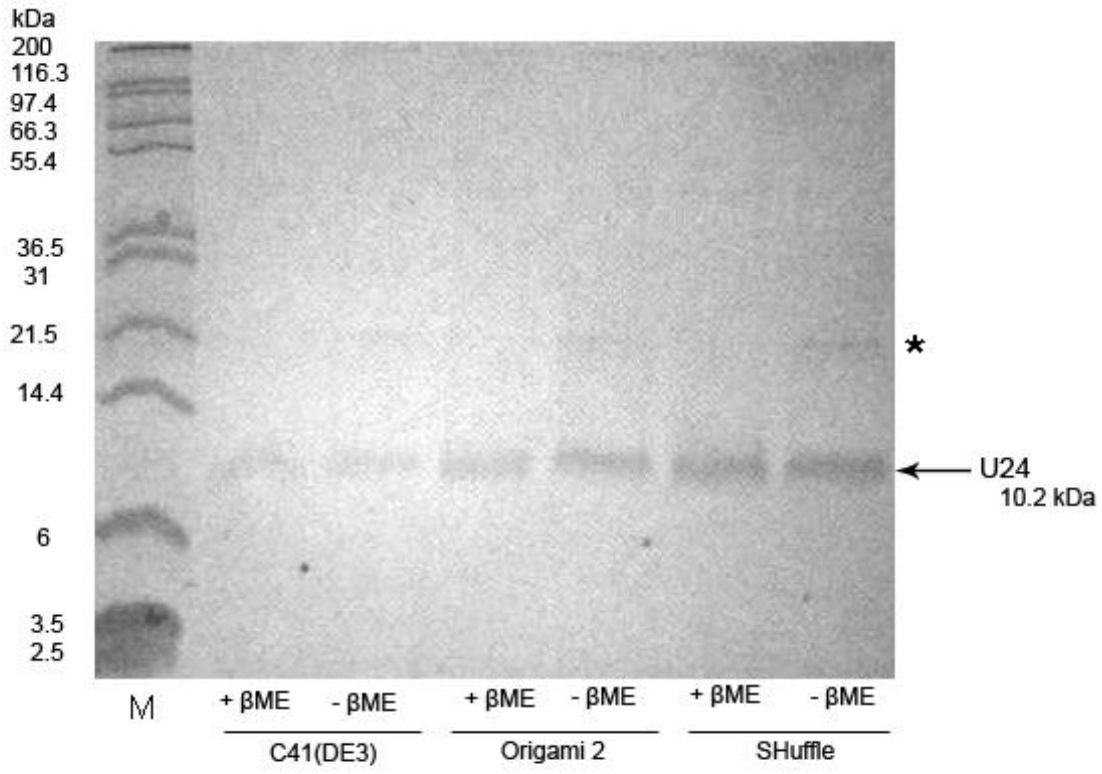

Figure 2.8 SDS-PAGE analysis of U24 purified from C41(DE3), Origami 2 and SHuffle *E. coli*, in the presence and absence of β-mercaptoethanol reducing agent Isolated U24 was from indicated strains, cultured in LB media. Protein solution was mixed 1:1 (vol:vol) with 2X SDS-PAGE buffer ± 2.5 % β-mercaptoethanol (βME) final concentration, and analysis carried out by Tris-Tricine SDS-PAGE. Protein amounts were approximately as follows: $U24_{C41(DE3)}$, 0.1 μg; $U24_{Origami2}$ and $U24_{SHuffle}$, 0.4 μg. M: molecular markers. Arrow points to location of monomeric U24 (10.2 kDa); * : U24 dimer.

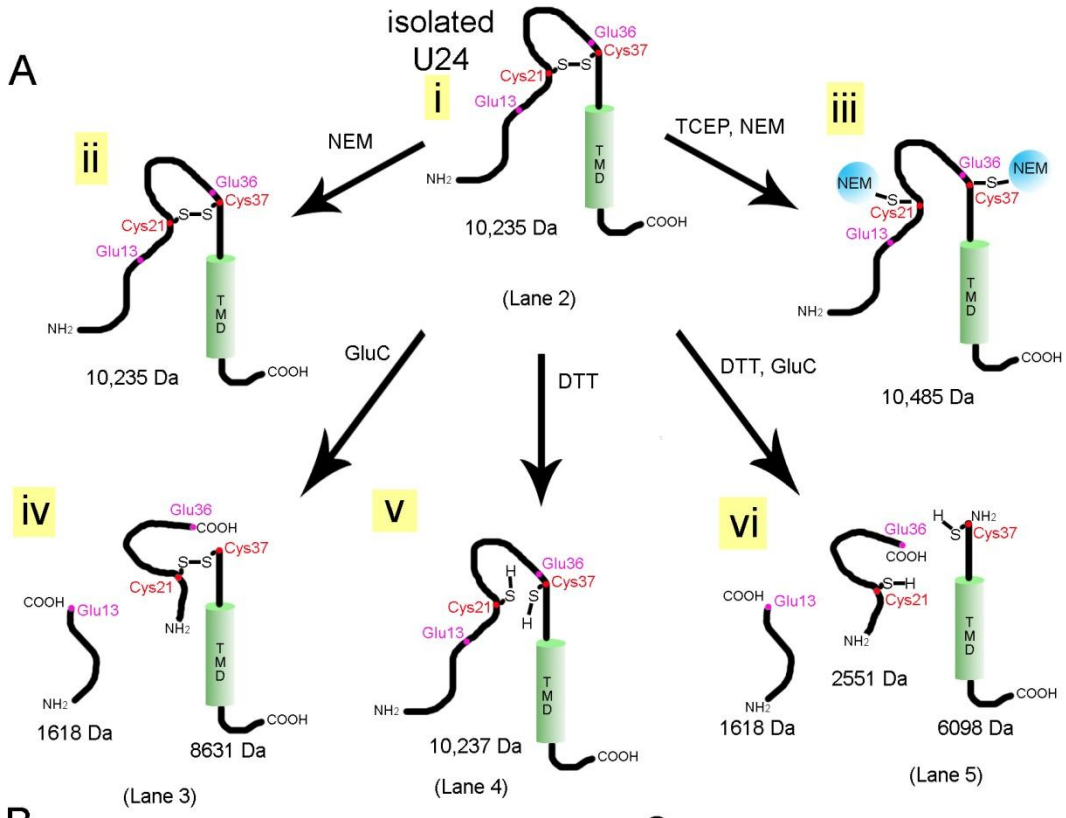

B

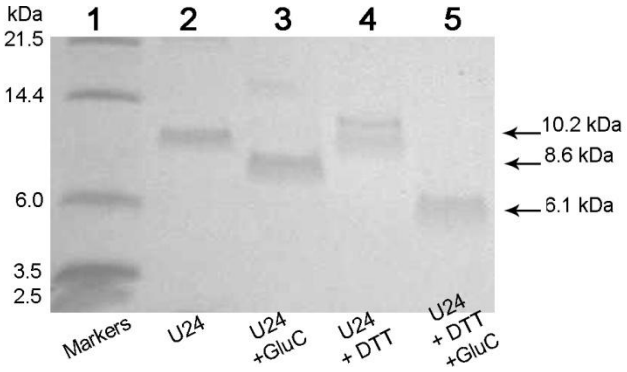

C

	Sample	Theoretical mass (Da)	Detected mass (Da)
i	Isolated U24	10,235	10,232
ii	U24 + TCEP	10,237	10,232
iii	U24 + NEM	10,235	10,241
iv	U24 + TCEP + NEM	10,485	10,492
v	U24 + GluC	1618, 8631	8632
vi	U24 + GluC + DTT	1618; 2551; 6098	2547; 6102

Figure 2.9 Characterization of the disulfide in isolated U24 protein. A) Illustration of isolated U24 protein, demonstrating the formation of a single intramolecular disulfide bond between the only two cysteines in the molecule (i). N-ethylmaleimide (NEM) does not react with the oxidized, disulfide bonded protein (ii) and NEM only modifies cysteines in the reduced form (+125 Da per cysteine) once they are reduced by TCEP (iii). Use of glutamyl endoproteinase (GluC), which cleaves peptide bonds primarily after glutamic acid under these conditions, yielded two fragments if U24 contained an intramolecular disulfide (iv). Using DTT to reduce the disulfide in U24 (v), GluC cleavage then gave three proteolytic fragments for U24 (vi). B) Tris-Tricine SDS-PAGE results of U24 (isolated from SHuffle) ± DTT and GluC-digested. M: molecular markers; oxidized U24 (10.2 kDa, lane 2) shifts to a lower mass once cleaved (lane 3, 8.6 kDa) and U24 reduced by DTT (10.2 kDa, lane 4) shifts to even lower mass when cleaved (6.1 kDa, lane 5). C) MALDI TOF MS analysis of U24 modifed with NEM ± TCEP, and cleaved by GluC ± DTT. Tabulated theoretical masses represent U24 species indicated in A) (i-vi). Experimental masses that were detected are ±0.2% the theoretical mass.

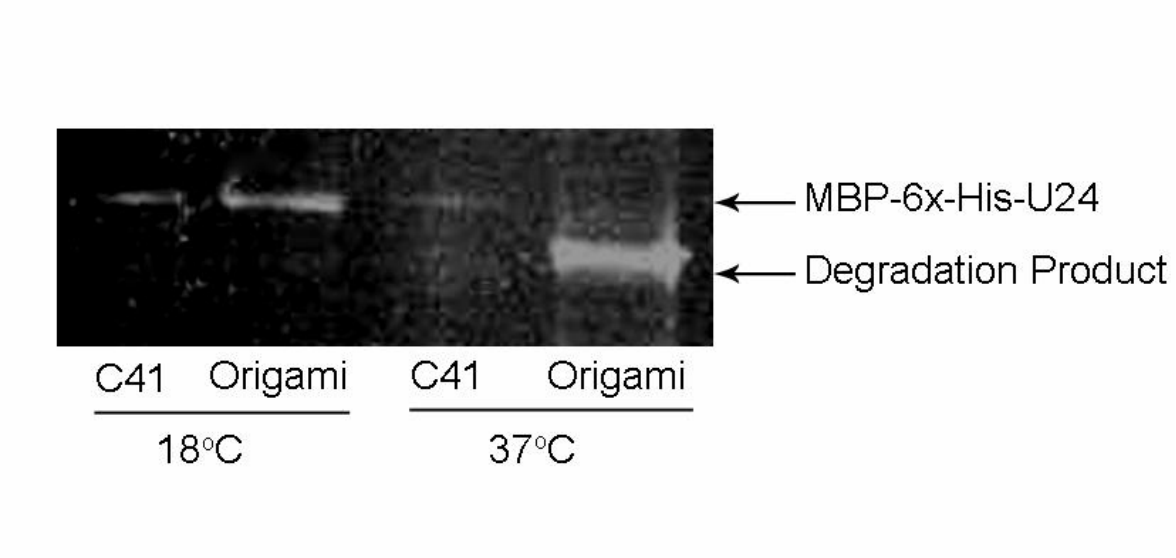

Figure 2.10 Examination of cysteine-free mutant U24 expression. The C21SC37S mutant U24 constructs were expressed: pMAL-p2x-U24 in C41(DE3) and pMAL-c2x-U24 in Origami 2 cells, at 18°C and 37°C. Removal of disulfide bond potential appeared to have no effect on *in vivo* stability of expressed MBP-6×His-U24, which exhibited the same expression characteristics as wild-type.

2.3 Discussion

In the course of expressing and isolating U24, we have shown that membrane protein expression levels can increase when the *E. coli* periplasm or an oxidizing cytoplasm is used in conjunction with the MBP-6×His dual tag, and that highly pure, soluble membrane protein can be readily obtained in good yields (2-3 mg, see Table 2.2). Using this as a model system, we conclude that use of the MBP-6×His tag, together with low temperature, and either the periplasm of C41(DE3) or strains with an oxidizing cytoplasm (Origami 2, SHuffle, etc.) is a worthwhile approach for obtaining other difficult-to-express membrane proteins in *E. coli.* These conditions were also useful for expressing and isolating another naturally cysteine-free membrane protein (unpublished results). In the current work, we have also determined that disulfide bonding of the target protein need not be a prerequisite for full-length expression of U24. Ultimately, we utilize the C41(DE3) in M9 media regime to produce isotopically labeled (e.g., ^{15}N) U24 protein for

NMR experiments, while reserving the Origami 2 in LB approach to routinely produce unlabeled U24 for all other biophysical studies.

While we are capable of forming (and reducing) a disulfide in our recombinant version of U24 from HHV-6A we must consider the fact that the cysteines are not conserved across the U24 proteins from other viruses, HHV-6B and HHV-7. All three versions of U24 have the ability to sequester cellular receptors in early and intermediate endosomes of human cells [198], yet while $U24_{HHV\text{-}6A}$ has two cytoplasmic cysteines, $U24_{HHV\text{-}6B}$ has only one and $U24_{HHV\text{-}7}$ has two which are exclusively located in the transmembrane region (and thus are not likely to form disulfide bonds). We cannot rule out whether these differences can affect the activity of U24 on a more precise level, or somehow are involved in regulatory mechanisms that have yet to be discovered.

The biological relevance of disulfide formation in U24 is clearly open for debate, and further experimentation is needed to determine whether the disulfide is formed *in vivo* or during the course of the subsequent purification scheme. G-protein-coupled receptors (GPCRs) represent one class of membrane proteins that may benefit from improved efficiency in disulfide bonding for stable high-yield expression in *E. coli*. About 30% of all marketed prescription drugs act on GPCRs, and they represent the most successful therapeutic target family [221]. GPCRs have a 7-transmembrane-pass structure and it is predicted that in 78.9% of these receptors, there is a conserved disulfide bond between the 2nd and 3rd extracellular loops [222]. The conserved GPCR disulfide bond is also present in rat neurotensin receptor (NTR1), which has been successfully expressed in *E. coli* but at low levels [223, 224]. In an attempt to create a more thermostable version of NTR1 to facilitate x-ray crystallography structural studies of the protein, 340 point mutations were introduced to NTR1 and expressed in *E. coli* using the aforementioned tags [225]. During the course of that work, it was interestingly discovered that the

only mutations which drastically reduced the overall yield of NTR1 were those made to Cys142 and Cys225, cysteines that form the conserved disulfide bond. Unable to form an essential disulfide bond, NTR1 is presumed to be heavily degraded by proteolysis, despite the presence of stabilizing fusion tags.

Using the MBP-6×His tagging system for a membrane protein of interest with a generic expression strain (i.e.: C41(DE3)), one should quickly be able to test both cytoplasmic and periplasmic expression strategies at high and low temperature. If there is the potential to form a disulfide bond in the membrane protein of interest, yet the oxidation state of the cysteines is unknown, one may benefit from using the reductase deficient SHuffle strain. Should the protein not have any disulfides, DsbC in SHuffle may still act as a chaperone to induce proper folding and avoid unwanted disulfide bonds. If co-overexpression of DsbC should fail to induce native disulfide bonding patterns of an MBP-fusion protein, it may be possible to correct disulfide mispairings by an *in vitro* incubation of MBP-fusions with DsbC [226], or by co-expression with the recently characterized sulfhydryl-oxidase, Erv1p [212].

Impaired disulfide bond formation may be but one of several key obstacles in obtaining stable full-length membrane proteins in *E. coli*, especially those from mammalian sources. Polypeptide synthesis is 4-10 times faster in prokaryotes than eukaryotes, and the apparatus by which membrane proteins are inserted into the membrane is different [227]. One approach may be to reduce the rate of synthesis by lowering expression temperature, or to use a weaker promoter. MBP appears superior to most other fusion tags in the literature for both increasing solubility and expression levels, as was consistent with our use of the GST tag as a comparison. Still, improvements in yield can result from using other unique tags [228]. Autoexpression media [206] or novel enzyme-based-substrate delivery media (EnBase [229]) also represents an attractive

approach for increasing both cell mass and protein yield. Still, other advances involve the reduction in toxicity associated with membrane protein overexpression [214, 215]. While these and other trial-and-error optimization techniques may give a modest improvement in membrane protein yield, increasing our mechanistic understanding of prokaryotic systems of membrane protein translation and folding is clearly warranted. Directed evolution studies [230] and genetic analysis of upregulation, downregulation and mutations [231] made to house-keeping genes [232] during membrane protein expression will undoubtedly continue to have an impact on yields of functional membrane proteins in *E. coli.*

2.4 Summary

The work presented in this chapter has demonstrated efficient methods to express and purify milligram quantities of U24 protein from an *E. coli* system. Discovering that strained metabolic conditions such as low temperature and oxidizing cytoplasm can enhance yield may find more global applications to obtaining membrane proteins in the future, where the MBP-6×His tag is also an indispensible tool for enhancing yield, solubility, and facilitating purification. These methods are currently being applied to successfully obtain other membrane proteins in our lab; the methodology may therefore find utility in future membrane isolation projects as well.

With sufficient amounts of protein in hand, we can now embark on an exciting journey into the realm of biophysical structure/function studies of U24, where the activity of U24 in possible disease and virus function can be more fully understood.

2.5 Materials and Methods

2.5.1 Gene Construction

The gene sequence for U24 from HHV-6A was obtained from NCBI [GenBank:**Q69559]**. Oligonucleotide fragments that represent the full-length U24 gene (Table 2.1) and primers were synthesized (Nucleic Acid Protein Service Unit, University of British Columbia), replacing codons which are rare in *E. coli* with ones more frequently used. The codon optimized U24 gene was assembled by overlap PCR for insertion into the pMAL-c2x and pMAL-p2x vectors (New England Biolabs) and also the pGEX-4T3 vector (GE Biosciences). For use with the pMAL-c2x and pMAL-p2x vectors, the amplified gene segment included a *Bam*HI site at the 5' end, followed by a sequence coding a hexahistidine tag followed by a thrombin cleavage site (LVPRGS), then the U24 sequence, followed by an amber stop codon then a *Hin*dIII site at the 3' end. For use with pGEX, the amplified gene segment contained a *Bam*HI site at the 5' end of the U24 sequence, flanked by an amber stop codon and *Xho*I site at the 3' end. DNA fragments were purified by agarose gel electrophoresis and subsequently extracted using a Qiaquick Gel Extraction Kit (Qiagen).

2.5.2 Cloning

The full length duplex DNA fragments obtained above for use in the pMAL vectors were incubated with Taq polymerase, pCR®2.1-TOPO® vector and dATP (all from Invitrogen) and the reaction mixtures were used to transform competent SURE® *E. coli* (Stratagene). The *E. coli* were then plated on Luria Bertani (LB) agar plates containing 50 μg/mL carbenecillin to grow overnight at 37°C. Colonies were selected and subjected to PCR using standard M13 forward and reverse primers to identify which colonies contained the vector with the correct inserted

gene. PCR reactions for colonies which did harbor the gene insert yielded a single band between 500-600 bp when run by agarose gel electrophoresis. These colonies were then grown in 5 mL of LB media with 50 μg/mL carbenecillin overnight and their plasmids were harvested using a QIAprep Spin Miniprep Kit (Qiagen). Isolated plasmid DNA was sent for sequencing (Nucleic Acid Protein Service Unit, University of British Columbia) to confirm that the correct gene sequences were obtained.

The pCR®2.1-TOPO® vectors containing the expected U24 gene inserts were digested by the appropriate endonculeases; *Hin*dIII / *Bam*HI for pMAL vectors, and *Bam*HI / *Xho*I for the pGEX vector. The digested fragments were isolated as previously described, then ligated into the corresponding pre-digested pMAL and pGEX vectors using T4 DNA ligase (Invitrogen). SURE® *E. coli* were transformed with the ligation products the plasmids were isolated and sequenced as before, and designated pGEX-U24, pMAL-c2x-U24 and pMAL-p2x-U24.

2.5.3 Site-directed Mutagenesis

Synthetic primers were purchased (Integrated DNA Technologies) and used according to Quikchange Site Directed Mutagenesis Kit instructions (Stratagene). Vectors pMAL-c2x-U24 and pMAL-p2x-U24 were used as the starting template. To construct the C21S mutant, the primers were 5'-CTGATGATGGACGTTATGTCCGGTCAGGTTTCC-3' and 5'-GGAAACCTGACCGGACATAACGTCCATCATCAG-3', which introduces an Eam1105I-sensitive restriction site. For the C37S mutant, the primers used were 5'-CCTTCGTTGAATCTATTCCGCCACCG-3'and 5'-GGACTGCGGTGGCGGAATAGATTCA-3' and they introduced a *XmnI*-sensitive restriction site. The C21S mutant plasmid was the

starting template for constructing the C21SC37S double mutant. All plasmids were isolated and sequenced as described above for wild-type plasmids.

2.5.4 Small Scale Protein Expression

The expression vector constructs pMAL-c2x-U24 and pMAL-p2x-U24 were used to transform XL1-Blue (Stratagene), BL21(DE3) (Stratagene), (C41(DE3) (Lugicen), Origami 2 (EMD Biosciences) and SHuffle (New England Biolabs) *E. coli* strains. The pGEX-U24 was used to transform C41(DE3), Origami 2 and SHuffle only. Transformed *E. coli* were then plated on LB agar plates containing 50 μg/mL carbenecillin to grow overnight at 37°C (30°C in the case of SHuffle, as per manufacturer's instructions). Single colonies were selected and grown at these temperatures overnight with shaking (225 r.p.m.) in 5 mL of LB, containing 50 μg/mL carbenecillin. Cells were pelleted by centrifugation, then resuspended in 100 mL of fresh medium with antibiotics and again grown for several hours until reaching an OD_{600} = 0.5-1.0. Isopropyl β-D-1-thiogalactopyranoside (IPTG) was added at a final concentration of 0.3 mM and the cells continued to grow for 3 hours at the same temperature (30 or 37°C). For growths carried out at lower temperature, the cultures were cooled in a cold-water bath for 30 minutes before addition of the IPTG, and these cultures were then grown at 18°C for 16-20 hours. All cultures were harvested by centrifugation at 4°C and the cells were stored at -80°C until further use.

2.5.5 Large Scale Protein Expression

Small starter cultures (5 mL) were set up as described for the small scale expression. In this case, the cultures were grown for only three to five hours before one mL of culture was used

to inoculate 100 mL of fresh LB or M9 minimal media containing 100 μg/mL ampicillin. The M9 minimal media was supplemented with 50 μg/mL thiamine. These cultures were grown overnight under the same conditions as the 5 mL cultures described in the section above, and then harvested by centrifugation. Cell pellets were resuspended in 4 × 1L of fresh medium with antibiotics and grown to an OD_{600} = 0.5-1.0. Cultures were cooled in a cold-water bath for 30 minutes before addition of IPTG at a final concentration of 0.3 mM, and they then continued to grow at 18°C for another 16-20 hours. Cultures were harvested by centrifugation at 4°C and the cells were stored at -80°C until further use.

2.5.6 Protein Extraction and Purification

The C41(DE3) cell pellets from 4L of culture, harboring expressed MBP-6×His-U24, were thawed on ice and resuspended in lysis buffer (20 mM Na^+/K^+ phosphate, 0.5 M NaCl, pH 7.4), adding DNase I (Roche) and EDTA-free protease inhibitor cocktail (Sigma). Cells were lysed by three passes through a French press, and the lysate was centrifuged for 90 minutes at 25,000 × *g*, 4°C. The pellet was resuspended in solubilization buffer (20 mM Na^+/K^+ phosphate, 0.5 M NaCl, 1% Triton X-100, 10 mM imidazole, pH 7.4), gently stirred for three hours at 4°C, and again centrifuged for 90 minutes at 25,000 × *g*, 4°C. Since a substantial amount of target protein was found in both the supernatant and pellet of Origami 2 and SHuffle cells treated with lysis buffer, the lysis buffer step was generally omitted and these cells were resuspended directly into solubilization buffer with protease inhibitor cocktail prior to being lysed by French press. Supernatants were filtered through a 45 μm filter and loaded on a 5 mL Histrap HP column (GE Biosciences) equilibrated with wash buffer (20 mM Na^+/K^+ phosphate, 0.5 M NaCl, 0.5% Triton

X-100, 10 mM imidazole, pH 7.4). The column was washed with 30 column volumes of wash buffer. The imidazole concentration of the wash buffer was raised to 45 mM, and the column was further washed with another 10 column volumes. The MBP-6×His-U24 protein was eluted from the column in 25 mL of elution buffer (20 mM Na^+/K^+ phosphate, 0.5 M NaCl, 0.5% Triton X-100, 500 mM imidazole, pH 7.4) and dialyzed overnight at 4°C against 1 L of dialysis buffer (20 mM Na^+/K^+ phosphate, 62.5 mM NaCl, 0.5 % Triton X-100) using a dialysis membrane with MWCO of 1000 (Spectrum Laboratories).

Dialyzed solution containing the MBP-6×His-U24 was transferred to a 50 mL polypropylene tube, and 50 units of bovine thrombin (GE Healthcare) were added. The digest was carried out for 48 hours at ambient temperature.

The digest solution was filtered through a 45 μm filter and re-loaded on a 5 mL Histrap HP column equilibrated with dialysis buffer. U24 was collected in the flowthrough, while MBP-6×His and any undigested MBP-6×His-U24 were eluted with elution buffer. To remove the thrombin and any trace contaminants that remained, U24 solution was loaded on a 5 mL Q-Sepharose column (GE Biosciences) equilibrated with dialysis buffer, and pure U24 was collected in the flowthrough. Purity was assessed by MALDI-TOF mass spectrometry and SDS-PAGE, and protein concentration was measured with the bicinchoninic acid (BCA) assay (Pierce).

The U24 protein isolated from SHuffle *E. coli* was dialyzed overnight at 4°C against 50 mM Tris·HCl, 100 mM NaCl, pH 7.5 with a 1,000 MWCO membrane. *Staphylococcus aureus* Protease V8 (GluC, from New England Biolabs) was dissolved in deionized water to a concentration of 0.1 μg/mL then mixed with U24 (1:17 w/w), ± 20 mM DTT, and incubated for two hours at 25°C. Reactions were quenched by addition of trichloroacetic acid (TCA) at a final

concentration of 20% (w/v). Pellets were collected by centrifugation and washed twice with ice-cold acetone, then air dried.

2.5.7 Far-UV Circular Dichroism

Protein stock solutions of U24 were precipitated by addition of TCA, 10 % (w/v), and collected by centrifugation. The protein pellets were then washed with two additions of ice-cold acetone, vortexing and centrifugation. After acetone was removed and the sample air-dried, the protein was reconstituted in 10 mM Tris·HCl, 10 mM NaCl, 10 mM SDS, pH 7.5 +/- 0.5 mM tris(2-carboxyethyl)phosphine (TCEP) with an estimated final protein concentration of 0.11 mg/mL. Protein solutions were sonicated in a water bath until the protein was completely dissolved, then centrifuged briefly to ensure the removal of any particulate matter. Final protein concentrations of the samples were determined by BCA assay.

Spectra were recorded with a J-810 spectropolarimeter flushed with nitrogen gas. Using a cell with a path length of 0.1 cm and a sample compartment that was thermostated to 20°C, samples were scanned at a rate of 50 nm/min with a step size of 1 nm. Spectra were averaged over three scans and corrected for background by subtracting the scans of buffer without protein.

2.5.8 SDS-PAGE Analysis of Protein Expression

Cell pellets from 0.5 mL of culture were mixed with 50µl 2× Novex dye (Invitrogen) supplemented with 5% β-mercaptoethanol and 50µl of 50% glycerol, vortexed and heated at 95°C for 5 minutes. Mark12 molecular weight markers (Invitrogen) and a 5 µl volume of each prepared sample were loaded on a 13% acrylamide gel and run by Tris-Glycine SDS-PAGE. The initial voltage was set to 50 V for one hour, and 100 V for the remainder of the run until the

dye front reached the bottom of the gel. Gels were stained with a Coomassie Blue-G250 solution for 1 hour and destained with 50% methanol / 10% acetic or deionized water alone. For Invision staining, the gels were treated according to manufacturer's instructions (Invitrogen).

Purified U24 samples were mixed with equal volumes of 2× Novex dye that contained 5% β-mercaptoethanol and then were heated to 95°C for 5 minutes. Samples used in the GluC digest experiment were not heated prior to loading on the gel, and only those that were previously exposed to DTT contained 2.5% β-mercaptoethanol. Gels were run, stained and destained as before, with the exception that a Tris-Tricine gel buffer was used in order to resolve the lower molecular weight proteins and peptides.

2.5.9 NEM Modification

U24 protein isolated from C41(DE3), Origami 2 and SHuffle *E. coli* strains were dialyzed overnight at 4°C against 50 mM Tris·HCl, 100 mM NaCl, pH 7.5 with a 1000 MWCO membrane. N-ethylmaleimide (NEM) was dissolved in the same buffer and diluted to 4 mM. TCEP was dissolved separately in this buffer to a concentration of 20 mM and the pH was made slightly basic by addition of NaOH before diluting further to a TCEP concentration of 2 mM. Samples of U24 were mixed 1:1 (v/v) with TCEP solution (+ TCEP samples) or with buffer (- TCEP samples) and incubated for 10 minutes at 37°C. These samples were then mixed 1:1 (vol:vol) with NEM solution (+ NEM samples) or buffer (- NEM samples) and incubated in the dark for 30 minutes at room temperature. Reactions were quenched by addition of trichloroacetic acid (TCA) to a final concentration of 20% (w/v). Pellets were collected by centrifugation and washed twice with ice-cold acetone, and then air dried.

2.5.10 MALDI-TOF Mass Spectrometry

Protein samples were dissolved in 50% acetonitrile with 0.1% trifluoroacetic acid. The matrix, sinapinic acid, was dissolved in the same solvent to a concentration of 10 mg/mL. The matrix was spotted on the MALDI target plate followed by the protein solution and another layer of matrix. Volumes added were 1 μL, and the spot was air dried between each addition. Experiments were performed on Bruker Biflex IV (Bruker Daltonics) MALDI-TOF mass spectrometer, operating in linear ion mode and externally calibrated with horse heart cytochrome C and bovine ubiquitin (Sigma), giving a mass accuracy of ±0.2%.

Chapter 3: Phosphorylation Studies of U24[†]

3.1 Introduction

In this chapter, the possibility that U24 can be phosphorylated by MAPK, on the basis of the sequence identity shared between MyBP and U24 is explored. There are many observed biochemical alterations associated with MS neural tissue (reviewed in Chapter 1), but the exact mechanisms which initiate or sustain the disease are unknown. Further confusion results in trying to discern whether the observed changes in physiology are directly involved in the pathogenesis of disease or more simply just a consequence of the disease (having no direct molecular relationship to disease progression). One such observation is that individuals with MS tend to have less phosphorylation at Thr97 of MyBP[50], but the cause and effect are both unknown. Substrate competition for phosphorylation by MAPK plays a pivotal role in eukaryotic development [233]. Demonstrating that U24 can be phosphorylated by a kinase that also recognizes MyBP supports the possibility that this may contribute to a pathological process that destabilizes the myelin sheath.

An excellent kinase substrate under both *in vitro* and *in vivo* conditions [234], MyBP experiences a rapid turnover of its phosphate groups [235]. Regulation of phosphorylation in MyBP is proposed to have both functional and structural implications for maintaining the efficiency of nerve conduction and physical integrity of the myelin sheath [236-238]. Thr97 (bovine numbering) is an *in vivo* phosphorylation site [239] that is recognized by both glycogen synthase kinase (GSK) and MAPK under *in vitro* conditions. The apparent Michaelis constant (K_M) for

[†] A version of this chapter has been published: "Tait, A.R., Straus, S.K., Phosphorylation of U24 from Human Herpes Virus type 6 (HHV-6) and its potential role in mimicking myelin basic protein (MBP) in multiple sclerosis. *FEBS Lett* **2008,** 582, 2685-2688."

MyBP phosphorylation by MAPK is 50 μM [239]. Phosphorylation at Thr97 attenuates the ability of MyBP to polymerize and bundle actin, and to bind actin filaments to a negatively charged lipid membrane [237]. This phosphorylation site has also been proposed to play a role in cell signalling and myelin development, with the discovery that MyBP that has been phosphorylated at Thr97 is specifically localized to lipid rafts [240, 241].

In studies on humans with MS and on a spontaneously demyelinating mouse model of MS, there was much less phospho-Thr97 MyBP detected compared to normal [50, 242]. The full consequences of this absence of posttranslational modification are as of yet unknown, but it has been shown that phosphorylation at Thr97 can protect against proteolysis of the Arg96-Thr97 peptide bond by at least three types of proteases [243]. Protection against MyBP degradation would have a direct positive impact on the integrity of the myelin sheath, and should further help by preventing MyBP epitopes from being released and exposed to the immune system.

The concept that a foreign protein substrate could compete with MyBP for phosphorylation was presented by Stoner *et al.* [244]. They noticed that the large T-antigen of papovaviruses JC shared a C-terminal subsequence with MyBP that was also a phosphorylation site in MyBP. JC virus lies dormant in a large number of the general population, but has been known to reactivate and cause a rare but deadly rapid demyelinating disease called progressive multifocal leukoencephapathy. Unfortunately, no cells expressing T-antigen were detected in plaque or periplaque regions of the MS brains or in control CNS tissue, therefore the study was inconclusive in corroborating a role for JC virus in MS. However, a larger sample set later revealed that JC virus DNA could be detected in cerebral spinal fluid of 11 of 121 (9%) MS patients [245], but none in normal patients, thus indicating a possible role for JC virus in at least a small subset of MS patients. In another study [246], large T-antigen expression was detected in

neurofilament-positive cells and astrocytes in the cortex juxtaposed to MS plaques, but not in the plaques themselves. While the molecular role of large T antigen as a phosphoacceptor competing with MyBP has not been followed up on, we sought to investigate a similar role for U24 protein from HHV-6.

While complex genetic traits may provide predisposition to MS, it is quite possible that an environmental factor, such as viral infection, is somehow involved with the progression of the disease [247]. Human Herpesvirus Type-6 (HHV-6), for example, has been shown to be associated with at least a subgroup of MS patients [248]. The exact mechanism by which HHV-6 may trigger or sustain disease pathology is as of yet unknown, but molecular mimicry is one proposed mode of action [249]. The concept of molecular mimicry is that a foreign protein (i.e.: viral or bacterial) triggers an immune response, and based on sequence or structural antigenic similarities with self proteins, the self proteins are degraded, leading to tissue damage such as demyelination. Myelin basic protein, a candidate autoantigen in MS, has a seven amino acid stretch identity with HHV-6 U24 protein, PRTPPPS ($MyBP_{92–104}$ =IV**PRTPPPS**QGK; $U24_{1–13}$ = MDP**PRTPPPS**YSE; identical sequence bold, potential MAPK phosphorylation sites underlined). It was demonstrated that greater than 50% of T-cells recognizing $MyBP_{95-105}$ cross-reacted with and could be activated by a synthetic peptide corresponding to $U24_{1-13}$ in MS patients [250]. Based on this sequence identity and the fact that MyBP has a phosphorylation site within this segment, we propose a mechanism by which U24 may additionally contribute to the pathogenesis of MS: by representing an alternative kinase target, U24 might interfere with essential phosphorylation of MyBP. In this light, we hope to extend the traditional molecular mimicry hypothesis that is immunologically based, to include a functional component in which U24 can be shown to mimic the function of MyBP, thereby precipitating a pathological process.

Here, in attempt to identify a factor which may contribute to the cause of low levels of phospo-Thr97 MyBP in MS patients, we explore the possibility that U24 protein from HHV-6 can be efficiently phosphorylated by MAPK, based on the sequence similarity between U24 and MyBP.

Unless specified otherwise, the term 'phospho-MyBP' refers to any isoform of MyBP being phosphorylated at the Thr97 position (bovine numbering), at the Thr95 position (murine numbering), or the Thr98 position (human numbering) in which all are considered equivalent phosphorylation sites.

3.2 Results

3.2.1 SDS-PAGE Purity Analysis of U24 and MyBP Proteins

Fresh solutions of MyBP and U24 were analyzed for purity by SDS-PAGE, and each protein migrated as a single band with no detectable contaminants (Figure 3.1). MyBP tended to degrade overnight at 30ºC to smaller peptide fragments, so phosphorylation experiments using MyBP were limited to 3 hours.

3.2.2 MAPK-mediated Phosphorylation Kinetics of U24 and MyBP

Figure 3.2 demonstrates the time course of protein phosphorylation, illustrating that U24 and MyBP can both be efficiently phosphorylated by MAPK. Under these conditions, we take 100 % phosphorylation of MyBP to be approximately 1 mol phosphate per mol protein [251], with the major phosphorylation site as Thr97 or TPR(phospho)TP [239]. Others have observed that Thr94 also represents a minor phosphorylation site *in vitro* [109], one that can be also be phosphorylated with increased kinase concentration and incubation time [237]. Our results

suggest that U24 can by phosphorylated up to approximately 50% that of MyBP or 0.5 mol phosphate per mol protein.

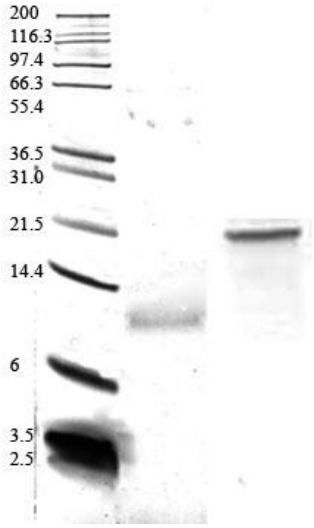

Figure 3.1 Tris-tricine SDS-PAGE analysis of U24 and MyBP, stained with Coomassie Blue G-250. Mark12 molecular weight markers (lane 1) were loaded and molecular weights in kilodaltons are indicated to the left of the gel. Amount of protein loaded was 1 µg for U24 (lane 2) and 3.6 µg for MyBP (lane 3).

3.2.3 Phosphoamino Acid Analysis

U24 has two potential MAPK target sites, Thr6 within the optimal PX(T/S)P consensus sequence, and S25 within the minimal (T/S)P consensus sequence [110]. To determine which one or if a mixture of both sites are phosphorylated, we performed a TLC analysis of the ^{32}P labeled phosphoamino acids that were released by acid hydrolysis (Figure 3.3). Using phosphoamino standards dyed with ninhydrin and the ^{32}P labeled phospho-threonine from MyBP acid hydrolysis, we confirmed that it is Thr6 in U24, part of the PRTPPPS sequence shared with

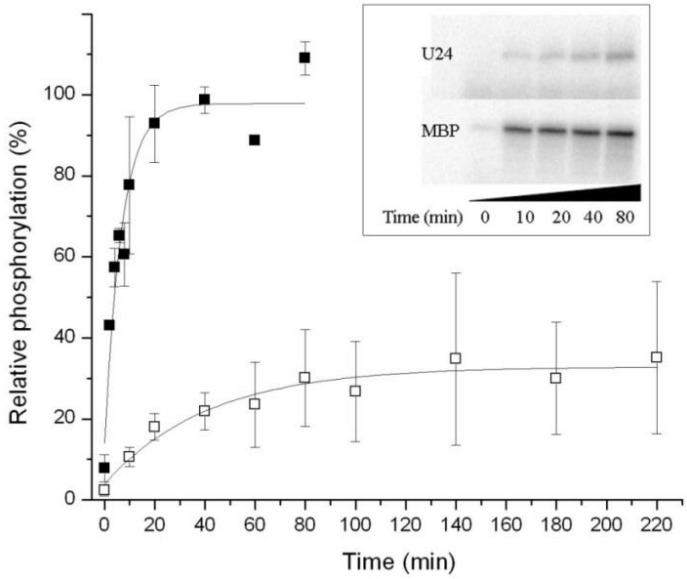

Figure 3.2: Phosphorylation kinetics data for U24 (open squares) relative to MyBP (closed squares), derived from SDS-PAGE/autoradiography results (inset). The error bars were obtained by repeating the measurements three times.

MyBP, and not Ser25 that is phosphorylated. It should be noted because MAPK does not phosphorylate tyrosine, the artifacts at the top of the TLC plate are not from phosphotyrosine, but rather, they are likely from partially hydrolyzed peptides containing phosphothreonine.

3.2.4 Evidence of U24 Phosphorylation by MALDI-TOF MS

A kinase reaction run overnight with 1 mM ATP subtrate resulted in U24 being fully phosphorylated at a single position, with no unphosphosphorylated or multiply phosphorylated species detected (Figure 3.4). Conversely, after only three hours of reaction and in the presence of 0.1 mM ATP, a mixture of both unphosphorylated and monophosphorylated forms could be observed (Figure 3.4C); no autophosphorylation activity was detected when kinase was not added. The mass of unphosphorylated U24 was measured to be 10235 Da, and

monophosphorylated (+80 Da) was 10313 Da. Kinase reactions carried out on MyBP for 3 hours and in the presence of 0.1 mM ATP appeared to give a mass increase corresponding to one phosphate.

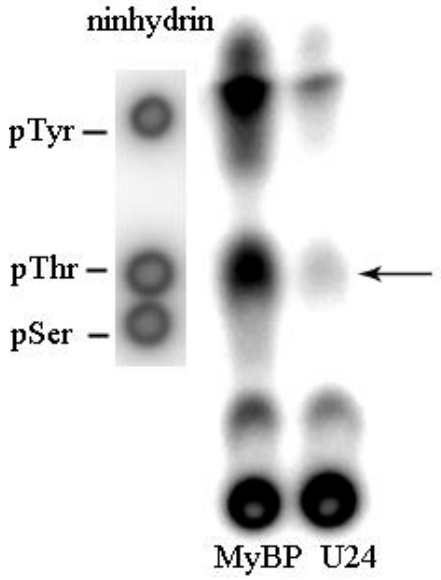

Figure 3.3 One dimensional TLC, followed by autoradiography of ^{32}P-phosphate labeled MyBP and U24 acid hydrolysates. Positions of pTyr (phospho-Tyrosine), pThr (phospho-Threonine), and pSer (phospho-Serine) were revealed by ninhydrin staining. Significant amounts of pThr only are detected in MyBP and U24 (arrow).

3.3 Discussion

We have successfully shown that U24 can be phosphorylated at the equivalent threonine in MyBP based on sequence similarity. Our results show that U24 can only be phosphorylated at a maximum of one site by MAPK, compared to MyBP which has previously been demonstrated to have two phosphorylation sites[109]. It is worth noting that the U24 sequence has an aspartic acid (underlined) near its phosphorylation site (M<u>D</u>PPRTPPS), which aligns within one position

of the second minor threonyl phosphorylation site (underlined) of MyBP (IVTPRTPPPS), thereby possibly making the aspartic acid a phosphorylation mimic due to the negative charge on the amino acid side chain.

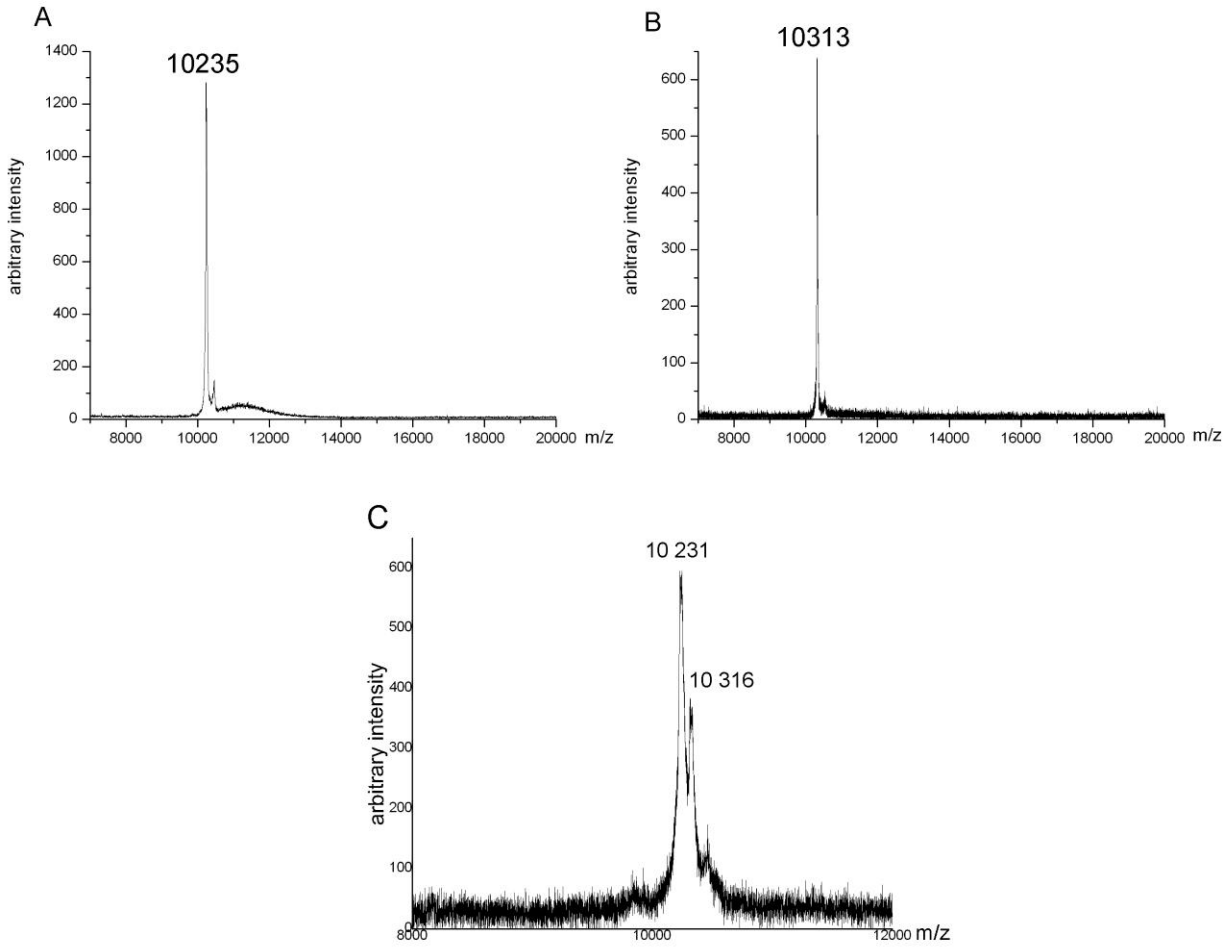

Figure 3.4 MALDI-TOF MS of unphosphorylated U24 (A) and U24 that has been phosphorylated by MAPK (B) after overnight incubation with 1 mM ATP and 200 units of kinase, or C) three hours of incubation with 0.1 mM ATP and 200 units of kinase. The mass shift of ~ +80 Da signifies the addition of one phosphate to the protein.

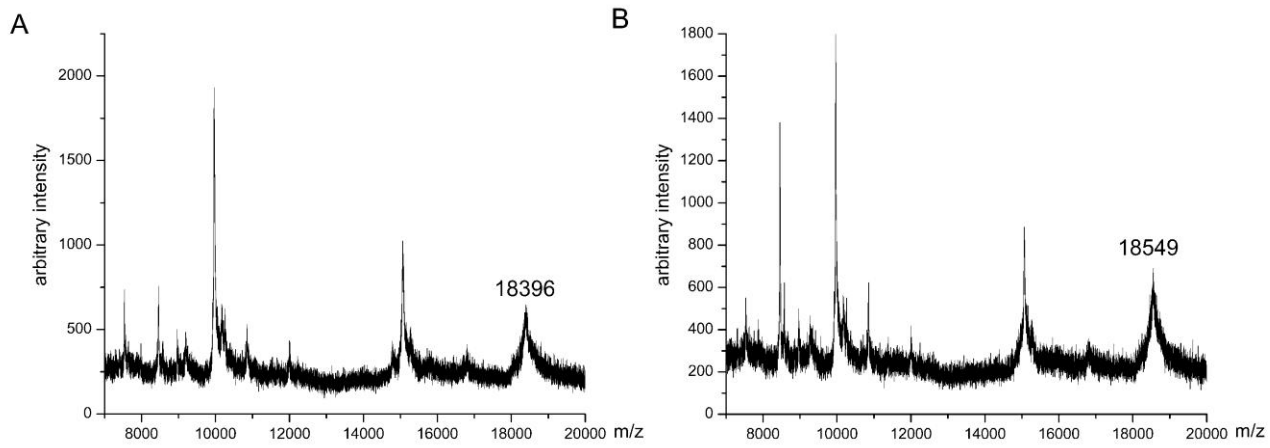

Figure 3.5 MALDI-TOF MS of unphosphorylated MyBP (A) and MyBP that has been phosphorylated by MAPK (B) after 3 hours of incubation with 0.1 mM ATP and 200 units of kinase. The mass shift of ~ +160 Da signifies the addition of two phosphates to the protein. Line broadening may indicate a mixture of mono- and unphosphorylated protein present; other peaks correspond to degradation products and trace contaminants that ionize well in comparison to the major MyBP species present.

The biological relevance of these findings is significant since HHV-6 genes have been detected in the brains of MS patients [252]. As reviewed in Chapter 1, it was shown that HHV-6A strain has been directly linked to MS, with a possible genetic factor placing those with certain MHC2TA gene polymorphisms at higher risk [248]. The U24 expressed by HHV-6 has been shown to down-regulate surface expression of CD3 receptors in T-cells [165], but the result of its expression in nervous tissue has yet to be examined. Here we propose that because of a stretch of sequence similarity between MyBP and U24, PRTPPPS, there may be cases of mistaken identity, resulting in essential interactions with and post-translational modifications done on the viral as opposed to the self-protein. This sequence is also a PXXP SH3-target consensus sequence [253], and ultimately there may be more examples in which U24 and MyBP compete for molecular recognition based on their identity[254], perhaps additionally contributing

to the destabilization of the myelin sheath and the pathogenesis of multiple sclerosis. One key example is the SH3 domain of Fyn tyrosine kinase, which will be discussed in Chapter 4. There are clearly many membrane-associated phosphorylation targets in myelin (e.g. MyBP, Tau [255]). Perhaps U24, with its putative transmembrane domain, sequesters phosphates to the membrane, thereby interrupting signalling or other pathways in which phosphorylated MyBP may participate. U24 has been demonstrated by us (this thesis) and by others [198] to behave as a membrane protein, and has the capacity to be abundantly expressed in neural tissue [256, 257]; the results are certainly suggestive that U24 colocalizes with MyBP or Fyn *in vivo*, although it remains to be proven. It can be further speculated that if U24 competes with MyBP for phosphorylation, than there will not be sufficient levels of phosphorylated MyBP in lipid rafts [240, 241] – a characteristic of mature myelin. Furthermore, phosphorylated U24 may signal to cellular machinery that myelin has matured, when in reality, the myelin remains in an immature, dysfunctional state.

There are several commercially available antibodies that are directed against phospho-Thr97 of MyBP (Santa Cruz Biotechnology, Inc.) and it would be of great interest to see if these antibodies could also bind to the phosphorylated form of U24 described here. If antibody cross-reactivity between phospho-MyBP and phospho-U24 were to be observed, the previously suggested hypothesis that U24 could mimic MyBP in an immunological sense [250] would further be strengthened.

It should be acknowledged that U24 expression alone may not bring about a pathological effect (MS-like symptoms), rather, a combination of other non-specific factors such as membrane lipid composition [258], physiological stress, genetic predisposition, the presence of other viruses [259, 260], or especially the full-functionality of the HHV-6 virus from which U24 is

expressed [261] may be required. A newly compiled on-line database called virPTM Web [262], details the existence of experimentally determined viral protein phosphorylation targets as well as makes predictions of potential viral protein phosphorylation based on primary sequence. Guided use of this database information coupled with future experimental evidence is likely to reveal that there are more examples of other viral proteins that have similar sequence to the phosphorylation site shared between U24 and MyBP. A first example of potential interest found in the database is the BRMF1 protein from HHV-4 (Epstein-Barr Virus), a protein which has the core PPRTP pentapeptide sequence shared with MyBP and U24, and which has the equivalent threonine phosphorylated [263]. HHV-4 has also been controversially implicated with MS [264]. It is therefore worth exploring whether there can be enough viral competitors present to block critical phosphorylation of MyBP, and in turn cause signalling mechanisms involved in myelination to go awry (i.e.: inhibition of actin cytoskeleton remodeling and clustering of phospho-MyBP in lipid rafts). Under the conditions we tested, U24 phosphorylation appeared to be slower than MyBP, and we can only speculate that if the dephosphorylation rates of U24 may be slow as well, the situation can arise where U24 can act as a phosphate sink and lock certain signalling processes constitutively on or off.

While the focus here has been on the relationship between U24 and MyBP phosphorylation, U24 phosphorylation by Erk2 MAPK may be important to U24's function in downregulating CD3/TCR cell-surface expression and cloaking HHV-6 virus from immune detection. Firstly, we know that the PPXY domain of U24 appears to be essential to its activity [132], which means that the U24 is likely to bind a WW domain-containing protein such as Nedd4 ubiquitin ligase. As mentioned in Chapter 1, the U24 phosphorylation sequence (PR<u>T</u>PPPSY; phosphorylated threonine underlined) is remarkably similar to that of the epithelial sodium

channel γ-subunit (PGTPPPKY), whose binding affinity towards Nedd4 ubiquitin ligase is strengthened by phosphorylation on the similarly positioned threonine [183]. Since we do not yet have confirmation that Nedd4 is the *in vivo* binding partner essential to U24 activity, future work should reveal if U24 phosphorylation increases its interaction towards its intended WW domain-binding partner.

Profiling of MyBP binding strengths to a cast of different SH3 domains has been carried out *in vitro* for both the phosphorylated and non-phosphorylated forms of MyBP[254]. While phosphorylation does not largely affect the affinity that MyBP has for SH3 domains directly, it is proposed that phosphorylation may negatively affect the ability that MyBP has to tether Fyn tyrosine kinase to the cell membrane. Fyn plays a critical role in the maintenance of CNS myelination [265]. More recently, it was discovered that Fyn has also has a role in PNS myelination [266] together with Lyn, another closely-related src kinase.

3.4 Summary

In this chapter, it was demonstrated that U24 can be efficiently phosphorylated by MAPK at the equivalent threonine that is in MyBP, strictly on the basis of both U24 and MyBP having the identical MAPK recognition site. The significance of phospho-U24 in the role of MS is only speculative at this point, but the fact that we have identified conditions under which U24 can be phosphorylated to virtual completion suggests that the polyproline region that contains the phosphorylation site is highly solvent accessible. This site-accessibility confirms that our isolated recombinant form of U24 may behave similarly in solution to the *in vivo* form of U24 expressed in T-cells[165], where the region has been shown to be important for activity and possible protein-protein interactions like WW domain modules[132].

In the following chapter, we continue exploring how U24 is able to further mimic MyBP such that the polyproline region of U24 can interact with the SH3 domain of Fyn in the same way that MyBP can. This brand of functional mimicry may in turn have an additional detrimental effect on the Fyn-Rcγ signalling pathway [267] – a pathway which is known to be important for myelination in the CNS [267-269].

3.5 Materials and Methods

3.5.1 Isolation of HHV-6 U24 Protein

The U24 protein was expressed and purified based on the method by Pryor *et al.* [204] with some changes. Full details of the expression and purification are discussed in Chapter 2 of this thesis. Briefly, the gene for U24 from HHV-6A was cloned into plasmid pMAL-p2x (New England Biolabs) and expressed in *E. coli* as a *C*-terminal fusion to maltose binding protein and a hexahistidine tag. Based on primary sequence analysis, U24 has a hydrophobic *C*-terminus that is possibly a transmembrane domain. Addition of Triton X-100 detergent was thus a requirement to solubilize the fusion protein from the *E. coli* pellet. The expressed fusion protein was purified using an immobilized metal affinity chromatography column, Histrap HP (GE Healthcare) charged with Ni^{2+}. Buffers contained 20 mM Na^+/K^+ phosphate, 1 mM dithiothreitol, 0.5% Triton X-100 and 0-500 mM imidazole, pH 7.4. The fusion protein included a thrombin cleavage site between the hexahistidine tag and U24 protein. After cleavage with bovine thrombin (GE Healthcare), the digested protein was reapplied to the column and the flowthrough was applied to an anion exchange column, Hitrap FF Q-Sepharose (GE Healthcare) to remove thrombin, liberated maltose binding protein with histag, undigested fusion protein, and

residual protein impurities. The U24 was collected from the flowthrough and its purity was determined by Tris-Tricine SDS-PAGE and found to be > 95% pure. The protein concentration was determined using the bicinchoninic acid method (Pierce) which included a procedure for removing interfering substances [270]. The yield of U24 was found to vary between 1-2 mg per l of minimal media M9 culture. The molecular mass of U24 was verified by MALDI-TOF MS; in agreement with the theoretical mass, MALDI-TOF MS data yielded an experimental mass of ~10 235 Da.

3.5.2 Preparation of ^{32}P-phosphate Labeled U24 and MyBP

Bovine MyBP (Sigma) was dissolved in water and its concentration was measured by the bicinchoninic acid method or by absorbance, using an extinction coefficient of $\varepsilon_{276.4}$ = 10300 $cm^{-1}M^{-1}$ [271]. The MAPK (Erk2) was obtained (New England Biolabs) and assays were set up for MyBP and U24 based on previously described methods [251]. In separate microfuge tubes, 480 pmol each of U24 and MyBP were diluted to a total volume of 60 µl with MAPK assay buffer (supplied by New England Biolabs; 50 mM Tris-HCl, 10 mM $MgCl_2$, 2 mM DTT, 0.1 mM EDTA, 0.01 % Brij 35, pH 7.5) 100 µM ATP (New England Biolabs) and 0.04 µCi/µl [γ-^{32}P]ATP. Reaction tubes were placed in a water bath or hotplate set at 30^{o}C, and reactions were started by the addition of 200 units of MAPK.

3.5.3 SDS-PAGE / Autoradiography Analysis of ^{32}P-labeled Proteins

At various time points, 40 pmol of protein were removed from the kinase reaction, and the reaction was quenched by addition of an equal volume of Novex 2X SDS buffer (Invitrogen) supplemented with 5 mM of 2-mercaptoethanol (Sigma) and heated to 95^{o}C for 5 minutes.

Samples were loaded on Tris-tricine polyacrylamide gels (13.5%) and run for 2 hours at 100 V. The gels were then wrapped in thin plastic film and exposed for varying lengths of time to a phosphoimager screen before being scanned with a Typhoon 9200 phosphoimager (GE Healthcare). Relative ^{32}P incorporation was quantified using ImageQuant 5.2 software (Molecular Dynamics).

3.5.4 Phosphoamino Acid Analysis

After an overnight kinase reaction, ^{32}P-phosphate labeled MyBP and U24 were precipitated by addition of trichloroacetic acid (20% w/v final) and the pellet was washed with three volumes of ice cold acetone. The pellets were then dissolved in 200 μL 6 M HCl and incubated for 1 hour at 110^{o}C. Acid was removed from the hydrolysate by speed-vac lyophilization, and the dried residue was suspended in 10 μl of water. A few microliters of hydrolyzed sample were spotted on a silica TLC plate (Merck). A small amount of a phosphoamino acid mixture containing of 1 mg/mL each of *O*-phospho-L-serine, *O*-phospho-L-threonine, and *O*-phospho-L-tyrosine (Sigma) was also spotted for reference. In a solvent composed of absolute ethanol:25% ammonia solution, 3.5:1.6 [272], the plate was developed by three rounds of thin layer chromatography. Phosphoamino acid standards were visualized with ninhydrin spray; identities of the ^{32}P-labeled phosphoamino acids were determined after the TLC plate was exposed to a phosphoimager screen overnight and scanned with a phosphoimager reader.

3.5.5 Characterization of Phosphorylated U24 by MALDI-TOF MS

Phosphorylation reactions were set up as mentioned in section 3.2.2, with the omission of [γ-^{32}P]ATP, and the unlabeled ATP concentration was either 0.1 or 1 mM. Control reactions did not have kinase added. All reactions were carried out for a minimum of 3 hours to overnight. After, U24 protein was precipitated by addition of trichloroacetic acid (20% w/v final) and the pellet was washed with three volumes of ice cold acetone. The MALDI matrix used was sinapinic acid, dissolved in 50 % acetonitrile with 0.1% TFA. The protein was also solubilized in 50 % acetonitrile with 0.1% TFA. Sample solution (1 µl) was spotted on a MALDI target plate, sandwiched between two layers of matrix solution (2 X 1µl), with air drying between applications. A Bruker Biflex IV (Bruker Daltonics) MALDI-TOF mass spectrometer was calibrated with bovine ubiquitin and horse heart cytochrome c (Sigma), and the samples were analyzed in positive linear ion mode. The theoretical mass of U24 was obtained from the primary sequence of the U24 protein of HHV-6A, computed using the ProtParam tool at www.expasy.org.

Chapter 4: Probing the Potential Interaction between U24 and Fyn Tyrosine Kinase[†]

4.1 Introduction

In this chapter, the possibility of U24 interacting with Fyn tyrosine kinase on the basis of U24's sequence identity with myelin basic protein (MyBP) is explored. The presence of Fyn in myelin, complete with its phosphorylating activity and protein-interaction modules, has been deemed critical for the growth and maintenance of the myelin sheath [273]. Therefore, it is worthwhile to explore the possibility that exogenous protein molecules, such as virally-encoded U24, may interfere with Fyn function to constitute a pathological process leading to demyelination or inefficient myelination, and contributing to the disease state of MS.

In the CNS, oligodendrocytes myelinate axons and permit nerve conduction. Through complex biochemical cues [274-276], oligodendrocytes recognize their target axons of nerve cells, and wrap their processes (finger-like projections) around axonal segments to result in the multilamellar membrane-stacked structure that is a familiar feature of mature, healthy myelin. The process of myelination is a rapid process requiring targeted delivery of both proteins and lipids towards the developing sheath. In rat brain, during the active phase of myelination, $\sim 10^5$ myelin protein molecules are produced per minute at the membrane surface in each oligodendrocyte. Interestingly, this is a rate comparable to that of viral membrane glycoprotein synthesis in virally infected cells [276].

[†] A version of this chapter is currently being prepared as a manuscript for publication. "Tait, A.R., Kumar, P., Scott, W.R.P., Straus, S.K. Probing the Interaction between U24 from Human Herpesvirus Type-6A and the SH3 Domain of Fyn Tyrosine Kinase."

A number of studies demonstrate that Fyn kinase has a pivotal function in translating complex communication signals into different cellular responses to direct CNS myelination (reviewed in [273]). The essential functional involvement of Fyn in myelination is highlighted in mutant mice lacking in Fyn, or expressing a single amino-acid mutant kinase-inactive form of Fyn [124, 125, 277]. Hypomyelination in these mice is found in different regions of the brain and optic nerve; the number of myelin fibres is drastically reduced. Blocking Fyn activity with selective inhibitors or with a dominant negative form of Fyn (lacking kinase activity) interferes with oligodendroglial maturation by reducing the oligodendroglial process formation and outgrowth [277, 278]. The full cast of molecules that Fyn functionally interacts with is unknown, but Fyn is considered thus far to mediate downstream signalling of three major pathways: (1) the Rho-family GTPases which in turn regulate actin cytoskeleton dynamics essential to cell survival and morphological differentiation, (2) recruitment of microtubule cytoskeleton component polarity to direct cargo transport, and (3) control the transport, stability and translation of mRNA of myelin proteins, especially MyBP [273].

Fyn kinase belongs to the Src-family of non-receptor tyrosine kinases and has a mass of 59 kDa. It has four Src homology (SH) domains [279]: an SH4 domain at the N-terminus with two acylation sites to anchor Fyn to the cell membrane, SH3 and SH2 protein-binding domains, and an SH1 domain with kinase activity. Description of the domains in the context of open/closed or active/inactive conformations can be found in Figure 4.1.

It has been demonstrated that the microtubule subunit α-tubulin interacts with both the SH2 and SH3 domains of Fyn. Microtubule-associated-protein Tau also specifically binds to the SH3 domain[127] specifically via one of its PXXP motifs at the N-terminus [280]. Tau is important for regulating the assembly and stability of microtubules. Removal of the PXXP domain of Tau

that interacts with Fyn reduces binding to the Fyn-SH3 domain by >90% [280]. The functional importance of the PXXP motif was demonstrated by co-expression experiments done by Klein *et al.*, showing that a deletion mutant of Tau lacking its microtubule domain, but with its PXXP intact, could out-compete native Tau for binding to Fyn-SH3 [127]. The result was that there was a reduction in the process number and length in myelinating oligodendrocytes. Belkadi *et al.* performed similar deletion-mutant Tau experiments, and found that Fyn was not present at the membrane processes as in normally developing oligodendrocytes, but was localized in the cell body [126]. The full significance of the Fyn/Tau interaction is not fully understood, but Fyn in the presence of Tau at the membrane may be required to inhibit to kinesin motor activity, causing kinesin's detachment from microtubules [281], and subsequent release of essential myelin cargo near the developing oligodendrocyte membrane surface.

It is conceivable that a foreign protein, such as from a virus or bacterium, can bind to the Fyn-SH3 domain and compete with essential interactions, such as the Fyn/Tau association, and thereby bring about a dysfunction in myelination. Hepatitis C-encoded NS5a protein has relatively high affinity for Fyn-SH3 (K_D = 629 nM), and as such it has previously been suggested to compete with native host proteins for binding to Fyn-SH3 [282]. K_D is the equilibrium dissocation constant, where K_D = [P][L]/[PL]; [P] and [L] are the concentrations of protein and ligand, respectively, and [PL] is the concentration of the protein-ligand complex. The U24 protein from HHV-6 has a PXXP motif sequence in common with MyBP, a protein which has been shown to bind to Fyn-SH3 [119], although a precise K_D for the MyBP·Fyn-SH3 complex has not been reported. Like Fyn, MyBP can also interact with actin and microtubule cytoskeletal components. Therefore, it is possible that U24 may bind to the Fyn-SH3 to prevent it from interacting with its cytoskeleton-organizing partners such as Tau or MyBP.

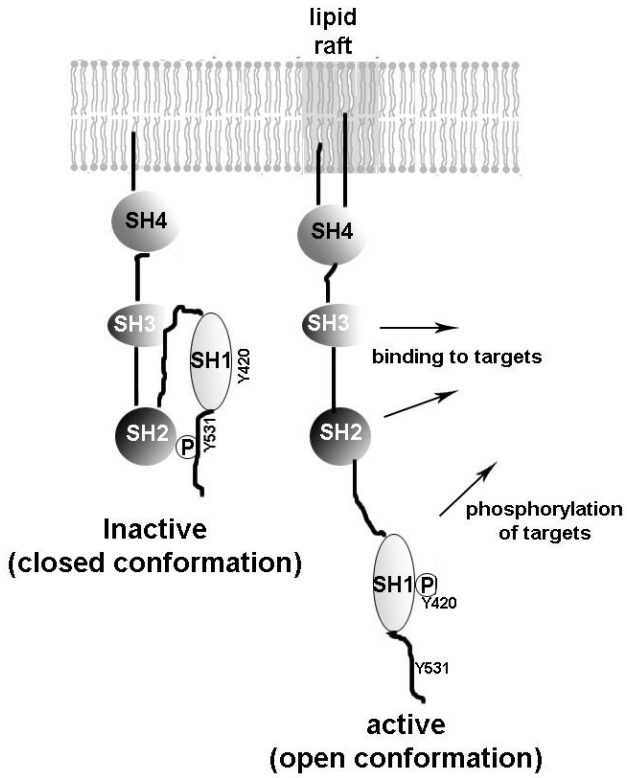

Figure 4.1 Depiction of the SH domain organization (open and closed conformations) of Fyn. In the closed conformation, the SH2 domain adopts an intramolecular contact with phosphorylated Y531 and SH3 domain. Upon dephosphorylation of Y531, Fyn adopts an open, active conformation which is further stabilized through autophosphorylation at Y420. Palmitoylation of the already myristoylated SH1 domain can direct Fyn into lipid raft domains (figure adapted from [273]).

It would not only be of interest to determine if U24 can bind to Fyn-SH3 on the basis of its sequence identity with MyBP (PPRTPPPS), but more precisely, how it does so on the basis of structural similarities. Like many SH3-binding domains, the proline-rich region of MyBP meets the canonical PXXP motif requirements and also adopts a polyproline type II helix [119]. Figure 4.2 is an NMR-derived structural model of Fyn-SH3 in complex with a polyproline-containing peptide PI3-kinase that can been seen adopting a PPII conformation [283]. Structural similarity may also impart a similar binding affinity: while the affinity that MyBP has for Fyn-SH3 has not been precisely calculated, it has been estimated that the interaction is in the micromolar range

[254], and U24 may follow suit. Weak but specific interactions with K_D values in the range of 10^{-4}-10^{-3} M may still be deemed physiologically relevant – a prime example is that of the SH3

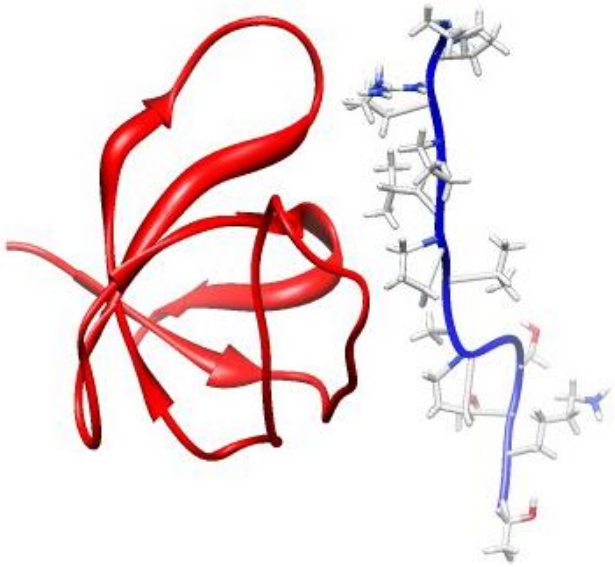

Figure 4.2 NMR-derived ribbon structure of Fyn-SH3 (red) in complex with a peptide (blue) corresponding to residues 91-104 of the p85 subunit of PI3-kinase (1azg.pdb) [283]. Peptide sequence is PPRPLPVAPGSSKT, and adopts a characteristic PPII helix.

domain of Nck binding to the PINCH focal adhesion protein, which has a K_D of 3.1 ±0.6 mM [284], calculated from NMR experimental results. An ultra-weak interface such as this signifies a transient Nck-2/PINCH-1 association process that may trigger rapid focal adhesion turnover during integrin signaling, a process related to cell shape change and migration[285].

The goal of this study was to probe for whether a specific interaction between U24 and Fyn-SH3 exists and to be able to further hypothesize how the interaction may relate to a dysfunction in myelination. To enable detection of weak interactions between U24 and Fyn-SH3, sensitive methods such as GST pulldowns and NMR spectroscopy are described (Table 4.1). Furthermore, to determine if the prolyproline motif in U24 can adopt a PPII helix, circular dichroism was used.

Table 4.1 Commonly-used experimental methods to probe protein-protein interactions and the corresponding sensitivity limitations in terms of the weakest dissociation constant (K_D) that can be detected [286].

Method	Weakest Detectable K_D
Co-immunoprecipitation	NA
GST-Pulldowns	~10 mM
NMR Spectroscopy	~ 1 mM
Isothermal Titrating Calorimetry	~ 100 μM
Yeast Two-hybrid System	10-100 μM
Surface Plasmon Resonance	~100 μM

4.2 Results

4.2.1 Pull-down Experiments with GST-Fyn-SH3 and U24

To determine if U24 could interact with the Fyn-SH3 domain via the PXXP motif in U24 that is common with MyBP, a pull-down experiment was performed using GST-Fyn-SH3 and full-length U24. GST-Fyn-SH3, GST, U24 and NΔ9-U24 were purified to homogeneity. Figure 4.3 is of an SDS-polyacrylamide gel depicting that full-length U24 could interact with GST-Fyn-SH3 that was bound to glutathione beads (lane 4), but U24 did not interact with GST alone (lane 3). This result indicates that U24 can bind to the SH3 domain of Fyn. To see if this interaction was mediated specifically by the polyproline region of U24, the NΔ9-U24 mutant, which lacks the 9 N-terminal amino acids (containing the PXXP SH3-recognition site) was mixed with GST-Fyn-SH3 and no interaction was observed. Control U24 (Lane 1) and NΔ9-U24 (Lane 5) proteins were loaded for reference; no other bands could be detected with control GST or GST-Fyn-SH3 when run in the absence of U24 protein (Lanes 2-3, 6-7). These results, taken together, suggest that U24 specifically binds to Fyn-SH3 via its polyproline domain.

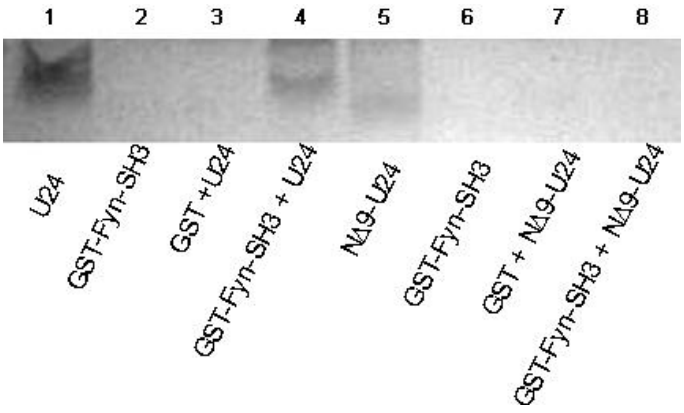

Figure 4.3 SDS-PAGE results of a GST pulldown experiment with Fyn-SH3, U24 and NΔ9-U24. U24 and NΔ9-U24 were loaded as reference in lanes 1 and 5, respectively. U24 appears to bind to Fyn-SH3 via its PXXP domain (lane 4), but truncated NΔ9-U24 without the PXXP cannot bind Fyn-SH3 (lane 8). Gel was stained with Coomassie Blue G-250.

4.2.2 Far-UV CD is Suggestive of a PPII Helix in U24

Using the method described by Polverini *et al.* [254] in their study of the polyproline region of MyBP, a peptide representing the N-terminal region of U24 was synthesized ($U24_{1\text{-}15}$: MDPPRTPPPSYSEVL), and was similarly investigated by temperature-variable circular dichroism (CD) spectroscopy. The presence of PPII helices is not readily apparent from the shape of far-UV CD spectra, which appears to yield very similar spectra as for random coil peptide (Figure 4.4A). However, it was recently shown by Polverini *et al.* that close examination of CD spectra of PPII helix-containing peptides can reveal spectral subtleties attributed to the left-handed chirality of the PPII helix [287, 288]. Due to its extended structural conformation and subsequent lack of NH···O interresidue hydrogen bonding in the peptide backbone to stabilize the PPII helices, the helical structure is readily lost when moving to higher temperature. Difference spectra obtained by subtracting the spectrum acquired at 45°C from the one obtained at 5°C is indicative of the PPII helix in the U24 peptide (Figure 4.4B), which gives a maximum at ~220 nm and an isoelliptic point at ~210 nm (Figure 4.4A). These results are very similar to those

obtained previously for the MyBP peptide which contained the identical polyproline core sequence, PRTPPPS [254]. Of note, however, is the finding that U24 appears to retain a significant amount of random coil signal even at 65°C (CD minima ~202 nm), while the signal for the MyBP peptide is virtually lost at this temperature. One speculative interpretation may be that the flanking residues to the polyproline helix may engage in intermolecular interactions to further stabilize the PPII content at higher temperatures. This type of stabilization was proposed for full-length MyBP, where a similar trend in residual signal at higher temperature was observed.

4.2.3 Probing of the Specific Interaction between U24 and Fyn-SH3 with NMR Spectroscopy

Using ^{1}H-^{15}N HSQC NMR spectroscopy, the binding interaction between the $U24_{1\text{-}15}$ peptide (sequence: MDPPRTPPPSYSEVL) and the Fyn-SH3 domain was examined. As the PXXP motif in U24 that is shared with MyBP was presumed to be the site of interaction, $U24_{1\text{-}15}$ containing this sequence was titrated with ^{15}N-labeled Fyn. Several amide chemical shifts of Fyn-SH3 changed in response to the $U24_{1\text{-}15}$ addition (Figure 4.5), and continued to change until a sufficiently high Fyn-SH3:$U24_{1\text{-}15}$ ratio was reached, indicative of binding saturation. Amide resonances were assigned according to [289]. The most notable shift changes were for residues Arg96 and Thr97, which are known to be part of the 'RT' loop [290], a flexible region of SH3 domains that is critical for peptide selectivity and binding interface. Fitting the binding data to several of the changing amide resonances (see Materials and Methods), an equilibrium binding constant (K_D) of 375 μM for $U24_{1\text{-}15}$ peptide binding to Fyn-SH3 was calculated, indicative of weak but specific binding between the two species. Figure 4.6 and Figure 4.7 are the titration

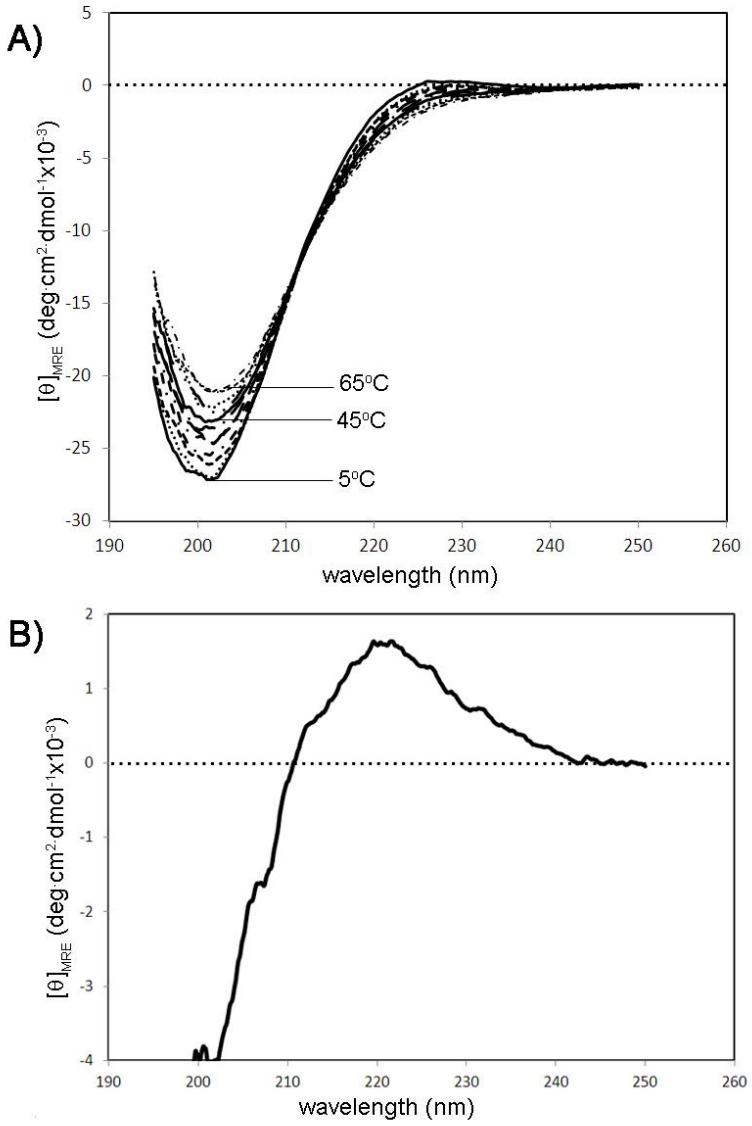

Figure 4.4 Probing the presence of a PPII helix in a 15-mer peptide containing the polyproline region U24 (sequence: MDPPRTPPPSYSEVL) with variable temperature far-UV CD. A) CD spectra were collected from 190-250 nm at increasing temperature, from 5°C to 65°C, with 5 degree intervals. Subtracting the spectra at 45°C from the one obtained at 5°C gives the difference spectra shown in B). The residual signal with maximum at approximately 220 nm and isochroic point at 210 nm is similar to results obtained for the polyproline-containing MyBP peptide studied by Polverini *et al.* [119], indicative of the chiral nature of the left-handed polyproline helix that is transiently lost at higher temperatures.

curves for the ^{1}H and ^{15}N chemical shift changes respectively for a number of residues as a function of protein:peptide.

Using a molecular model that was previously derived from NMR spectroscopy in which Fyn-SH3 is bound to the proline-rich p85 subunit of PI3-kinase [283], the amino acid amides that were perturbed by the presence of $U24_{1-15}$ peptide were colored according to the magnitude of chemical shift change (Figure 4.8). As can be observed in the figure, the residues perturbed the most form what appears to be a potential binding pocket. However, visualization of the PI3-kinase peptide in the model suggests that the mode of $U24_{1-15}$ peptide binding may be different as different residues are perturbed (Figure 4.9).

The ^{1}H-^{15}N HSQC NMR experiments were also performed on ^{15}N-labelled Fyn-SH3 in the presence of full-length U24 and truncation mutant NΔ9-U24. Optimization of the DPC lipid concentration and sample handling of the U24 proteins was a prerequisite for success in this study. Through a series of initial solubility screens, U24 was found to be soluble in 20 mM MES buffer, pH 6.2 containing 100 mM DPC, but generally not in phosphate-based buffers (discussed in Chapter 5). However, Fyn-SH3 did not appear stable in MES buffer, as spectra changed over time and resonances disappeared. Fortunately, solubilized U24 could be readily exchanged into NMR buffer (20 mM phosphate, pH 6.0) containing 100 mM DPC although DPC at this concentration appeared to perturb many of the Fyn-SH3 resonances compared to sample without the lipid. The DPC concentration was then successively lowered to the point that the resonances were no longer perturbed by the lipid, while still being able to keep the U24 proteins soluble; 6 mM DPC was the final concentration that was arrived at for the U24 and NΔ9-U24 NMR experiments. Figure 4.10 is the overlaid ^{1}H-^{15}N-HSQC spectra of the Fyn-SH3 domain alone, with full-length U24, and with NΔ9-U24. Indicative of binding, only full-length

U24 is able to perturb resonances in Fyn-SH3, while the spectrum acquired in the presence of NΔ9-U24 is virtually identical to the control spectrum that has no additional protein added to Fyn-SH3. This result further confirms that the full-length form of U24 is able to interact with Fyn-SH3 and that the PXXP motif is specifically required for this interaction.

4.3 Discussion

Further to the demonstration in Chapter 3 where it was experimentally shown that U24 could be phosphorylated by MAPK, this chapter provides evidence that the polyproline region in U24 is also available to interact with the SH3 domain of Fyn tyrosine kinase. U24 fulfills the structural requirements for binding to an SH3 domain by forming a PPII helix. Also, GST-tagged Fyn-SH3 can successfully bind to U24 via its PXXP region, and titrating a peptide of U24 containing this same region with Fyn-SH3 confirms a weak but specific interaction between U24 and the SH3 domain of Fyn (K_D = 375 μM). Identifying the key regions of the Fyn-SH3 that are perturbed as a result of binding to the $U24_{1-15}$ peptide suggest that different residues of the SH3 domain are involved compared to those for PI3 kinase peptide [283].

It is unknown what such a weak interaction between U24 and Fyn-SH3 may mean in a physiological sense, but is worth further study. There are other binding partners for Fyn-SH3 such as the NS5a protein from Hepatitis C whose affinity for Fyn-SH3 is three orders of magnitude greater than what was calculated for U24 here, so it is unlikely that U24 binds to and sequesters Fyn from its endogenous ligand substrates (such as MyBP, Tau). However, the presence of U24 in the membrane even with its weak interaction with Fyn may have measurable effects, such that the presence of U24 colocalized near Fyn in the cell membrane may constitute pathological interference with Fyn signalling relating to microtubule arrangements, myelin

protein/mRNA cargo transport, and perhaps other yet-unknown Fyn functions. While an equilibrium dissociation constant, K_D, in the high micromolar range observed here suggests weak affinity, even a small amount of U24 may be capable of interfering with the precisely timed and localized protein-protein interactions with Fyn that are needed to carry out a coordinated rearrangement of cytoskeleton required for myelin development.

As it is, the polyproline region in U24 itself is being shown to have tremendous potential as a veritable signalling hub. For example, the potential WW binding domain in U24, a PPXY-motif, is also part of the same polyproline region that recognizes the Fyn-SH3 domain. An intriguing new possibility is that the region in U24 serves as a scaffold to bring other proteins quickly in contact with each other. It has already been suggested that U24 can interact with a variety of WW domain proteins [198, 291]. A WW domain containing protein like a NEDD4 ubiquitin ligase could then bind to U24, and colocalization with other proteins such as Fyn and MAPK may enhance their ubiquitination and subsequent degradation.

Guided by the data obtained previously for MyBP, U24 may also have the potential to bind with other SH3 domains besides the one for Fyn [119], and the biological significance of other SH3-based interactions should also be considered. Ultimately, *in vivo* experimentation in the future will serve to uncover which ligands for U24, SH3 or otherwise, do or do not have a direct impact on myelin integrity.

It terms of U24's *in vivo* ability to downregulate cell-surface expression of CD3 T-cell receptors for viral immunoevasion strategy, SH3 domain interactions do not appear to be critical for function [132]. They may, however, be somehow involved in modulating the activity of U24, because of the virtual overlapping between the PXXP SH3 binding site and of the essential PPXY sequence that binds WW domains. Important to note is that there are subtle differences in

sequence surrounding the PXXP SH3 binding site in versions of U24 from HHV-6A and -6B, and the PXXP site in U24 from HHV-7 is absent.

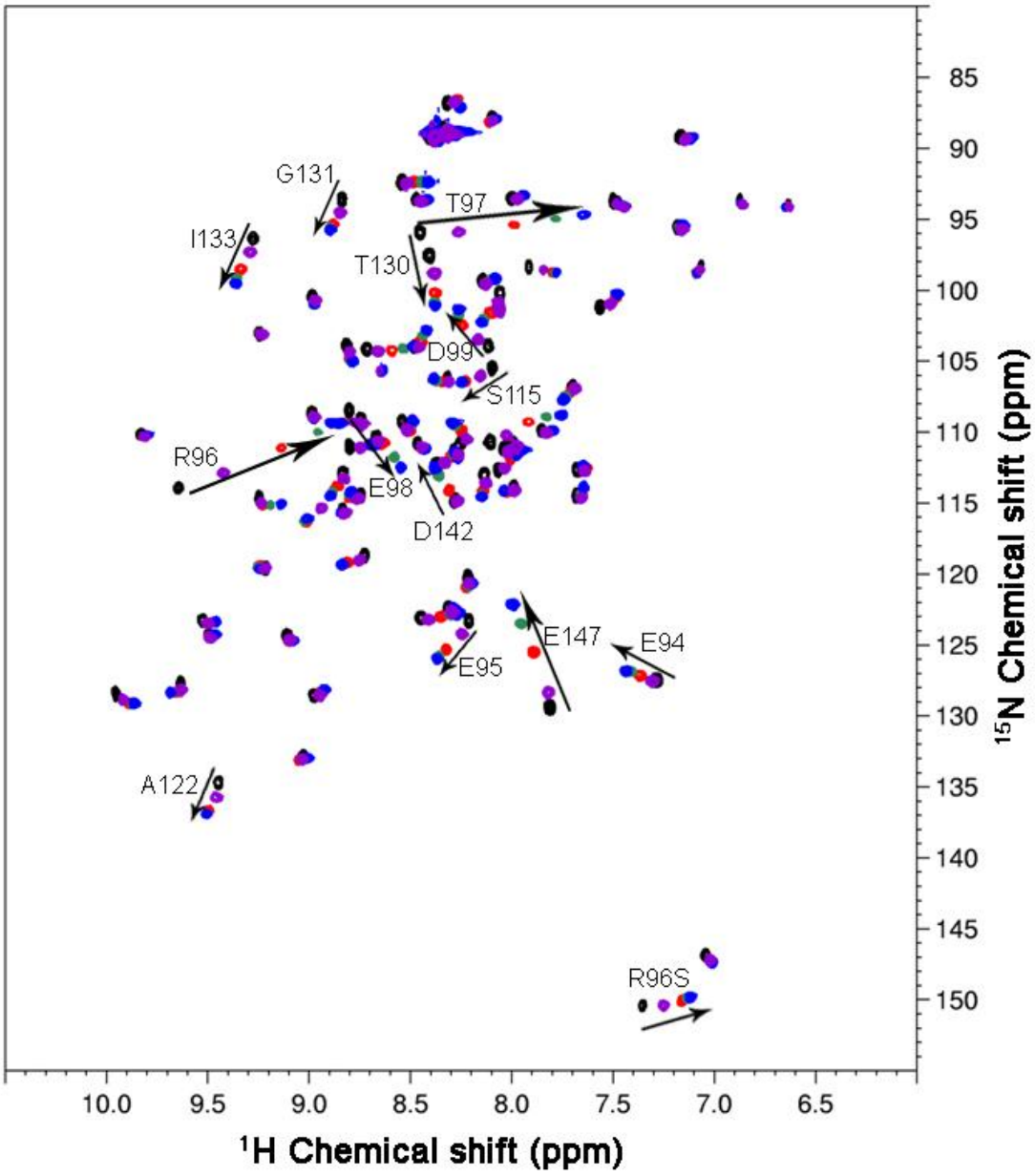

Figure 4.5 Overlay of ^{1}H- ^{15}N HSQC spectra of Fyn-SH3 with the U24$_{1-15}$ peptide MDPPRTPPPSYSEVL added in different ratios: Fyn-SH3 to peptide ratio= 1:0 (black); 1:0.94 (purple); 1:2.50 (red); 1:5.00 (green); and 1:8.74 (blue). Some of the key residues affected are indicated. The assignment is based on that reported by Mal *et al.* [289]. "S" indicates side-chain. Starting concentration of Fyn-SH3 was 0.5 mM, in 10 mM Na phosphate, pH 6.0, with 10% D_2O.

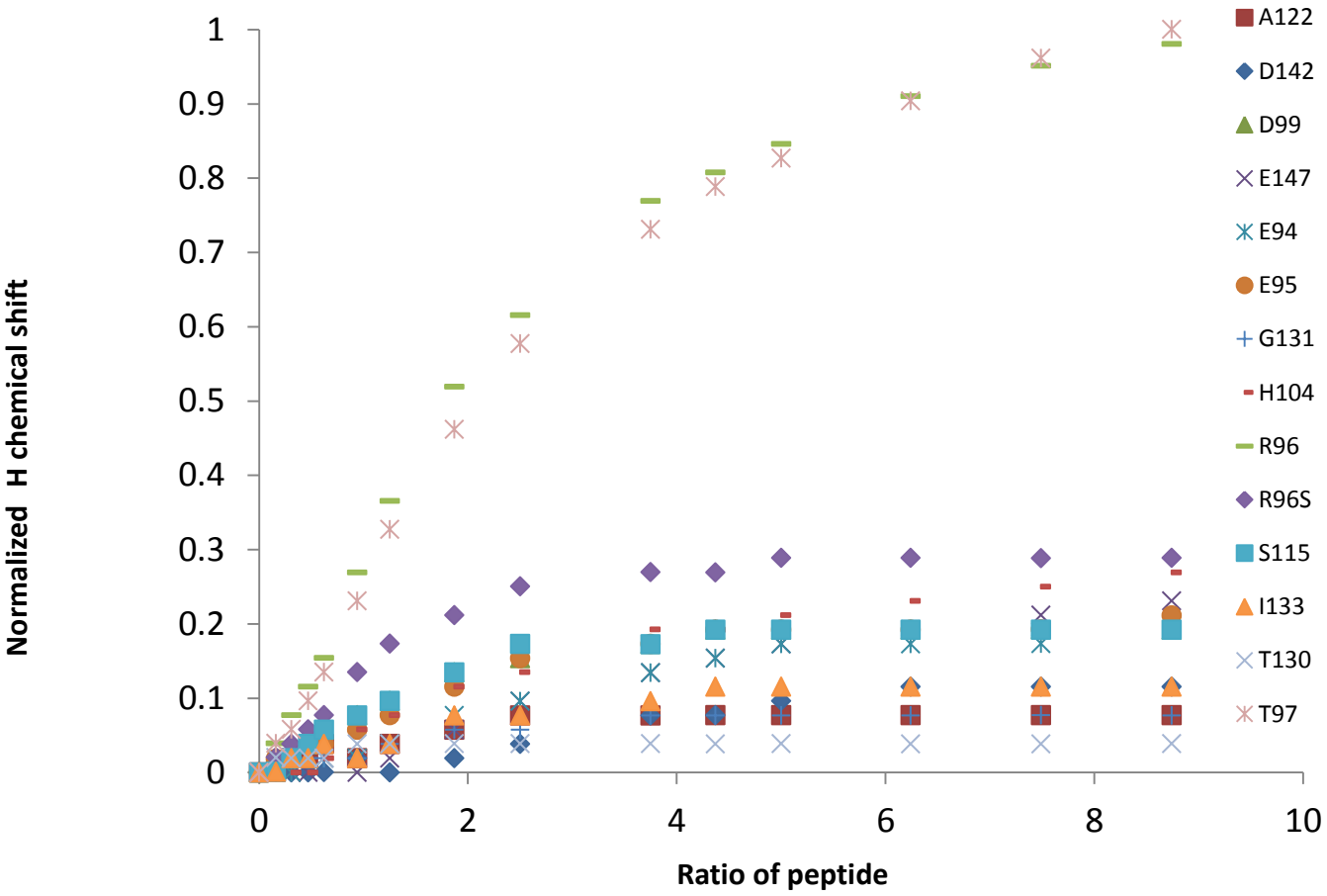

Figure 4.6 Normalized ^{1}H chemical shift changes for different residues of Fyn-SH3 when the peptide MDPPRTPPPSYSEVL added in Fyn-SH3 to peptide ratio ranging from 1:0 (data points at x=0) to 1:8.74 (data points at x=8.74). The shifts are normalized relative to the largest difference, which was observed for T97.

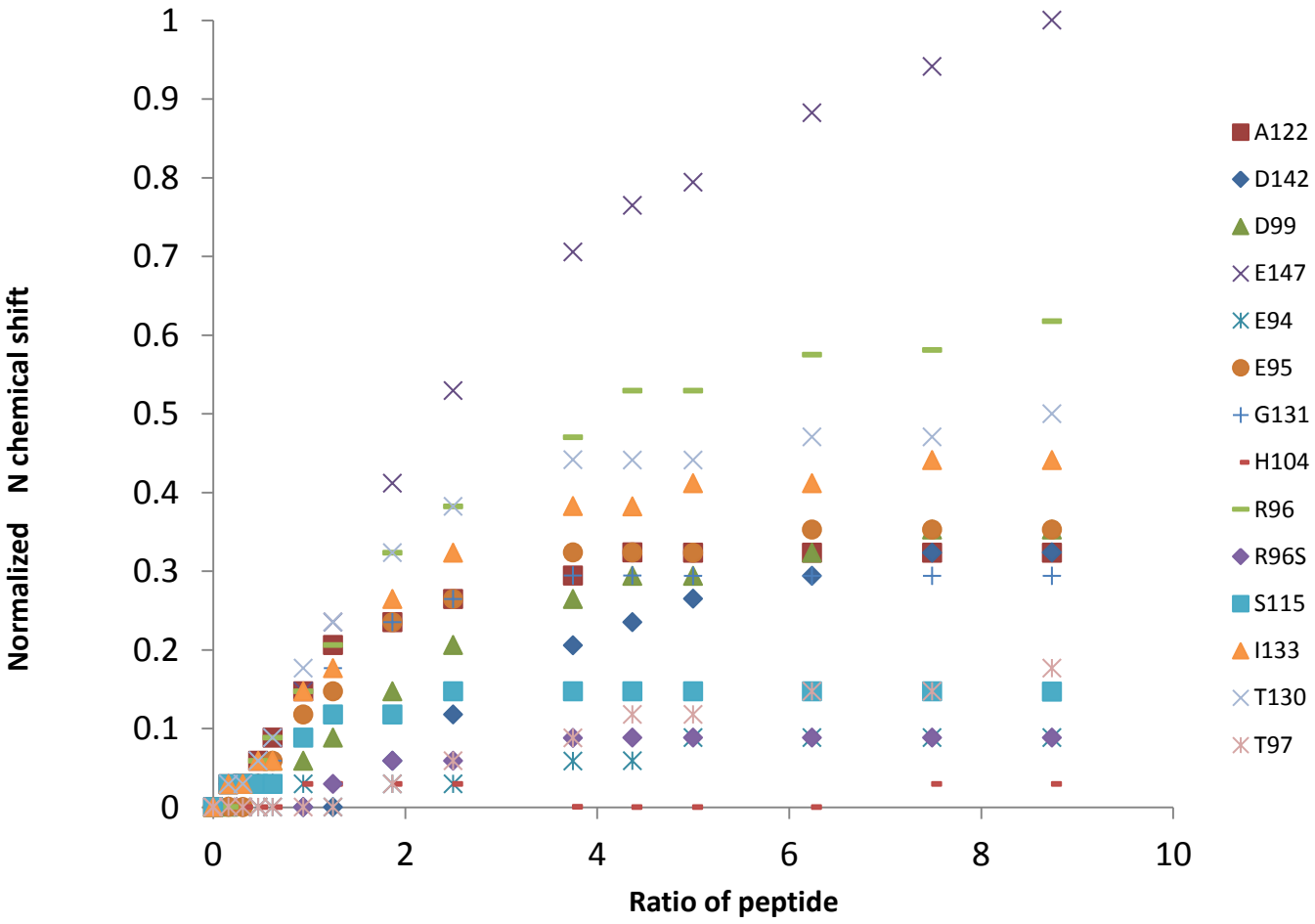

Figure 4.7 Normalized ^{15}N chemical shift changes for different residues of Fyn-SH3 when the peptide MDPPRTPPPSYSEVL added in Fyn-SH3 to peptide ratio ranging from 1:0 (data points at x=0) to 1:8.74 (data points at x=8.74). The shifts are normalized relative to the largest difference, which was observed for E147.

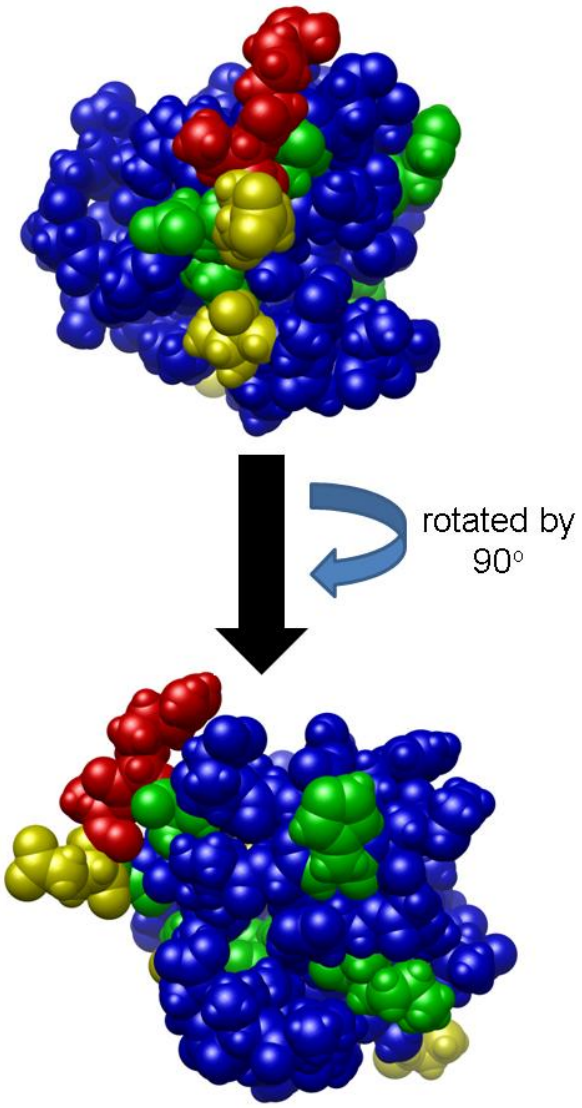

Figure 4.8 Model of Fyn-SH3 with the residues most affected by the presence of the U24 peptide indicated: red (80-100% change in chemical shift); orange (60-79%); yellow (40-59%); green (20-39%); blue (0-19%). The model is derived from the PDB structure 1A0N and was generated using UCSF CHIMERA [129].

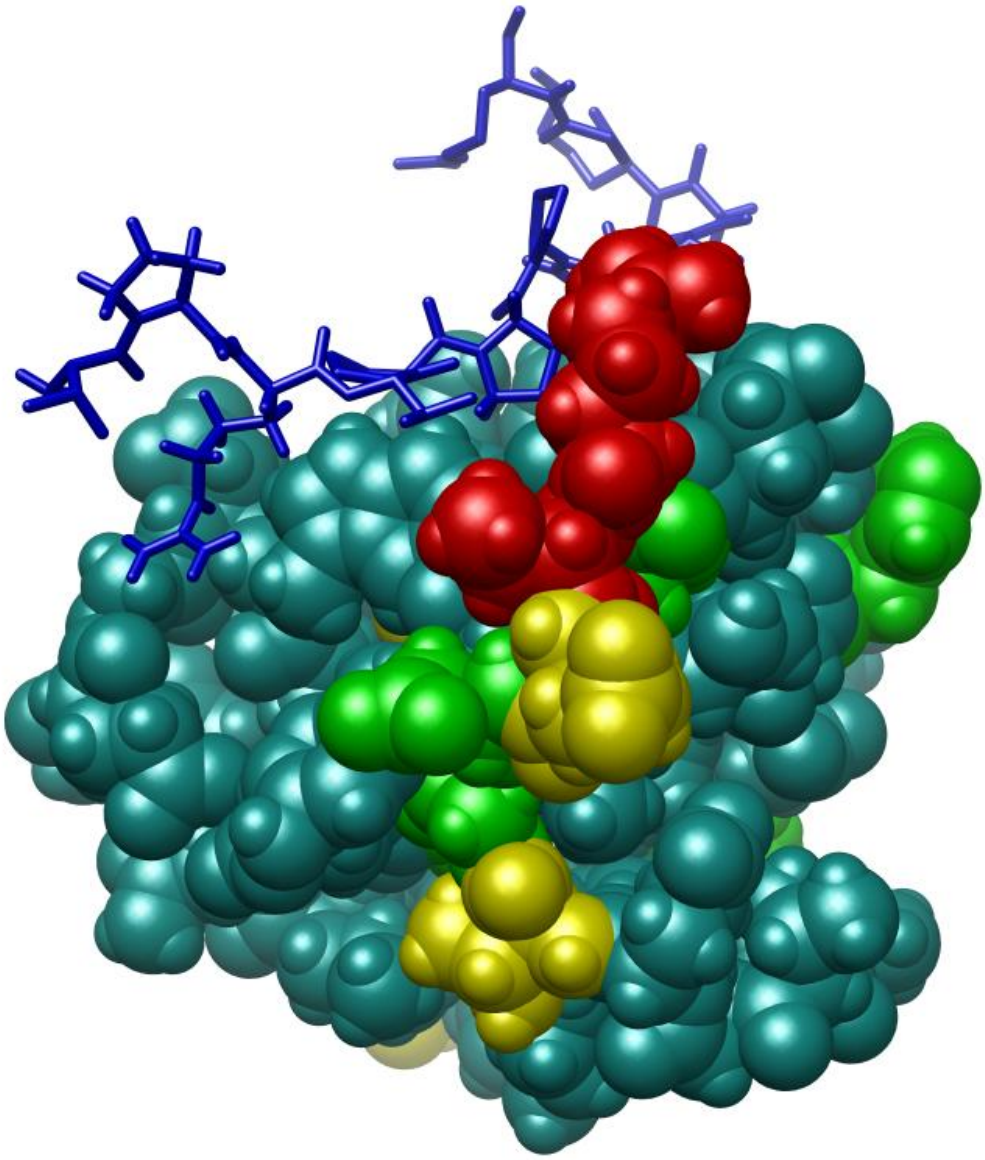

Figure 4.9 Model of Fyn-SH3 (CPK) with the peptide PPRPLPVAPGSSKT bound (stick). The color coding of the Fyn is similar to that used in Figure 4.8 and suggests that the binding proposed for U24 peptide may be different, as different residues are perturbed. The model is derived from the PDB structure 1A0N and was generated using UCSF CHIMERA.

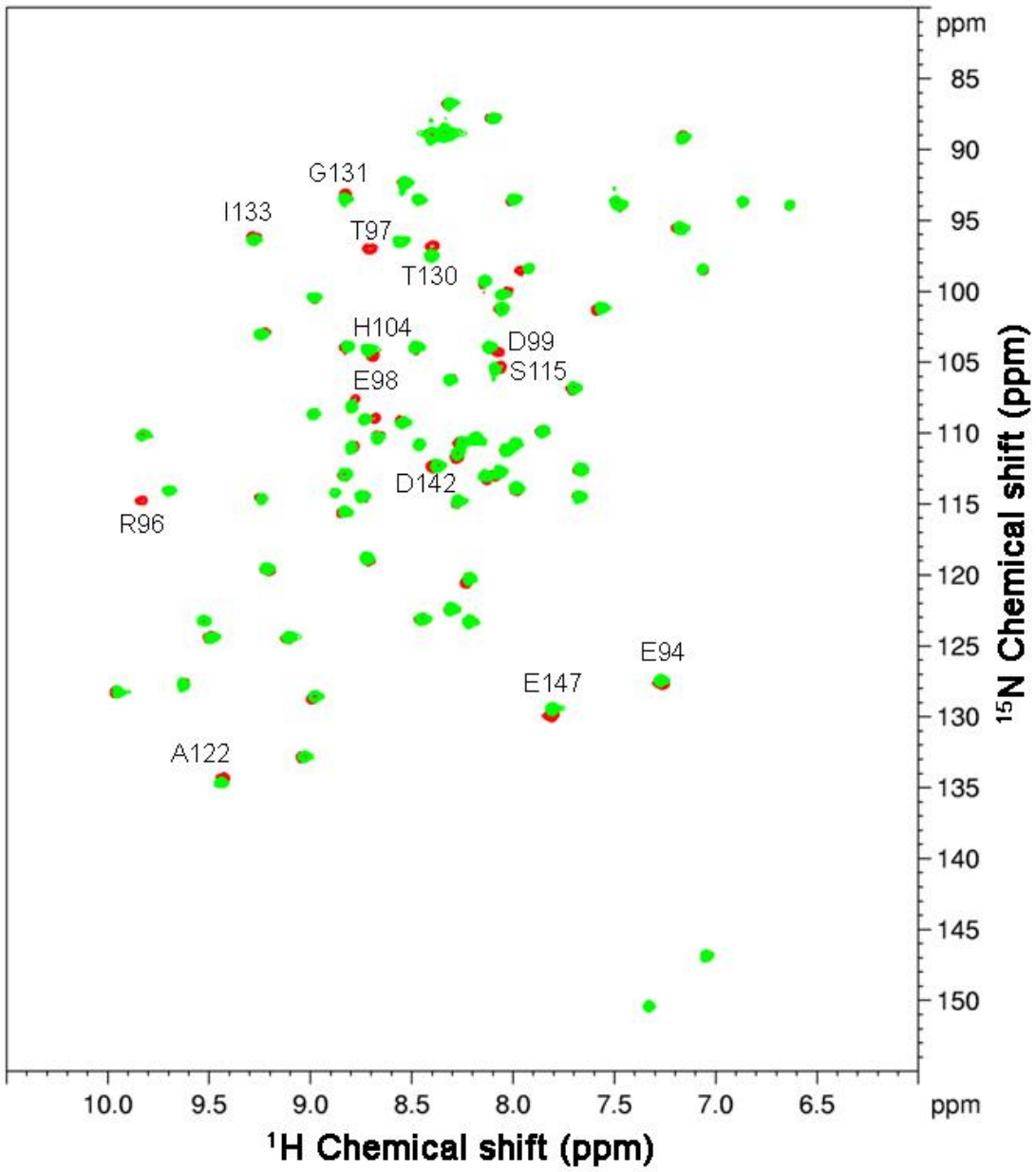

Figure 4.10 Overlay of ^{1}H- ^{15}N HSQC spectra of ^{15}N-Fyn-SH3 alone (green), Fyn-SH3 in the presence of full length U24 (red) and Fyn-SH3 in the presence of NΔ9-U24 (black) (i.e. U24 with the first 9 residues removed). The samples consisted of 0.25 mM Fyn-SH3 in 6 mM DPC, 10 mM phosphate buffer, pH 6.0, 7% D_2O. The U24 proteins were present in a ratio of 1:0.6 (Fyn-SH3 to U24). The black and the green spectra overlap completely.

4.4 Summary

Using GST pull-down assays and NMR spectroscopy, U24 was found to bind specifically to the SH3 domain of Fyn tyrosine kinase, specifically via its polyproline PXXP SH3-binding motif. A U24 peptide representing this binding domain can also form a PPII helix, as suggested by CD spectroscopy. Finally, when the peptide was titrated with ^{15}N-labelled Fyn-SH3 and examined by ^{1}H-^{15}N HSQC NMR spectroscopy, a K_D of 375 μM was found. Binding of U24 to the Fyn-SH3 domain further supports the possibility that U24 may have a role in MS by interfering with signalling pathways pertinent to the structure and maintenance of the myelin sheath.

4.5 Materials and Methods

4.5.1 Expression GST-Fyn-SH3

The plasmid expressing the GST-Fyn-SH3 protein was a kind gift from Dr. Catherine Pallen (Child & Family Research Institute, Vancouver, BC). The vector is pGEX-KG with the SH3 domain of human Fyn (from residues TGVTLF to TVAPVD) cloned into the *Hin*dIII/*Xba*I site. The protein expressed is the Fyn-SH3 domain at the C-terminus of GST, with a thrombin cleavage site in between.

The plasmid was transformed into BL21(DE3) *E. coli*, then plated on LB-agar plates containing 50 μg/mL carbenecillin and incubated overnight at 37°C. Single transformant colonies were grown for 3-5 hours in LB containing 50 μg/mL carbenecillin, shaking at 225 rpm, 37°C and 0.5 mL of this culture was used to inoculate 100 mL of fresh LB containing 100 μg/mL ampicillin. This 100 mL culture was grown overnight with shaking at 225 rpm, 37°C for 12-16

hours, transferred to 4×50 mL sterile Falcon tubes and cells were collected by centrifugation for 10 minutes, 3750 ×*g*, 4°C. The cell pellet was gently resuspended with a Pasteur pipette into 1 L of fresh LB containing 100 μg/mL ampicillin and grown with shaking at 225 rpm, 37°C, for 1 hour before protein expression was induced by addition of a concentrated, filter-sterilized IPTG solution to a final IPTG concentration of 0.1 mM. After 4 hours, the cells were harvested by centrifugation, 5000 ×*g*, 20 minutes, 4°C, and then stored at -80°C until purification was carried out.

To obtain ^{15}N-labeled protein, M9 minimal supplemented with 1 g/L ^{15}N-NH_4Cl was used in place of nutrient rich LB media from the 100 mL overnight culture step onwards.

4.5.2 Purification of GST-Fyn-SH3

To initiate purification of the GST-fusion protein, the cell pellets were thawed on ice and 10 mL of binding buffer (PBS with 1% Triton X-100, pH 7.3) was added and supplemented with a spatula tip of DNase I (Boehringer) and 100 μL of protease inhibitor cocktail (Sigma). Cells were resuspended and then lysed by two passes through a French press. The resulting cell lysate was centrifuged at 25,000 ×*g* for 1 hour and the supernatant was syringe-filtered through a 0.45 μM filter.

Approximately 2 mL of Glutathione-Sepharose 4B beads (GE Healthcare) were placed in a 15 mL Falcon tube and equilibrated by addition of 10 mL of binding buffer. The beads were pelleted by centrifugation at 500 ×*g* for 5 minutes, the buffer removed, and the procedure was repeated twice more. The cell lysate supernatant was added and mixed for 30 minutes with end-over-end rotation at ambient temperature. The beads were pelleted by centrifugation, and the supernatant removed. Fresh binding buffer was added (10 mL) and centrifuged again. The

beads were again washed with binding buffer and centrifuged, then repeated two more times. Elution buffer, which consisted of 50 mM Tris·HCl, 10 mM reduced glutathione, 1% Triton X-100, pH 8.0, was added in the amount of 2 mL to the beads. The resulting slurry was rotated end-over-end overnight at ambient temperature.

The next day, the beads were pellet by centrifugation at 500 ×*g* for 5 minutes, and approximately 2 mL of solution containing the liberated GST-fusion protein was removed and collected. The beads were slurried again with another 2 mL of elution buffer and immediately centrifuged. After the supernatant was collected, the beads were slurried with a final addition of elution buffer and centrifuged a final time. All three supernatants had aliquots removed for analysis by SDS-PAGE, then were pooled for a total volume of ~6 mL. The protein was dialyzed against 3×1L of buffer containing 20 mM K phosphate, 75 mM NaCl, 0.5 % Triton X-100, pH 7.4 to remove the glutathione. The dialyzed GST-Fyn-SH3 protein was stored at 4°C and the concentration was determined by BCA assay.

4.5.3 Purification of Fyn-SH3 (unlabeled or ^{15}N labelled) and GST Proteins

The purification procedure for Fyn-SH3 and GST was begun essentially in the same way as for the GST-Fyn-SH3 fusion as detailed in the previous section, up until after the third wash with binding buffer. After this step, Triton X-100 was removed by three more successive washing/centrifugation steps using PBS (binding buffer without detergent). Afterwards, 2 mL of PBS with 100U of thrombin protease (GE Healthcare) was added, and the bead slurry was rotated end-over-end at ambient temperature overnight. The beads were centrifuged 500 ×*g* for 5 minutes, and the supernatant was collected. Fresh PBS was added, the beads were slurried and

immediately centrifuged. The supernatant was collected and the process was repeated a third time. The supernatants were pooled to a total volume of ~6 mL.

The still-bound GST protein was removed from the beads with elution buffer using the same method as for isolating the full-length uncleaved GST-Fyn-SH3, starting with incubation with 2 mL of elution buffer and incubating overnight with end-over-end-rotation.

4.5.4 Construction, Expression and Isolation of the NΔ9-U24 – a Deletion Mutant of U24 with the 9 N-terminal Amino Acids Removed

The U24 lacking the 9 amino acids at its N-terminus (MDPPRTPPS removed) was obtained by performing site-directed mutagenesis on plasmid encoding wild-type U24, designated pMAL-p2x-U24 (see Chapter 2 for details), which expresses U24 protein at the C-terminus to a hexahistine tag and maltose binding protein, MBP-6×His-U24. Procedures were carried out according to instructions in the Quikchange II Site-Directed Mutagenesis Kit (Stratagene). Briefly, mutagenic primers were designed with the following sequences: 5'-catcatcacagcagcggcctggtgccgcgcggcagctactccgaagttctg-3' (forward primer) and 5'-gtgcggggaaacctgaccgcacataacgtccatcatcagaacttcggatgagctgccgcg-3' (reverse primer). After PCR was carried out, parental plasmid was digested with 10 U of *Dpn*I restriction endonuclease (Invitrogen) and the amplified mutagenic plasmid was used to transform XL1-Blue *E. coli*. Transformed *E. coli* was plated on LB-agar plates containing 50 μg/mL carbenecillin and incubated overnight at 37°C. Single colonies were selected for colony-PCR using the primers pMAL-seq and pMAL-seqrv (sequences listed in Table 2.1). Amplified reactions were run on agarose gel electrophoresis and bands of smaller size than wild-type control plasmid reactions were suggestive of successful mutagenesis in those colonies. These colonies were selected for

growth in 5 mL of LB containing 50 μg/mL carbenecillin overnight at 37°C, shaking at 225 rpm. Plasmids were isolated using QIAprep Spin Miniprep Kits (Qiagen) and sent for sequencing at the NAPS Unit, University of British Columbia, Vancouver, BC.

Purification was carried out in the same fashion as was done for wild-type U24 (see Materials and Methods, Chapter 2). Mass of the isolated mutant NΔ9-U24 protein was obtained by MALDI-TOF MS, and confirmed that the protein had the desired mutation, having an N-terminal sequence truncated of 9 amino acids (MDPPRTPPS) and beginning with the sequence GSYSEVL.

4.5.5 GST-Fyn-SH3 Pull-down Assays with Full-length U24 and Mutant NΔ9-U24

In separate microfuge tubes, 30 μL of Glutathione-Sepharose 4B beads were added and equilibrated by adding 1 mL of pull-down buffer containing 20 mM K phosphate, 75 mM NaCl, 0.5 % Triton X-100, pH 7.4 with centrifugation at 2000 rpm in a microfuge for 5 minutes at 4°C. The buffer was removed, and 1 mL of fresh buffer was added and centrifuged again. This procedure was carried out a third time. To the equilibrated beads, 30 μL of GST or 15 μL of GST-Fyn-SH3 were added, GST stock concentration had been determined to be 1.52 mg/mL and GST-Fyn-SH3 was 1.22 mg/mL. Pull-down buffer was added to a final volume of 500 μL with the bead slurry. Afterwards the beads were pelleted by centrifugation, and rinsed 3 times with 0.5 mL of pull-down buffer with intermittent centrifuging and replacing with fresh buffer. Stock solution of either wild type U24 or mutant NΔ9-U24 (0.15 mg/mL protein in pull-down buffer) was added in a volume of 500 μL to the beads, and the slurry was mixed again with end-over-end rotation for 30 minutes at 4°C. The beads were pelleted by centrifugation and the supernatant was removed. The beads were washed with three successive rounds of 0.5 mL of

Glascow Lysis Buffer (GLB) [292], which is 10 mM PIPES·NaOH, 120 mM KCl, 30 mM NaC1, 5 mM $MgC1_2$, 1% Triton X-100, 10% glycerol, with centrifuging and removal of supernatant before each addition of fresh buffer. The beads were then mixed with 30 μL 2× Novex dye (Invitrogen) supplemented with 5% β-mercaptoethanol, vortexed briefly, then heated for 5 minutes at 95°C. A volume of 25 μL was removed and run by SDS-PAGE using a Tris-Tricine buffer system.

4.5.6 Construction of a 15-mer Peptide Representing the Polyproline-containing N-Terminus of U24

A synthetic 15-mer peptide representing the N-terminus of U24 (sequence: MDPPRTPPPSYSEVL) was obtained by standard solid-phase peptide synthesis procedures [293] employing 9-fluorenylmethyloxycarbonyl (Fmoc)-based N-α-amino acid group protection. Double-coupling was required of the proline residues and the two final amino acids. Synthetic peptide was purified by preparative gradient RP-HPLC on a Waters 600 system with Waters 2996 Photodiode Array Detector with 229 nm UV detection using a Phenomenex C4 column (20 μm, 2.1×25 cm) at a flow rate of 10 mL/min, with a gradient of 25 to 45% buffer B (10% deionized water, 90% acetonitrile containing 0.1% TFA) in buffer A (90% deionized water, 10% acetonitrile containing 0.1% TFA) over 40 minutes. The peptide solution was lyophilized, and its final purity and mass was confirmed by MALDI-TOF MS.

4.5.7 Circular Dichroism

The CD experiments were conducted on a Jasco J-815 equipped with a circulating temperature-controlled water bath. The synthetic U24 peptide was dissolved in 10 mM Na

phosphate, 10 mM KCl, pH 6.5 to a final concentration of 0.3 mg/mL. A volume of 300 µL of peptide solution was placed in a cuvette with a path length of 0.1 cm. Scans were collected at a rate of 100 nm/min 0.1 nm intervals, in the 190-250 nm region. Starting at 5°C, scans were collected at 5 degree increments to 65°C. A total of four scans were collected at each temperature and averaged. Buffer blank spectra were similarly collected at each temperature, then subtracted from the corresponding peptide spectra. The CD machine units in millidegrees were converted to mean-residue-ellipticity. To characterize the PPII helical content, the spectrum at 45°C was subtracted from the one taken at 5°C [119].

4.5.8 ^{1}H-^{15}N HSQC NMR Titrations and K_D Calculations for the Fyn-SH3 Protein and U24 Peptide Interaction

Solutions of ^{15}N-Fyn-SH3 protein were prepared by successive rounds of concentration and dilution with NMR buffer [294] (10 mM Na phosphate, pH 6.0) using a 15 mL regenerated cellulose centrifugal filter device with a MWCO of 3,000 Da (Millipore). The final protein concentration was determined using an extinction coefficient of ε_{280} = 16,960 $cm^{-1}M^{-1}$, calculated using the method of Edelhoch [295] but with the extinction coefficients of Trp and Tyr determined by Pace [296] (the Protparam algorithm at www.expasy.ch). Protein solutions were centrifuged briefly and diluted to a final volume of 500 µL with NMR buffer, having 10% D_2O and a ^{15}N-Fyn-SH3 concentration of 0.5 mM. These were placed in a 5 mm NMR tube and a ^{1}H-^{15}N HSQC spectrum was recorded at 30°C using a Bruker 500-MHz NMR spectrometer (Milton, Ontario, Canada). Peptide binding was analyzed by adding small volumes of unlabeled U24 peptide (MDPPRTPPPSYSEVL) stock solution which had a concentration of 11.86 mM in NMR buffer and recording a subsequent HSQC spectrum after each new addition. A total of 15

different protein:peptide ratios were examined between 1:0 to 1:8.74. The amide chemical shifts of Fyn-SH3 were assigned according to Mal *et al.* [289]. The dissociation constant (K_D) was calculated according to the method by Morton *et al.* [294], by fitting with non-linear regression the change in chemical shift versus U24:Fyn-SH3 ratio to the following equation:

$$\Delta = \Delta_0 . \frac{([K_D]+[L]+[P]) - \sqrt{(([K_D]+[L]+[P])^2 - 4[P][L])}}{2[P]}$$

where Δ is the measured change in chemical shift and Δ_o is the is the total change in chemical shift at saturation, [*L*] and [*P*] are the ligand (U24) and protein (Fyn-SH3) concentrations respectively. Both ^{1}H and ^{15}N chemical shift changes for several amides were used in the calculation, and were fitted assuming a 1:1 binding model.

4.5.9 ^{1}H-^{15}N HSQC NMR of ^{15}N-Fyn-SH3 with Full-length U24 and NΔ9-U24

Full-length U24 or NΔ9-U24 proteins were prepared from an acetone precipitation procedure (described in Chapter 5, Materials and Methods section). Dodecylphosphocholine (DPC) (Avanti Polar Lipids) in chloroform was placed in a 5 mL round bottom flask and was dried to a thin film under nitrogen. Enough DPC was added so that a final concentration of 6 mM in 500 µL could be obtained. Residual chloroform was removed overnight under vacuum. A volume of 500 µL of 20 mM MES, pH 6.2 was used to reconstitute the lipid solution and the resulting solution was used to dissolve full-length U24 or NΔ9-U24 with extensive sonication in a water bath. The dissolved protein was transferred to a Vivaspin 500 (GE Healthcare) centrifugal filtration unit with a MWCO of 3,000, and buffer exchanged into NMR buffer according to manufacturer's protocols. After several rounds of concentration and re-dilution into NMR buffer, U24 or NΔ9-U24 was reconstituted to a final concentration of 0.15 mM together with 0.25 mM ^{15}N-Fyn-SH3, 7% D_2O, and NMR buffer to a final volume of 500 µL. These

solutions were placed in a 5 mm NMR tube and a ^{1}H-^{15}N HSQC spectrum was recorded at 30°C using a Bruker 500-MHz NMR spectrometer.

Chapter 5: Preliminary Animal Model and Structural Studies of U24

5.1 Introduction

The aim of this chapter is to present preliminary results obtained from pilot studies testing the immunogenicity of U24 in an animal model, and to summarize the ongoing efforts to characterize the structure of U24 by NMR spectroscopy. Much progress has been made on each of these two fronts, and promising data have paved the way for future studies to be carried out.

As reviewed in Chapter 1 (Section 1.3), there are a plethora of animal models that mimic various aspects of multiple sclerosis (MS) [46]. Unfortunately, due to the heterogeneous nature of MS, individual animal models cannot completely mimic all aspects of the human disease – MS is too complex a disease to be adequately represented by just one animal model. Nevertheless, experimental autoimmune encephalitis (EAE), the quintessential animal model of MS that comes in many variations, plays a critical role in our understanding of MS and development of treatments for the disease [297]. One common form of EAE is the inflammatory, demyelinating autoimmune response triggered by injection of immunogenic peptides, either those derived from neural 'self' proteins (MyBP, PLP, MOG, MAG, etc.) or 'foreign' proteins such as those from viruses and bacteria. The idea that a foreign protein can trigger an autoimmune response towards a self protein is termed *molecular mimicry* (reviewed in Section 1.5) [83], and the concept still remains as a possible mechanistic explanation for initiating or sustaining MS. The large-T antigen from the JC virus, for example, which harbours a sequence similar to MyBP, was able to cause T-cell cross reactivity which resulted in clinical signs of EAE in Lewis rats [86]. These rats exhibited mild signs of paralysis, and histological analysis revealed T-cell infiltration into the spinal cord. The peptide sequences of large-T antigen, MyBP and U24 from HHV-6 are all remarkably similar (Figure 5.1); it is therefore possible that U24 may also trigger EAE

symptoms. U24 has already been shown to trigger cross-reactivity in a sub-population of T-cells isolated from MS patients [88]. Using the recombinant form of U24 obtained from expression in *E. coli* (described in Chapter 2), the experimental goal was set to determine if U24 could also trigger EAE symptoms in Lewis rats. A positive EAE result would further support the possibility that U24 may trigger an autoimmune response in human MS.

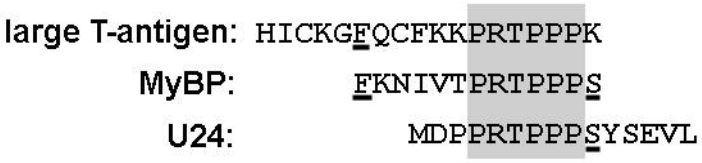

Figure 5.1 Sequence comparison of the large T-antigen from the JC-virus, human MyBP, and U24 from Human Herpesvirus Type 6A. The core identical sequence shared by all three proteins is shaded, other identical flanking residues are underlined.

The other main focus of this thesis chapter is the description of the continuing research efforts to understand more about the overall structure of U24 by NMR spectroscopy. Based on CD experiments described in chapters 2 and 4 of this thesis, a picture was formed on how U24 generally behaves as an α-helical membrane protein (in the presence of membrane-mimetic SDS detergent), and that the N-terminus of U24 appears to form a poly-proline type II helix. This data is still far from being able to give a detailed structural understanding of the protein, which NMR experiments may provide [298]. To underscore the overall difficulty in determining high-resolution structural data for membrane proteins, approximately 30% of the human genome is predicted to encode for membrane proteins [299] yet only 1% of the structures in the Protein Data Bank [300] are of these systems. At the time that this thesis is being prepared, there are 281 membrane proteins of known unique structure [301]. There are many non-trivial technical considerations which make solving a protein structure by solution NMR spectroscopy a not-so-straightforward task (reviewed in [302]). Once the initial hurdle of obtaining sufficient amounts of

pure membrane protein has been overcome, conditions must be carefully screened to enable solubilisation and optimal spectral resolution - while at the same time ensuring that the protein remains in a biologically-relevant form. Conditions for running NMR experiments must therefore be selected quite carefully. One general approach [303, 304] is to screen the protein of interest against a variety of different lipids and detergents at set pH and buffer composition for solubility, and then evaluate the subsequent quality of ^{1}H-^{15}N Heteronuclear Single-Quantum Coherence (HSQC) NMR spectra [305] for sufficiently solubilized ^{15}N-labeled protein. The goal is to observe well-resolved N-H resonances corresponding to the expected number of amides in the protein backbone (except for proline, which does not have an N-H group) and perhaps extra resonances corresponding to the sidechains of tryptophan, arginine, histidine, glutamine and asparagine (for examples of optimal spectra, see any of those for Fyn-SH3 in Chapter 4). This screening strategy was employed here for U24 where we would expect to see approximately 79 backbone resonances for the 89 amino acids where 10 residues are prolines.

5.2 Results and Discussion

5.2.1 Probing for U24 Immunogenicity in an EAE Animal Model

Full-length recombinant U24 was emulsified in Freund's Complete Adjuvant and injected into female Lewis rats. Saline solution as a negative control and guinea pig MyBP as a positive control were similarly emulsified with adjuvant and injected into separate rats. Clinical signs of the EAE, such as tail limpness and rear leg paralysis were monitored, along with weight and temperature. Only the positive control rats exhibited any sign of disease; Figure 5.1 demonstrates their clinical EAE score and associated weight loss.

U24-injected animals did not show any sign of disease, and there may be several reasons for this finding. Firstly, U24 may have aggregated in the adjuvant solution and thus prevented presentation of epitopes efficiently to the immune system. If this were the case, perhaps using the soluble synthetic peptide of the sequence MDPPRTPPPSYSEVL that is described in Chapter 4 would help circumvent such an aggregation problem. Another consideration for sample handling would be to extrude the adjuvant mixtures between two syringes, instead of performing the sonication that was done in these experiments. While there has been some evidence that sonication can improve immunogenicity in some instances[306], most protocols still favour the use of extrusion [307]. Indication that the samples used in these experiments were slightly inhomogeneous comes from the observation that there was a large variation of clinical signs in the MyBP-injected control, and the fact that one animal developed experimental autoimmune arthritis [308] (swelling in the joints) – an indicator that the animal received a higher dose of inactivated *M. tuberculosis* in the adjuvant of the injection than the other animals.

The second possible explanation of negative findings with U24 is that the sample size is too small, and more animals are needed in the study. Mao *et al.* [86] only observed mild signs of EAE in 6/12 rats when they were injected with the large T antigen form JC virus Figure 5.1, with an overall average severity of 0.7 on the EAE scoring system. A larger sample size would enable for more thorough monitoring for clinical signs. Also, some animals could be sacrificed midway through the experiment (i.e.: day 15) to analyze for inflammatory infiltrates in the spinal cord.

A third and most obvious explanation is that the U24 protein is simply unable to trigger EAE in Lewis rats. Antibodies and Major Histocompatibility Complex (MHC) molecules require stringent sequence and/or structure in peptides to enable their binding. While U24 has a

sequence similarity between MyBP and large-T antigen of the JC virus, it may not fulfill binding requirements to bind immune-recognition molecules that trigger cross-reactivity. On the other hand, it is possible that U24 could be recognized through clonal expansion, or epitope spreading (see Section 1.4), and in this case, U24 may exacerbate already-induced EAE symptoms rather than act as an initiator. Ultimately, a lack of ability for U24 to cause EAE further strengthens the hypotheses presented in Chapters 3 and 4, that U24 may have more of a subtle signal interference role (MAPK and Fyn tyrosine kinase recognition) rather than a direct immunologic role in myelin disease pathology.

5.2.2 Solubility Trials and ^{1}H-^{15}N-HSQC Solution NMR

Three methods to avoid having Triton X-100 in a final protein sample were summarily evaluated: removal by polystyrene beads or acetone precipitation, and use of an alternative detergent, 3-[(3-Cholamidopropyl)dimethylammonio]-1-propanesulfonate (CHAPS). The reason for Triton X-100 avoidance in NMR samples is because poor spectral quality normally is the result [304]. Triton X-100 is used at concentrations of 0.5% w/v in the buffers used in the purification of U24 (described in Materials and Methods of Chapter 2), and is not readily removed by dialysis because it has a low critical micelle concentration (CMC) of 0.019% w/v or 0.3 mM [309]. Dilution past the CMC and then dialysis would not be economically efficient, since such a large volume of dilutant and a great deal of dialysis tubing would be required. CHAPS was therefore evaluated as a substitute for Triton X-100, because it has a much higher CMC of 0.4% w/v or 6.4 mM [310] and is readily dialyzable. It was found that 1% was effective in solubilizing the fusion expressed in C41(DE3) cells, and that it could be purified on a Ni affinity

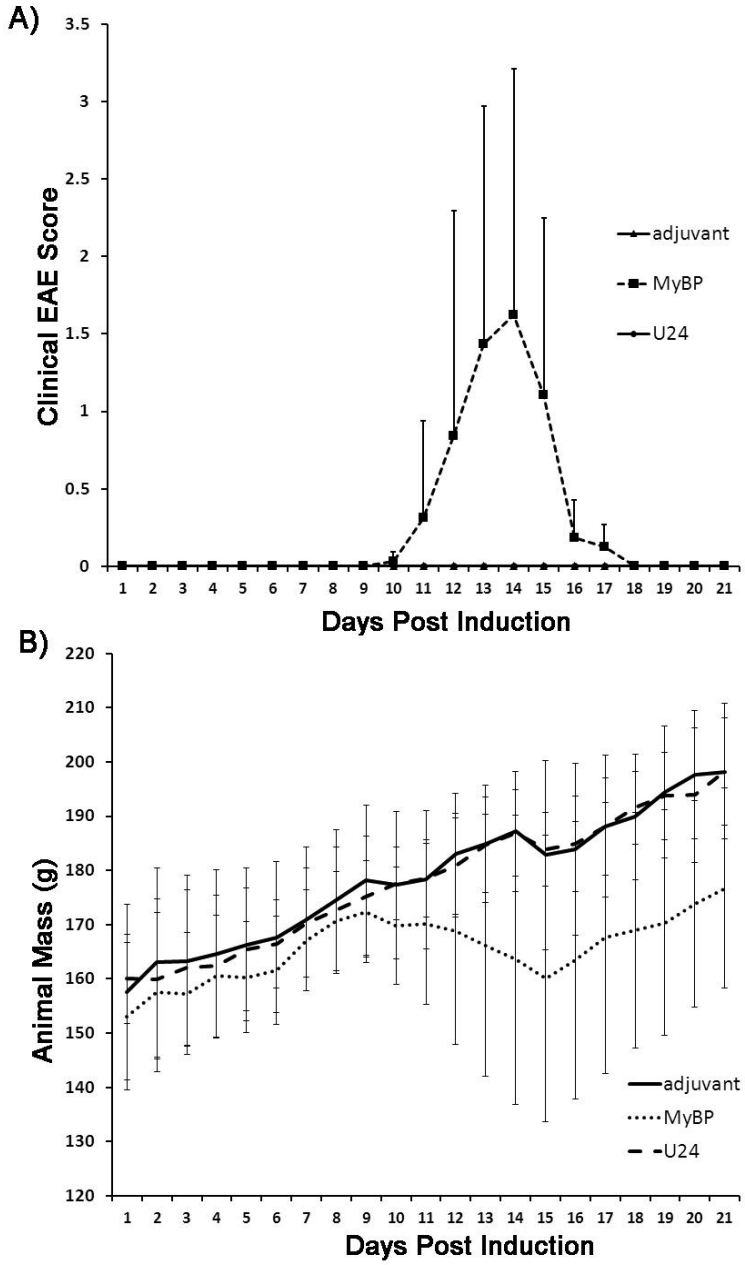

Figure 5.2 Test of U24 immunogenicity – experimental autoimmune encephalitis experiments on female Lewis rats. A) EAE score chart. MyBP (positive control) induced varying levels of clinical signs of EAE, whereas adjuvant alone (negative control) did not produce any EAE symptoms; U24 was not found to induce any detectable symptoms of EAE. B) Animal masses corresponding to EAE scoring. Weight loss is consistent with EAE symptoms seen in MyBP-injected animals. (Standard deviation is from n=4 for adjuvant, MyBP; n=3 for U24.)

column that was equilibrated with buffer containing 0.1% CHAPS. Once eluted, brought to 0.5% CHAPS, and dialyzed (to remove salt, not CHAPS at this point) the protein was digested with 50 U of thrombin. Digestion was inefficient, as only approximately half of the protein was cleaved. The largest obstacle presented itself when the protein was rerun on the Ni column to isolate the U24 in the flow-through fraction – the uncleaved MBP-6×His-U24 bound very poorly and thus flowed through the column along with U24. It is possible that under the low salt conditions (~ 75 mM NaCl) CHAPS acted as an ionic interfering substance that prevented the Histag from binding to the resin, a result that was seen in the purification of rat neurotensin receptor[311]. These conditions were also not favourable for thrombin digestion. Careful adjustment of salt and CHAPS concentration would be needed to enhance the binding of the Histag-containing proteins to the column after cleavage, as well as to improve thrombin digestion of the fusion. The method of using CHAPS in place of Triton X-100 was deemed promising, but it was abandoned to evaluate procedures that required less trouble-shooting.

The second method that was attempted to remove Triton X-100 was polystyrene beads. This approach consistently resulted in approximately half of the sample being lost (as determined by protein assay). It is possible that sample loss is due primarily to the precipitation of the protein and its adsorption into the beads in the slurry. One way to avoid precipitation may be to remove the Triton X-100 by running the protein solution through a column of the polystyrene beads, then immediately adding an NMR-compatible detergent of choice. This method may take only a couple hours to complete as opposed to the overnight batch preparation that was used here. The supposition is that U24 aggregation may be time-dependent and occur after lengthy exposure in a detergent-free solution, but further testing would be required to determine if this is what is actually occurring.

Acetone precipitation was selected as the method of choice for Triton X-100 removal from the U24 samples. The method has been widely used to selectively precipitate proteins while leaving the detergent miscible with the solvent, and has been used more specifically in preparing small membrane proteins for characterization by NMR. PufX is one such an example of a membrane protein that was precipitated by ice-cold acetone prior to being reconstituted for NMR spectroscopy [312]. Precipitation of U24 by acetone also proved very efficient at avoiding protein loss, as determined by BCA protein assay.

Reconstitution of U24 protein powder after acetone precipitation, dialysis against water and lyophilisation was a difficult task. A variety of different solvents normally effective at dissolving membrane proteins did not appear to be able to dissolve U24. These solvents included trifluoroethanol, hexafluoroisopropanol and chloroform/methanol, and have been used as membrane-mimetics to stabilize the protein for NMR structural analysis [312, 313]. Since U24 dissolved readily in 2-chloroethanol at concentrations of 1 mg/mL for use in our animal studies, the solvent was tested and found to be equally effective at dissolving U24 at higher concentrations of 4 mg/mL. The use of 2-chloroethanol in NMR structural studies is rare (in part probably due to the solvent's extreme toxicity), but it has been used at a concentration of up to 4% to disaggregate the NAP-2 protein into monomers for successful solution NMR structural determination [314]. Figure 5.3 shows the HSQC spectra obtained for U24 dissolved in 90% 2-chloroethanol and 10% D_2O. The spectra reveal some well-defined N-H resonances with others broad and overlapping. Additional resonances appear when going to higher temperatures, an observation characteristic of some membrane proteins [315]. The broad overlapping spectra could be indicative of several features, such as protein aggregation and/or certain protein regions capable of adopting a mixture of different conformations.

Attempting to solubilize U24 at 4 mg/mL (~0.4 mM) concentration directly in many different aqueous conditions was initially unsuccessful. Most of the initial screens involved using 20 mM sodium or potassium phosphate buffer at pH 5.5-7.5 as a starting point, with the commonly used lipids dihexanoylphosphocholine (DHPC), dodecylphosphocholine (DPC) and the detergent sodium dodecyl sulfate (SDS) at concentrations above 100 mM. NaCl was also included at varying concentrations, up to 300 mM. Remarkably, U24 was still relatively insoluble in the relatively harsh SDS detergent at detergent concentration up to even 400 mM. An initial hypothesis was that U24 was not soluble at concentration of 4 mg/mL in an aqueous solution, but MES or MOPS containing buffers were then found to be effective at solubilizing U24 at a pH range of 6-7 (and included lipids/detergents). MES is 2-(*N*-morpholino)ethanesulfonic acid, whereas MOPS has a propane moiety instead of an ethane. We can only speculate why these buffers provided solubility enhancement over phosphate at the same pH, but it has recently been suggested that MES can bind to proteins, affecting their dynamics in solution [316]. Figure 5.4 shows the HSQC spectra of U24 solubilized in conditions used by Ellena *et al.* to solve the NMR solution structure of synaptobrevin 2 [315]. DPC was the solubilizing lipid, present at a concentration of 200 mM. Like with 2-chloroethanol, the spectra with DPC exhibits a mixture of resolved and heavily overlapped resonances. Whereas resolution appears to improve with increasing temperature, many of the expected 79 backbone resonances still appear to be absent.

Several other lipids/detergents were attempted with U24 for HSQC study. There have been several successes mixing DPC and other detergents to modulate spectral quality by reducing protein aggregation associated with using DPC alone, for example, DPC/SDS at 5:1

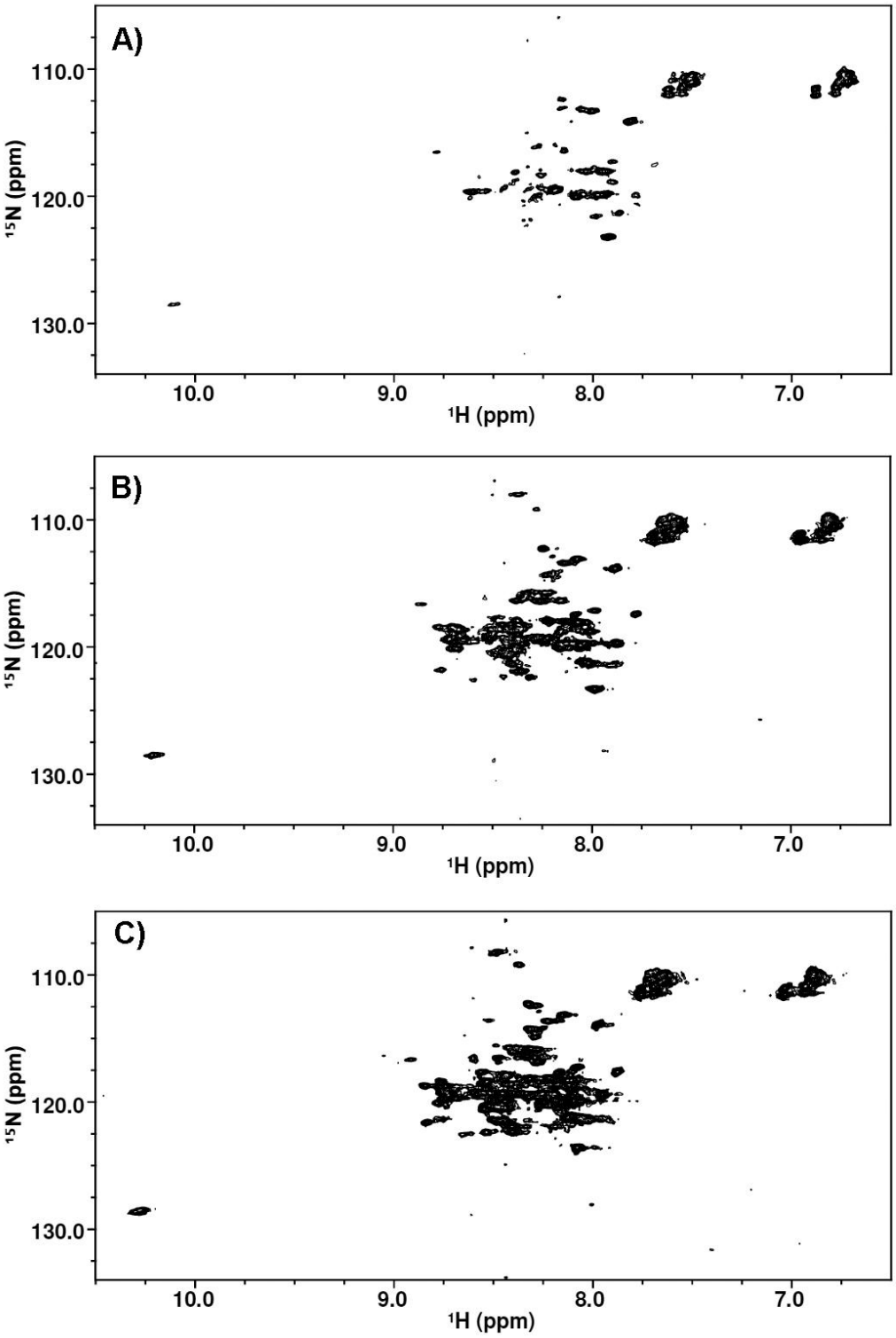

Figure 5.3 ^{1}H-^{15}N HSQC spectra of ^{15}N-labelled U24 (~0.4 mM) in 90% 2-chloroethanol, 10% D_2O at A) 17°C; B) 25°C; C) 40°C. As is characteristic of helical membrane proteins, it appears that increasing temperature improves detection of N-H resonances of U24.

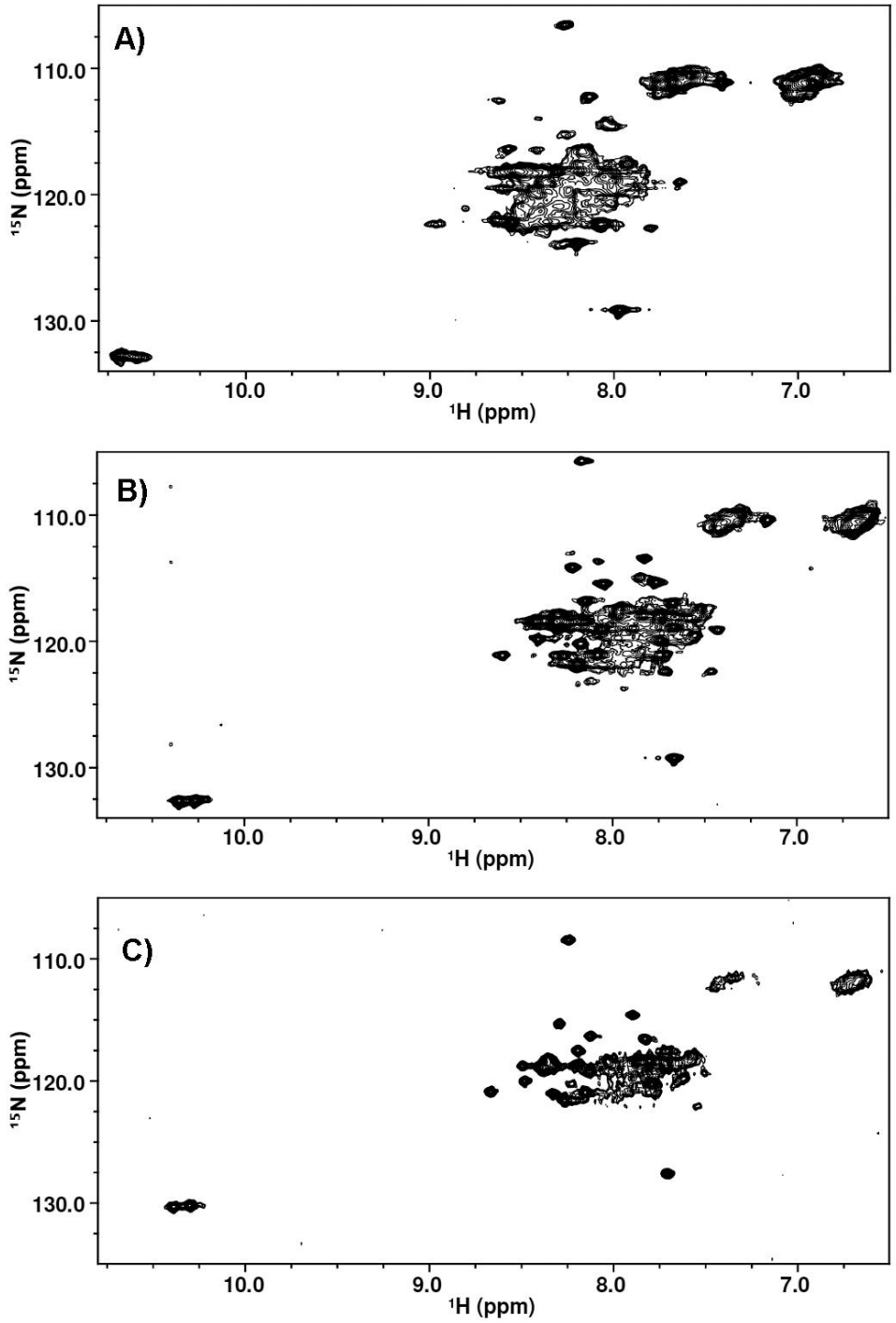

Figure 5.4 ^{1}H-^{15}N HSQC spectra of ^{15}N-labelled U24 (~0.4 mM) with 200 mM DPC in 20 mM MES, pH 6.0 buffer with 150 mM NaCl, 5 mM DTT, and 1 mM EDTA at A) 17°C; B) 40°C and C) 55°C. Line widths sharpen for certain resonances at higher temperatures, yet other resonances disappear. The two closely-clustered resonances at >10 ppm on the ^{1}H scale likely correspond to the N-H resonances of the side chains of U24's two tryptophans.

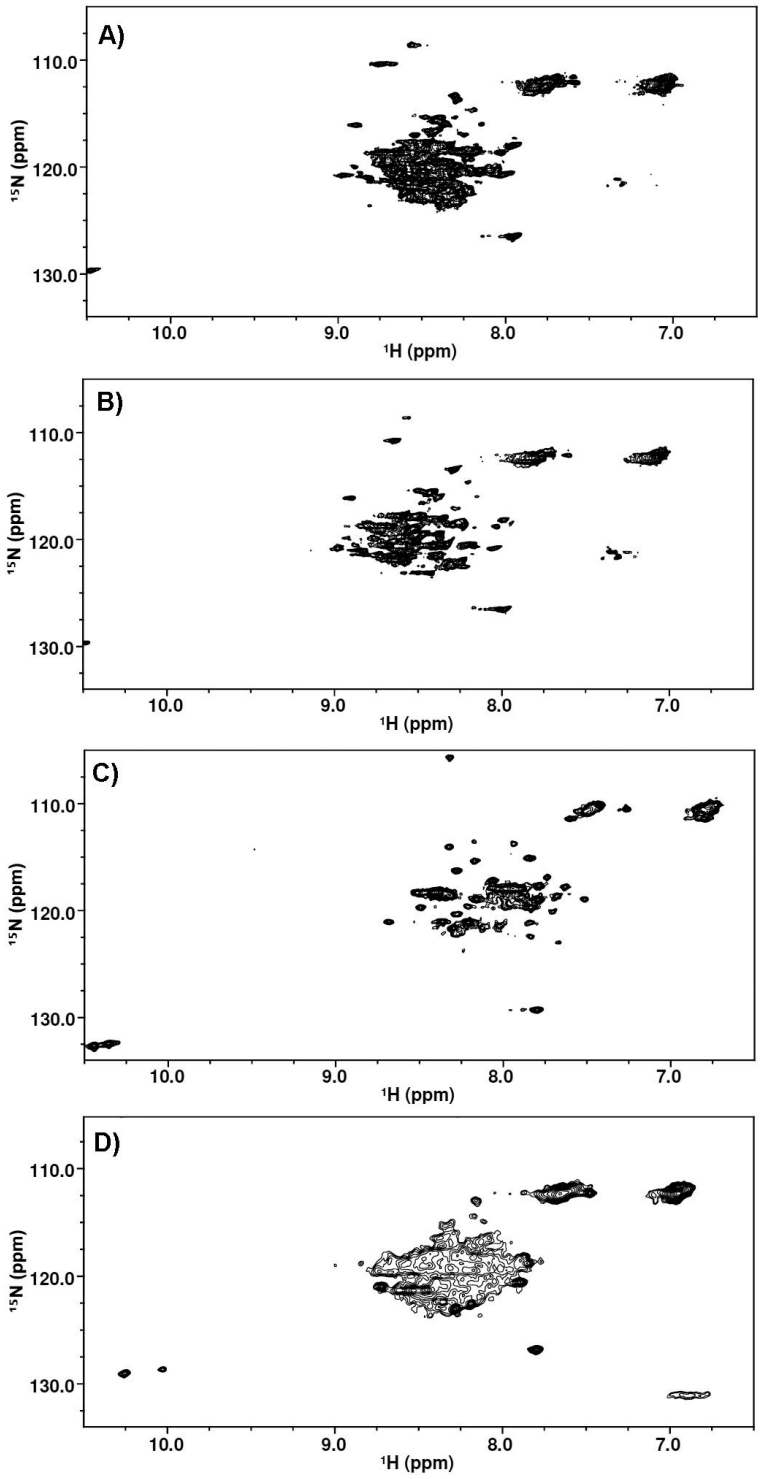

Figure 5.5 ^{1}H-^{15}N HSQC spectra of ^{15}N-labelled U24 (~0.4 mM) at 40°C in A) 30 mM SDS/150 mM DPC in 20 mM Na phosphate, pH 7, 5% D2O; B) same as A), but included 1 mM DTT; C) 16.6 mM LDAO/150 mM DPC in 20 mM MES pH 6.2, 10% D_2O.

mol/mol [317] and DPC/ lauryldimethylamine-oxide (LDAO) at 9:1 [318]. Using these conditions, the spectra for U24 shown in Figure 5.5A-C were obtained. Figure 5.5A&B are the spectra for the DPC/SDS mixture ± 1 mM DTT reducing agent, respectively. Knowing that U24 has a potential disulfide bond (discussed in Chapter 2), the desire was to see if its presence in the protein had any effect on the quality of the HSQC spectrum. The addition of DTT had marginal effect on the spectra. Of note is that phosphate buffer was used in the DPC/SDS samples, despite the protein having limited solubility in this buffer; interestingly, clarification by centrifugation demonstrated that there was at least some protein that could be solubilized, as evidenced by the spectra that were obtained. The DPC/SDS mixture appeared to give different spectra than for DPC alone at similar temperatures, and the same observation can be made for U24 in the DPC/LDAO mixture. This latter mixture appeared to give the best resolved resonances of all conditions attempted (Figure 5.5C). The lipid lysopalmitoyl phosphatidylcholine (LPPG) was also attempted as it has been previously touted as a detergent capable of producing high-quality well-resolved HSQC spectra of membrane proteins [304]. Unfortunately, this was not the case for U24, where the spectra were broad and overlapped, possibly indicating aggregation and/or unstructured protein (Figure 5.5D).

5.2.3 Prediction that U24 is Partially Disordered

The program PONDR VL-XT uses databases of CD, NMR, and X-ray crystallography data for disordered proteins to predict ordered and disordered regions of proteins based on their primary amino acid sequence [319]. The software has been used in the context of high-throughput screening to preferentially select targets that are predicted to be ordered in structure [320]. As shown in Chapter 2, far-UV CD data for U24 in membrane-mimetic detergent SDS shows that

the protein adopts an α-helical conformation, and the data shown in Chapter 4 for the N-terminal peptide of U24 suggests that the region is largely disordered – but can transiently form a polyproline type II helix. PONDR results suggest that the first 20 of the 87 amino acids of U24 are highly disordered. Other regions of the protein may also be somewhat disordered, with only the predicted transmembrane domain (amino acids 57-79) attaining highly ordered structure.

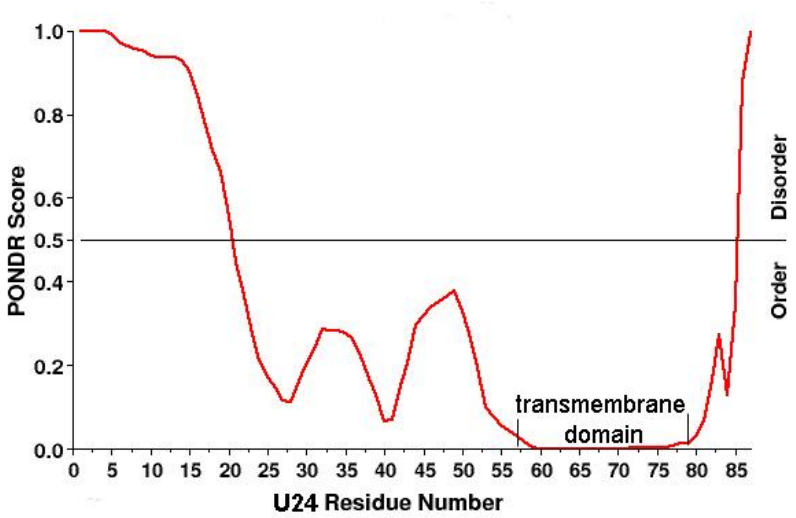

Figure 5.6 PONDR VL-XT [319] scoring for the U24 primary sequence. The N-terminal 20 amino acids are largely disordered; only the transmembrane domain (residues 57-79) are predicted to be highly ordered.

5.3 Summary

This chapter described preliminary results for the U24 protein in two different areas of study: testing if U24 is capable of causing EAE (an MS disease mimic) in an animal model and structural analysis of U24 by NMR spectroscopy.

U24 was not found to be able to initiate EAE disease symptoms in Lewis rats, but this result should not be interpreted as conclusive; a larger number of rats, different sample handling procedures, use of a short peptide instead of full-length protein, and histological analysis may yet demonstrate different findings. However, lack of a positive immunologic result strengthens the

hypothesis that U24 alternatively contributes to disease mechanisms by interfering with signal modalities governed by MAPK, Fyn tyrosine kinase, and myelin basic protein that are important for efficient myelination.

The ^{1}H-^{15}N HSQC results for U24 indicate that the protein may have regions that are largely disordered and/or that the protein is partially aggregated. Results obtained by Sullivan *et al.* [198] suggest that U24 expressed in native mammalian cells is heavily postranslationally modified (with unknown modifications), and it is possible that these modifications (i.e.: disulfide bonding, N-glycosylation, phosphorylation, etc.) may need to be present to confer structural stability. The observation that different conditions yield different quality spectra suggests that continued screening may yet further improve spectral quality and peak count. Labelling the protein with ^{13}C may provide better resolved spectra through the use of higher dimensional NMR datasets. Studying of the protein in piecewise truncated segments (i.e.: cytoplasmic vs. transmembrane) has also been a useful strategy for gleaning specific structural information about a protein that has differential ordered and disordered regions [315]. *In silico* prediction suggests that U24 is largely disordered at the N-terminus, which is in good agreement with our experimental results in previous chapters highlighting the possibility of U24 acting as a signal domain *in vivo* (binding to multiple protein targets, being phosphorylated, etc.); *intrinsic* disorder is common in proteins implicated in cell signaling [321]. Binding of U24 to its cognate ligands may signal disordered-to-order structural transitions that can be well observed by NMR spectroscopy.

5.4 Materials and Methods

5.4.1 Animal Model Studies

This section describes the procedures that were carried out to determine if U24 could cause experimental EAE in Lewis rats. Phosphate-buffered saline (PBS)-based injections were the negative control, and MyBP-based injections were the positive control.

5.4.1.1 Procedural Approval

All animal procedures were approved by the University of British Columbia Animal Care Committee and an Animal Care Certificate was awarded (cert# A07-0663). Additional training certificates were awarded after successful completion of the Animal Husbandry of the Laboratory Rodent Course (cert# RBH-327-08) and the on-line Animal Care Training Course (cert# 2529-07) offered by the University of British Columbia Animal Care Centre. Animals were housed in the Animal Centre at the University of British Columbia Hospital, and basic care was provided by the staff there.

5.4.1.2 Preparation of Proteins to be Injected into Lewis Rats

Approximately 8 mL of U24 protein isolate (~0.15 mg/mL protein in 20 mM potassium phosphate, 75 mM NaCl, 0.5 % Triton X-100, pH 7.4) was precipitated by addition of trichloroacetic acid (TCA) (20% w/v final) and after brief vortexing the precipitate was collected by centrifugation at 4°C at 3750×*g* for 10 minutes. The supernatant was discarded and the pellet was resuspended in 200 µL of ice-cold acetone with vortexing, then centrifuged in a microcentrifuge at maximum speed at 4°C for 5 minutes. The supernatant was discarded, the

pellet was washed again with the same volume of cold acetone, and the procedure was repeated once more for a total of three acetone washes. The pellet was air dried and resuspended in 25 mL of deionized water, then sonicated until the solution became a cloudy homogeneous suspension. The solution was then frozen at -80°C and lyophilized. The PBS solution was prepared and filter-sterilized through a 0.45 µm filter. One milligram of U24 powder was resuspended in 400 µL of PBS to a final concentration of 0.5 mg/mL protein. The U24 in this form is a milky suspension of water-insoluble protein.

To prepare a water-soluble form of U24 for injection, 10 mL of U24 isolate (~0.15 mg/mL protein in 20 mM potassium phosphate, 75 mM NaCl, 0.5 % Triton X-100, pH 7.4) was divided evenly by placing 1 mL in each of 10 microfuge tubes. Precipitation was initiated by addition of 300 µL of 72% TCA (w/v) to each tube and vortexing. Pellets were collected by centrifugation at maximum speed in a microcentrifuge at 4°C for 5 minutes. With the supernatant removed, 300 µL of ice cold acetone was added to each pellet, then vortexed and centrifuged again for 5 minutes. The acetone wash was repeated another two times. The pellets were left standing in a fume hood until dry. Protein powder was solubilized in 500 µL of 2-chloroethanol [322] with transferring and collecting into a single microfuge tube. This solution was transferred to a home-made dialysis button fitted with a 1,000 MWCO regenerated cellulose membrane and dialyzed with stirring against 2×1L of deionized water at 4°C over 48 hours.

One milligram of guinea pig myelin basic protein (MyBP, Sigma) was dissolved in 2 mL of filter-sterilized PBS for a final concentration of 0.5 mg/mL. Solutions of either water-soluble or insoluble U24 had concentrations of 2.5 mg/mL. A pestle and mortar were sterilized with ethanol and air dried in a biosafety cabinet. In the mortar, 40 mg of heat-killed *M. tuberculosis* powder (strain H37RA, Difco) was ground with 10 mL Freund's Incomplete Adjuvant (Difco),

to yield a Freund's Complete Adjuvant paste containing 4 mg/mL *M. tuberculosis.* Protein solutions of U24 and MyBP, as well as a PBS control solution lacking protein were added separately 1:1 (v:v) to the adjuvant for a total volume of 500 µL of each. Solutions were vortexed and thoroughly sonicated intermittently for >2 hours to maximize the homogeneity. Solutions were then sucked 100 µL each into sterile 3 mL luer-lock syringes fitted with 19-gauge needles, and the needles were replaced with 25-gauge, 3/8" needles prior to injection. Excess solution and air bubbles were pushed out, and the needle cap was replaced. Loaded syringes were stored at room temperature for use in same-day injections.

5.4.1.3 Injection and Monitoring for Clinical Signs of EAE

Female Lewis rats (6-8 weeks old, 150-170 g mass) were purchased from Charles River Laboratories and were allowed to acclimatize to their surroundings for 1-2 weeks before experiments began. The animals were handled daily to acclimatize them to the monitoring procedures. Animals were housed two to a group in three groups and given an identity label on their tail skin with indelible marker. The mass of each rat was measured and recorded daily. Also recorded daily was the measurement of skin temperature by use of an infrared thermometer. To initiate injections, animals were calmed by wrapping their head in a towel and the site of injection at the base of the tail was shaved and swabbed with isopropyl alcohol. As an alternative to towel-wrapping, particularly skittish animals were subdued with a general anaesthetic supplied by the Animal Care Facility prior to shaving and injections. The two animals of each group were given subcutaneous injections at the base of the tail with 100 µL of adjuvant mixed with either of the PBS, MyBP, or U24 solutions. The identity of each group was kept blinded to the observer until the end of the experiment.

Clinical scoring for EAE was done on a five-point scale as follows: 0 – asymptomatic; 0.25 – paralysis in the distal tail; 0.5 – limp tail; 1 – ataxia; 2 – hind limb paresis; 3 – hind limb paralysis; 4 – tetraplegia; 5 – moribund. After injection, animals were monitored for clinical signs, weighed and had their temperature taken twice daily. If an animal`s clinical score was between 2-3, or if they required manual feeding, they were monitored three times each day. If an animal`s basal temperature fell more than 2°C or if their weight decreased by 20%, they were euthanized according to procedures approved by the Animal Care Committee.

5.4.2 NMR Structural Studies

In this section, experimental details are described in which the U24 protein is screened for optimal conditions for use in ^{1}H-^{15}N-HSQC NMR. Triton X-100 is useful for purification procedures but must be removed due to its tendency to generate poor protein NMR spectra [304]. Once removed, protein must be adequately solubilized in an NMR-compatible detergent or lipid; protein concentration, buffer composition, temperature, pH and other parameters must be critically evaluated in order to obtain quality NMR spectra.

5.4.2.1 Acetone Precipitation

To 10 mL U24 protein isolate (~0.15 mg/mL protein in 20 mM potassium phosphate, 75 mM NaCl, 0.5 % Triton X-100, pH 7.4), ice cold acetone was added to a final total volume of 50 mL (80 % acetone v/v). After vortexing, flocculent white precipitate could be observed. The suspension was let stand for two hours at -20°C, then centrifuged at 3750×*g* at 4°C for 10 minutes. The pellet was washed with cold acetone and centrifuged twice more before being allowed to air dry in the fume hood. The pellet was resuspended in 30-35 mL of deonized water

and placed in a sonicating water bath until a thinly clouded homogenized solution was the result. The cloudy solution was transferred to regenerated cellulose dialysis tubing (Spectrapor) with a MWCO of 1,000. The solution was dialyzed at 4°C with stirring against 3×1L of Milli-Q deionized water over a 24 hour period.

5.4.2.2 Buffer Exchange Using Polystyrene Beads

Approximately 1 g of Biobeads SM-2 was transferred to a beaker containing 50 mL of 20 mM phosphate, 75 mM NaCl, pH 7.4. The beaker was placed under vacuum and stirred overnight. Residual floating beads were discarded along with the solution and the wet beads were collected and determined to have a wet weight of 1.5 g. The wet beads were placed in 8 mL of U24 protein isolate (~0.15 mg/mL protein in 20 mM potassium phosphate, 75 mM NaCl, 0.1 % Triton X-100, pH 7.4) and gently stirred overnight at 4°C. The result was a cloudy solution of protein precipitate that could be removed from the beads with a Pasteur pipette. The suspension was transferred to cellulose dialysis tubing with a 1,000 MWCO and dialyzed against 3×1L changes of deioninzed water over 24 hours. The protein content of the dialyzed sample was measured by BCA assay (Pierce).

5.4.2.3 Purification of U24 in CHAPS – a Low CMC Detergent

Expression of MBP-6×His-U24 was carried out from the pMAL-p2x-U24 expression vector in 1L of M9 minimal media culture, and purification was initiated essentially as described in Chapter 2 of this thesis, except that CHAPS (3-[(3-cholamidopropyl)dimethylammonio]-1-propanesulfonate) was used in place of Triton X-100 in the purification buffers, and 1 mM DTT

was included as well. The solubilization buffer contained 1% CHAPS and column buffers had 0.1% CHAPS. CHAPS has a critical micelle concentration of ~ 5 mM (0.3%) in salt-containing solutions [310]. After elution of MBP-6×His-U24 from the 5 mL Ni^{2+}-affinity Histrap column, solid CHAPS was added to 0.5%, above the CMC. The protein was dialyzed against detergent-free buffer. Thrombin was added and the protein was digested as previously described. The protein digest was reloaded on the Histrap column, and the flowthrough was collected. SDS-PAGE was used to analyze the efficiency of initial solubilization of MBP-6×His-U24 from the cell lysate, and each subsequent purification step.

5.4.2.4 Solubility Screens and ^{1}H-^{15}N-HSQC NMR of U24

Starting with lyophilized U24 powder obtained through acetone precipitation (see Section 5.4.2.1), approximately 1-2 mg of protein was subjected to a variety of solution conditions in order to resolubilize the protein in conditions suitable for NMR spectroscopy. This step involved mixing the protein together with select organic solvents or detergents/lipids in aqueous buffer in a 5 mL round-bottom flask. The flask was sealed with a glass plug and parafilm, and then sonicated in a water bath until solubilized, for up to 6 hours. Efficiency of solubilisation was determined by visual inspection of the samples and samples that were reasonable solubilized were centrifuged to remove any remaining particulate matter, then placed in a 5 mm NMR tube. The volume was final volume was adjusted to 500 μL. The ^{1}H-^{15}N-HSQC spectroscopy was performed [305] on either a 500 MHz Varian Unity or 600 MHz Varian Inova NMR spectrometer.

5.4.2.5 Protein Structure Order and Disorder Prediction

The relative order/disorder based on the amino acid composition of U24 was predicted by the neural network program PONDR VL-XT [319, 320] which is available from Molecular Kinetics Inc. at http://www.pondr.com.

Chapter 6: Conclusions and Future Work

6.1 Thesis Summary

This thesis presented my work to obtain a recombinant form of U24 protein from HHV-6 using an *E. coli* expression system. The motivation for initiating research on U24 stemmed from the original report on U24 by Tejada-Simon *et al.* [88], which suggested that U24 played a role in the pathogenesis of multiple sclerosis. Experimental evidence supported the hypothesis that U24 was a molecular mimic of myelin basic protein (MyBP), a protein found primarily in the central and peripheral nervous system, and that this mimicry could perhaps trigger a pathological autoimmune reaction leading to degradation of myelin, the insulation of nerve fibres. The proposed mimic region consists of a seven amino-acid stretch with sequence PRTPPPS, identical to both proteins. Their pioneering work involved the use of short synthetic peptides only, so obtaining a full-length form of the U24 protein for study was of obvious interest.

Chapter 1 of the thesis provided background information to introduce the hypothesis that U24 has a relationship to the disease multiple sclerosis (MS) on the basis of the U24 sequence similarity to MyBP. Also reviewed in the chapter was what is known about the *in vivo* function of U24 in immunomodulation of infected T-cells. Chapter 2 focused on the development of methods to obtain U24 and described some initial analysis of the isolated full-length protein. Chapter 3 summarized the study of the *in vitro* phosphorylation of U24 by Erk2 MAPK. To further characterize protein-protein interactions with U24, Chapter 4 described probing the *in vitro* interaction between U24 and the SH3 domain of Fyn tyrosine kinase, and the chapter also described experiments to investigate the structure of a U24 peptide representing the binding interface between U24 and Fyn. Finally, Chapter 5 discussed the attempted development of an

EAE model using U24, and the chapter also presented initial NMR structural data for U24, concluding with a brief prediction of U24 acting as a membrane bound protein with intrinsically disordered regions.

6.2 Overarching Experimental Conclusions

The U24 protein from HHV-6 had not previously been isolated for study prior to work begun in this thesis. The main two goals that were laid out in the Introduction have been achieved: to acquire a large amount of pure U24 protein using a heterologous *E. coli* expression system, and to see if U24 could then behave as a structural and functional mimic of MyBP on the basis of its PRTPPPS identical sequence. A yield of ~3 mg of highly pure U24 protein per litre of culture can now be obtained. It was established that use of an oxidizing strain of *E. coli*, together with a MBP-6×His dual tag could enhance protein expression at lower growth temperatures, and that formation of a disulfide linkage was not critical for protein expression. The limitation of this *E. coli*-based system is such that post-translational modifications (i.e.: glycosylation) may still need to be done to obtain a form of U24 that is comparable to that which is expressed in eukaryotic cells; U24 expressed in *E. coli* gives the expected molecular weight of 10 kDa, compared to the heterogeneous ~20 and 23 kDa forms expressed in mammalian cells [132]. The 10 kDa form of U24 described here behaved much like a membrane protein as expected, being highly hydrophobic and attaining up to 60% α-helical structure in the membrane-mimetic environment of SDS-detergent micelles when examined by CD spectroscopy. Despite being able to adopt a defined structure, portions of U24, especially the N-terminus, appear to be largely disordered. Structural analysis of the peptide $U24_{1\text{-}15,}$ MDPPRTPPPSYSEVL, representing the N-terminus of U24, predicted a random coil structure

and thermal denaturation studies of the peptide in conjunction with CD spectroscopy suggested the presence of a transient PPII helix. The observation that U24 has a transiently-structured polyproline region is in agreement with the hypothesis that this region is responsible for engaging in protein-protein interactions. Based on the sequence identity with MyBP, U24 was found to be phosphorylated by MAPK on the equivalent threonine, and U24 could also bind to the SH3 domain of Fyn tyrosine kinase. U24 does not appear to be as efficient as substrate for MAPK as MyBP, and U24 only very weakly binds to Fyn-SH3 (K_D = 375 μM), perhaps somewhat more weakly than has been predicted for MyBP binding to Fyn-SH3 [119].

Despite the observation that these proteins interact *in vitro*, there is still no direct evidence to show that U24 can interfere with *in vivo* MyBP functioning on the basis of sequence identity. Experimental results presented here also do not act purely as circumstantial evidence to infer a link between U24 and demyelinating mechanisms of diseases such as MS. What we have shown is that the version of U24 studied here is capable of interacting with other proteins, Fyn-SH3 and MAPK, on the basis of its sequence shared with MyBP, thus making this version of U24 suitable for use in further *in vitro* protein-protein interaction studies, and for guiding *in vivo* work. Demonstrating that U24 can interact with some of the same molecules as MyBP definitely warrants further study to determine what *in vivo* relevance these interactions have in terms of the dynamic biochemical processes of myelin maintenance and repair - for which both Fyn and MyBP are critical. Only through more research can a definitive relationship between U24 and MS be established.

Methodology established here to obtain a high yield of U24 protein makes many more interesting biophysical experiments possible; for example, preliminary NMR structural studies of U24 have shown promise.

Initial attempts to establish an EAE model of U24 failed; direct injection of U24 into animal subjects did not appear to cause symptoms of demyelination. While U24 might not be capable of inducing EAE, this negative result is not to be taken as conclusive, as a larger number of test subjects are needed and different sample preparation procedures should be attempted. Taken with the other results showing how U24 can interact with Fyn-SH3 and be phosphorylated by MAPK, it is tempting to speculate that U24 may play more of a signal-interference role in demyelinating mechanisms, rather than a direct immunological one (i.e.: by triggering T-cell and/or antibody cross-reactivity against MyBP).

6.3 Future Work

While much of this thesis centred on the comparison of U24 and MyBP and a relationship to multiple sclerosis, it should be reiterated with emphasis that much more study is needed to prove that such a connection actually contributes to disease. The *in vitro* studies done here strongly suggest that U24 interacts with both MAPK and Fyn tyrosine kinase *in vivo*, but it remains to be seen. Performing *in vivo* expression of U24 in cultured oligodendrocytes followed by immunoprecipitation and probing for Fyn and MAPK is an obligatory next step. However, interactions may be weak and not be observed in this kind of experiment, especially in the case of Fyn. Therefore, monitoring of certain enzyme activity and protein levels (such as for participants in the Fyn-Rcγ pathway [49]) in the presence and absence of U24 may show what effect U24 expression has on levels of proteins that are critical to myelin development. Ultimately, MAPK and Fyn will need to be validated as *bona fide in vivo* interaction targets of U24 to further strengthen the hypothesis that U24's interference with them and with the normal functioning of MyBP contribute to demyelination in MS. A co-worker is currently performing

amylose-affinity pull-down experiments using the MBP-6×His-U24 fusion protein and T-cell lysates to probe for these and other proteins that can interact with U24.

To follow up on NMR structural studies of U24, study of the individual component cytoplasmic domain (residues 1-56) and transmembrane domain (residues 57-79) will give a greater understanding of each of these domains, such as relative disorder and lipid membrane interactions, respectively. The single Cys mutants of U24 (C21S and C37S, described in Chapter 2) may be useful for attaching thiol-reactive spectroscopic probes to examine local conformation and dynamics of the protein. Specific focus on examining the mammalian cell expressed U24 will also characterize why this version of the protein appears at 20 and 23 kDa by SDS-PAGE, whereas the *E. coli* expressed protein runs at the expected 10 kDa. Perhaps refolding of U24 and adding posttranslational modifications such as N-glycosylation and intermolecular disulfide bonding to form a dimer are still needed to attain a stable, physiologically-relevant form of U24.

Other future work will definitely centre on studying the underlying molecular mechanisms that U24 engages in to help HHV-6 to avoid detection and elimination by the immune system. Screens of SH3 and WW domains for binding to U24 using commercially-available kits (Affymetrix, Ltd.) can also provide leads as to which domains bind tightly to U24. Sullivan *et al.* [132] confirmed through mutagenesis that the PPXY motif in U24 is critical its activity in blocking endosomal recycling. Interestingly, additional mutation of the threonine in the MAPK phosphorylation site or mutation of the first proline in the PXXP motif of the SH3 binding site had no effect on this recycle-blocking activity. While MAPK and SH3 domain-containing protein (such as Fyn) may not be essential for U24's endosomal blockade actions, they may still provide an added level of control. Versions from U24 from HHV-6A, HHV-6B

and HHV-7 all have similar type of activity, but the actual activity levels may be somewhat different. This speculation is linked to the fact that the regions flanking the essential PPXY sequence are not conserved and may as a result exhibit differential binding to regulator molecules. Because its sequence lacks the PXXP core motif, U24 from HHV-7 may especially lack the ability to be efficiently phosphorylated by MAPK and to bind to SH3 domains like Fyn, and work is underway by a co-worker to see if this is the case.

Sullivan *et al.* [132] alluded to U24 being capable of binding to a variety of WW domain containing proteins (that recognize the PPXY motif) but did not speculate which one(s) might be the actual *in vivo* binding target. The Nedd4 ubiquitin ligase is therefore a good candidate, especially since it binds to a sequence in the sodium channel ENaCγ [183] that is similar to U24 (ENaCγ: PGTPPPKY; U24: PRTPPPSY; phosphorylation site underlined), and ubiquitin

Figure 6.1 Sequences of the first 15 amino acids from U24 proteins of HHV-6A, -6B and -7, aligned via the conserved TPPPSY region (shaded). U24 from HHV-6A and 6B only differ at one position (Arg/Pro substitution), but U24 from HHV-7 also lacks the optimal MAPK phosphorylation sequence PX(T/S)P and the PXXP SH3-binding motif. Phosphorylation at the threonine of the minimal MAPK recognition site (T/S)P is still possible.

ligase activity is also implicated in endosomal recycling [323]. Phosphorylation of the equivalent threonine in ENaCγ resulted in tighter binding of MAPK to the protein, and it can be predicted that phosphorylation of U24 may also result in enhanced Nedd4 binding [183].

Pull-down assays and NMR titration experiments as described in Chapter 4 of this thesis are a logical next step, now using the physiologically-relevant WW domain binding partner(s) required by U24 to block endosomal recycling. Understanding more about this interaction from a structural point of view may lead to the design of novel therapeutics which block the U24/WW interaction, thereby helping the immune system to detect and eradicate the persistent HHV-6 virus – for which there is currently no vaccine or cure.

Bibliography

[1] J. H. Noseworthy, C. Lucchinetti, M. Rodriguez, B. G. Weinshenker, Multiple sclerosis. *N Engl J Med* **2000**, *343*, 938-952.

[2] C. Confavreux, S. Vukusic, T. Moreau, P. Adeleine, Relapses and progression of disability in multiple sclerosis. *N Engl J Med* **2000**, *343*, 1430-1438.

[3] A. Auty, C. Belanger, J. P. Bouchard, D. G. Brunet, P. Duquette, G. S. Francis, M. S. Freedman, W. J. Hader, S. C. Marshall, C. E. Maxner, L. Metz, T. J. Murray, P. O'Connor, J. Oger, J. E. Paulseth, W. E. Pryse-Phillips, G. P. A. Rice, G. Alcock, R. Amaoutelis, P. Lewis, L. Armstrong, D. Boucher, B. Davis, C. Edger, D. Hiser, J. Lesaux, P. Vandervoort, M. Hader, S. McGuiness, W. Morrison, J. Nelson, D. Pack, B. Neufeld, J. A. Haynes, M. Perera, J. Poirier, K. Stevenson, M. Riviere, R. Tretiak, M. Belanger, S. Laplante, J. F. Grenier, G. Canadian Burden Illness Study, Burden of illness of multiple sclerosis: Part I: Cost of illness. *Canadian Journal of Neurological Sciences* **1998**, *25*, 23-30.

[4] G. Rosati, The prevalence of multiple sclerosis in the world: an update. *Neurological Sciences* **2001**, *22*, 117-139.

[5] C. A. Beck, L. M. Metz, L. W. Svenson, S. B. Patten, Regional variation of multiple sclerosis prevalence in Canada. *Multiple Sclerosis* **2005**, *11*, 516-519.

[6] A. Y. Poppe, C. Wolfson, B. Zhu, Prevalence of Multiple Sclerosis in Canada: A Systematic Review. *Canadian Journal of Neurological Sciences* **2008**, *35*, 593-601.

[7] S.-M. Orton, B. M. Herrera, I. M. Yee, W. Valdar, S. V. Ramagopalan, A. D. Sadovnick, G. C. Ebers, Sex ratio of multiple sclerosis in Canada: a longitudinal study. *The Lancet Neurology* **2006**, *5*, 932-936.

[8] D. A. Dyment, G. C. Ebers, A. Dessa Sadovnick, Genetics of multiple sclerosis. *The Lancet Neurology* **2004**, *3*, 104-110.

[9] C. Lock, G. Hermans, R. Pedotti, A. Brendolan, E. Schadt, H. Garren, A. Langer-Gould, S. Strober, B. Cannella, J. Allard, P. Klonowski, A. Austin, N. Lad, N. Kaminski, S. J. Galli, J. R. Oksenberg, C. S. Raine, R. Heller, L. Steinman, Gene-microarray analysis of multiple sclerosis lesions yields new targets validated in autoimmune encephalomyelitis. *Nature Medicine* **2002**, *8*, 500-508.

[10] G. C. Ebers, A. D. Sadovnick, N. J. Risch, A genetic basis for familial aggregation in multiple sclerosis. *Nature* **1995**, *377*, 150-151.

[11] H. Schmidt, D. Williamson, A. Ashley-Koch, HLA-DR15 Haplotype and Multiple Sclerosis: A HuGE Review. *American Journal of Epidemiology* **2007**, *165*, 1097-1109.

[12] S. A. Bahreini, M. R. Jabalameli, M. Saadatnia, H. Zahednasab, The role of non-HLA single nucleotide polymorphisms in multiple sclerosis susceptibility. *Journal of Neuroimmunology* **2010**, *229*, 5-15.

[13] J. R. Oksenberg, S. E. Baranzini, S. Sawcer, S. L. Hauser, The genetics of multiple sclerosis: SNPs to pathways to pathogenesis. *Nat Rev Genet* **2008**, *9*, 516-526.

[14] N. Grigoriadis, G. M. Hadjigeorgiou, Virus-mediated autoimmunity in Multiple Sclerosis. *J Autoimmune Dis* **2006**, *3*, 1.

[15] A. Ascherio, K. L. Munger, E. T. Lennette, D. Spiegelman, M. A. Hernán, M. J. Olek, S. E. Hankinson, D. J. Hunter, Epstein-Barr Virus Antibodies and Risk of Multiple

Sclerosis. *JAMA: The Journal of the American Medical Association* **2001**, *286*, 3083-3088.
[16] J. L. Blond, F. Beseme, L. Duret, O. Bouton, F. Bedin, H. Perron, B. Mandrand, F. Mallet, Molecular characterization and placental expression of HERV-W, a new human endogenous retrovirus family. *Journal of Virology* **1999**, *73*, 1175-1185.
[17] P. B. Challoner, K. T. Smith, J. D. Parker, D. L. Macleod, S. N. Coulter, T. M. Rose, E. R. Schultz, J. L. Bennett, R. L. Garber, M. Chang, P. A. Schad, P. M. Sewart, R. C. Nowinski, J. P. Brown, G. C. Burmer, PLAQUE-ASSOCIATED EXPRESSION OF HUMAN HERPESVIRUS-6 IN MULTIPLE-SCLEROSIS. *Proceedings of the National Academy of Sciences of the United States of America* **1995**, *92*, 7440-7444.
[18] J.-M. Charcot, Histologie de la sclérose en plaques. *Gazette des Hôpitaux (Paris)* **1868**, *41*, 554-555, 557-558, 566.
[19] J. Murray, Prelude to the framing of a disease: multiple sclerosis in the period before Charcots Lecons. *Int MS J* **2004**, *11*, 79-85.
[20] R. Medaer, Does the history of multiple sclerosis go back as far as the 14th century? *Acta Neurol Scand* **1979**, *60*, 189-192.
[21] A. Compston, A. Coles, Multiple sclerosis. *Lancet* **2002**, *359*, 1221-1231.
[22] F. D. Lublin, S. C. Reingold, Defining the clinical course of multiple sclerosis: Results of an international survey. *Neurology* **1996**, *46*, 907-911.
[23] M. J. Tullman, R. J. Oshinsky, F. D. Lublin, G. R. Cutter, Clinical characteristics of progressive relapsing multiple sclerosis. *Multiple Sclerosis* **2004**, *10*, 451-454.
[24] V. V. Brinar, M. Habek, Rare infections mimicking MS. *Clinical Neurology and Neurosurgery* **2010**, *112*, 625-628.
[25] L. A. Rolak, J. O. Fleming, The differential diagnosis of multiple sclerosis. *Neurologist* **2007**, *13*, 57-72.
[26] C. M. Poser, D. W. Paty, L. Scheinberg, W. I. McDonald, F. A. Davis, G. C. Ebers, K. P. Johnson, W. A. Sibley, D. H. Silberberg, W. W. Tourtellotte, New diagnostic criteria for multiple sclerosis: guidelines for research protocols. *Ann Neurol* **1983**, *13*, 227-231.
[27] W. I. McDonald, A. Compston, G. Edan, D. Goodkin, H.-P. Hartung, F. D. Lublin, H. F. McFarland, D. W. Paty, C. H. Polman, S. C. Reingold, M. Sandberg-Wollheim, W. Sibley, A. Thompson, S. Van Den Noort, B. Y. Weinshenker, J. S. Wolinsky, Recommended diagnostic criteria for multiple sclerosis: Guidelines from the international panel on the diagnosis of multiple sclerosis. *Annals of Neurology* **2001**, *50*, 121-127.
[28] A. L. Hodgkin, B. Katz, The effect of sodium ions on the electrical activity of the giant axon of the squid. *The Journal of Physiology* **1949**, *108*, 37-77.
[29] B. Zalc, D. Goujet, D. Colman, The origin of the myelination program in vertebrates. *Current Biology* **2008**, *18*, R511-R512.
[30] D. W. Paty, J. J. F. Oger, L. F. Kastrukoff, S. A. Hashimoto, J. P. Hooge, A. A. Eisen, K. A. Eisen, S. J. Purves, M. D. Low, V. Brandejs, W. D. Robertson, D. K. B. Li, MRI IN THE DIAGNOSIS OF MS - A PROSPECTIVE-STUDY WITH COMPARISON OF CLINICAL-EVALUATION, EVOKED-POTENTIALS, OLIGOCLONAL BANDING, AND CT. *Neurology* **1988**, *38*, 180-185.
[31] F. Barkhof, M. Filippi, D. H. Miller, P. Scheltens, A. Campi, C. H. Polman, G. Comi, H. J. Ader, N. Losseff, J. Valk, Comparison of MRI criteria at first presentation to predict conversion to clinically definite multiple sclerosis. *Brain* **1997**, *120*, 2059-2069.

[32] F. Fazekas, R. Kleinert, H. Offenbacher, R. Schmidt, G. Kleinert, F. Payer, H. Radner, H. Lechner, PATHOLOGICAL CORRELATES OF INCIDENTAL MRI WHITE-MATTER SIGNAL HYPERINTENSITIES. *Neurology* **1993**, *43*, 1683-1689.
[33] N. A. Losseff, L. Wang, H. M. Lai, D. S. Yoo, M. L. GawneCain, W. I. McDonald, D. H. Miller, A. J. Thompson, Progressive cerebral atrophy in multiple sclerosis - A serial MRI study. *Brain* **1996**, *119*, 2009-2019.
[34] B. D. Trapp, J. Peterson, R. M. Ransohoff, R. Rudick, S. Mork, L. Bo, Axonal transection in the lesions of multiple sclerosis. *New England Journal of Medicine* **1998**, *338*, 278-285.
[35] M. H. Barnett, J. W. Prineas, Relapsing and remitting multiple sclerosis: Pathology of the newly forming lesion. *Annals of Neurology* **2004**, *55*, 458-468.
[36] C. Stadelmann, C. Wegner, W. Brück, Inflammation, demyelination, and degeneration -- Recent insights from MS pathology. *Biochimica et Biophysica Acta (BBA) - Molecular Basis of Disease* **2011**, *1812*, 275-282.
[37] J. M. Frischer, S. Bramow, A. Dal-Bianco, C. F. Lucchinetti, H. Rauschka, M. Schmidbauer, H. Laursen, P. S. Sorensen, H. Lassmann, The relation between inflammation and neurodegeneration in multiple sclerosis brains. *Brain* **2009**, *132*, 1175-1189.
[38] H. Lassmann, W. Brück, C. F. Lucchinetti, The Immunopathology of Multiple Sclerosis: An Overview. *Brain Pathology* **2007**, *17*, 210-218.
[39] C. Lucchinetti, W. Brück, J. Parisi, B. Scheithauer, M. Rodriguez, H. Lassmann, Heterogeneity of multiple sclerosis lesions: Implications for the pathogenesis of demyelination. *Annals of Neurology* **2000**, *47*, 707-717.
[40] H. L. Weiner, The challenge of multiple sclerosis: How do we cure a chronic heterogeneous disease? *Annals of Neurology* **2009**, *65*, 239-248.
[41] J. W. Prineas, E. E. Kwon, E. S. Cho, L. R. Sharer, CONTINUAL BREAKDOWN AND REGENERATION OF MYELIN IN PROGRESSIVE MULTIPLE-SCLEROSIS PLAQUES. *Annals of the New York Academy of Sciences* **1984**, *436*, 11-32.
[42] T. Berger, P. Rubner, F. Schautzer, R. Egg, H. Ulmer, I. Mayringer, E. Dilitz, F. Deisenhammer, M. Reindl, Antimyelin Antibodies as a Predictor of Clinically Definite Multiple Sclerosis after a First Demyelinating Event. *New England Journal of Medicine* **2003**, *349*, 139-145.
[43] J. Kuhle, C. Pohl, M. Mehling, G. Edan, M. S. Freedman, H.-P. Hartung, C. H. Polman, D. H. Miller, X. Montalban, F. Barkhof, L. Bauer, S. Dahms, R. Lindberg, L. Kappos, R. Sandbrink, Lack of Association between Antimyelin Antibodies and Progression to Multiple Sclerosis. *New England Journal of Medicine* **2007**, *356*, 371-378.
[44] G. A. Rosenberg, J. E. Dencoff, N. Correa, M. Reiners, C. C. Ford, Effect of steroids on CSF matrix metalloproteinases in, multiple sclerosis: Relation to blood-brain barrier injury. *Neurology* **1996**, *46*, 1626-1632.
[45] H. Lassmann, R. M. Ransohoff, The CD4-Th1 model for multiple sclerosis: a crucial re-appraisal. *Trends in Immunology* **2004**, *25*, 132-137.
[46] R. Gold, H.-P. Hartung, K. V. Toyka, Animal models for autoimmune demyelinating disorders of the nervous system. *Molecular Medicine Today* **2000**, *6*, 88-91.
[47] S. M. Molineaux, H. Engh, F. Deferra, L. Hudson, R. A. Lazzarini, RECOMBINATION WITHIN THE MYELIN BASIC-PROTEIN GENE CREATED THE

DYSMYELINATING SHIVERER MOUSE MUTATION. *Proceedings of the National Academy of Sciences of the United States of America* **1986**, *83*, 7542-7546.
[48] J. M. Kwiecien, L. T. O'Connor, B. D. Goetz, K. H. Delaney, Morphological and morphometric studies of the dysmyelinating mutant, the Long Evans shaker rat. *Journal of Neurocytology* **1998**, *27*, 581-591.
[49] C. Seiwa, M. Yamamoto, K. Tanaka, M. Fukutake, T. Ueki, S. Takeda, R. Sakai, A. Ishige, K. Watanabe, M. Akita, T. Yagi, K. Tanaka, H. Asou, Restoration of FcRγ/Fyn signaling repairs central nervous system demyelination. *Journal of Neuroscience Research* **2007**, *85*, 954-966.
[50] J. K. Kim, F. G. Mastronardi, D. D. Wood, D. M. Lubman, R. Zand, M. A. Moscarello, Multiple sclerosis: an important role for post-translational modifications of myelin basic protein in pathogenesis. *Mol Cell Proteomics* **2003**, *2*, 453-462.
[51] C. L. Vanderlugt, S. D. Miller, Epitope spreading in immunemediated diseases: Implications for immunotherapy. *Nature Reviews Immunology* **2002**, *2*, 85-95.
[52] S. D. Miller, W. J. Karpus, The immunopathogenesis and regulation of T-cell-mediated demyelinating diseases. *Immunology Today* **1994**, *15*, 356-361.
[53] M. M. Lipton, J. Freund, E. Brady, The Transfer of Experimental Allergic Encephalomyelitis in the Rat by Means of Parabiosis. *The Journal of Immunology* **1953**, *71*, 380-384.
[54] L. Ortiz-Ortiz, R. M. Nakamura, W. O. Weigle, T Cell Requirement for Experimental Allergic Encephalomyelitis Induction in the Rat. *The Journal of Immunology* **1976**, *117*, 576-579.
[55] L. P. Weiner, Pathogenesis of Demyelination Induced by a Mouse Hepatitis. *Arch Neurol* **1973**, *28*, 298-303.
[56] S. D. Miller, C. L. Vanderlugt, W. S. Begolka, W. Pao, R. L. Yauch, K. L. Neville, Y. KatzLevy, A. Carrizosa, B. S. Kim, Persistent infection with Theiler's virus leads to CNS autoimmunity via epitope spreading. *Nature Medicine* **1997**, *3*, 1133-1136.
[57] G. J. Atkins, B. J. Sheahan, N. J. Dimmock, SEMLIKI FOREST VIRUS-INFECTION OF MICE - A MODEL FOR GENETIC AND MOLECULAR ANALYSIS OF VIRAL PATHOGENICITY. *Journal of General Virology* **1985**, *66*, 395-408.
[58] M. Sospedra, R. Martin, Immunology of multiple sclerosis. *Annual Review of Immunology* **2005**, *23*, 683-747.
[59] D. O. Willenborg, EXPERIMENTAL ALLERGIC ENCEPHALOMYELITIS IN THE LEWIS RAT - STUDIES ON THE MECHANISM OF RECOVERY FROM DISEASE AND ACQUIRED-RESISTANCE TO REINDUCTION. *Journal of Immunology* **1979**, *123*, 1145-1150.
[60] F. Mor, T. R. Cohen, SHIFTS IN THE EPITOPES OF MYELIN BASIC-PROTEIN RECOGNIZED BY LEWIS RAT T-CELLS BEFORE, DURING, AND AFTER THE INDUCTION OF EXPERIMENTAL AUTOIMMUNE ENCEPHALOMYELITIS. *Journal of Clinical Investigation* **1993**, *92*, 2199-2206.
[61] N. Karin, D. J. Mitchell, S. Brocke, N. Ling, L. Steinman, REVERSAL OF EXPERIMENTAL AUTOIMMUNE ENCEPHALOMYELITIS BY A SOLUBLE PEPTIDE VARIANT OF A MYELIN BASIC-PROTEIN EPITOPE - T-CELL RECEPTOR ANTAGONISM AND REDUCTION OF INTERFERON-GAMMA AND TUMOR-NECROSIS-FACTOR-ALPHA PRODUCTION. *Journal of Experimental Medicine* **1994**, *180*, 2227-2237.

[62] C. C. A. Bernard, T. G. Johns, A. Slavin, M. Ichikawa, C. Ewing, J. Liu, J. Bettadapura, Myelin oligodendrocyte glycoprotein: A novel candidate autoantigen in multiple sclerosis. *Journal of Molecular Medicine-Jmm* **1997**, *75*, 77-88.
[63] M. M. Morris-Downes, K. McCormack, D. Baker, D. Sivaprasad, J. Natkunarajah, S. Amor, Encephalitogenic and immunogenic potential of myelin-associated glycoprotein (MAG), oligodendrocyte-specific glycoprotein (OSP) and 2',3'-cyclic nucleotide 3'-phosphodiesterase (CNPase) in ABH and SJL mice. *Journal of Neuroimmunology* **2002**, *122*, 20-33.
[64] C. L. Vanderlugt, K. L. Neville, K. M. Nikcevich, T. N. Eagar, J. A. Bluestone, S. D. Miller, Pathologic Role and Temporal Appearance of Newly Emerging Autoepitopes in Relapsing Experimental Autoimmune Encephalomyelitis. *The Journal of Immunology* **2000**, *164*, 670-678.
[65] H. L. Lipton, THEILERS VIRUS-INFECTION IN MICE - UNUSUAL BIPHASIC DISEASE PROCESS LEADING TO DEMYELINATION. *Infection and Immunity* **1975**, *11*, 1147-1155.
[66] E. J. McMahon, S. L. Bailey, C. V. Castenada, H. Waldner, S. D. Miller, Epitope spreading initiates in the CNS in two mouse models of multiple sclerosis. *Nature Medicine* **2005**, *11*, 335-339.
[67] C. Genain, *Vol. US 2006 0130161 A1*, Carantech Inc., Mill Valley, CA, United States, **2006**, p. 25
[68] C. Genain, in *World Congress on on Treatment and Research in Multiple Sclerosis*, Montreal, QC, CANADA, **2008**
[69] F. Santoro, P. E. Kennedy, G. Locatelli, M. S. Malnati, E. A. Berger, P. Lusso, CD46 Is a Cellular Receptor for Human Herpesvirus 6. *Cell* **1999**, *99*, 817-827.
[70] M. Hammarstedt, J. Ahlqvist, S. Jacobson, H. Garoff, A. Fogdell-Hahn, Purification of infectious human herpesvirus 6A virions and association of host cell proteins. *Virology Journal* **2007**, *4*.
[71] A. L. Astier, T-cell regulation by CD46 and its relevance in multiple sclerosis. *Immunology* **2008**, *124*, 149-154.
[72] R. Alvarez-Lafuente, M. Garcia-Montojo, V. De Las Heras, M. I. Dominguez-Mozo, M. Bartolome, R. Arroyo, CD46 expression and HHV-6 infection in patients with multiple sclerosis. *Acta Neurologica Scandinavica* **2009**, *120*, 246-250.
[73] J. E. Wohler, M. I. Gaitan, E. Harberts, A. Huebner, A. C. Silva, D. S. Reich, Effects of HHV-6A Infection in the Common Marmoset. *Journal of Neurovirology* **2010**, *16*, 90-91.
[74] J. Reynaud, Jégou, J., Welsch, J., Horvat, B., in *7th INTERNATIONALConference on HHV-6 & 7*, Reston, Virginia, USA, **2011**
[75] L. Messori, A. Casini, C. Gabbiani, L. Sorace, M. Muniz-Miranda, P. Zatta, Unravelling the chemical nature of copper cuprizone. *Dalton Transactions* **2007**, 2112-2114.
[76] G. K. Matsushima, P. Morell, The Neurotoxicant, Cuprizone, as a Model to Study Demyelination and Remyelination in the Central Nervous System. *Brain Pathology* **2001**, *11*, 107-116.
[77] P. Zatta, M. Raso, P. Zambenedetti, W. Wittkowski, L. Messori, F. Piccioli, P. L. Mauri, M. Beltramini, Copper and zinc dismetabolism in the mouse brain upon chronic cuprizone treatment. *Cellular and Molecular Life Sciences* **2005**, *62*, 1502-1513.

[78] F. Benetti, M. Ventura, B. Salmini, S. Ceola, D. Carbonera, S. Mammi, A. Zitolo, P. D'Angelo, E. Urso, M. Maffia, B. Salvato, E. Spisni, Cuprizone neurotoxicity, copper deficiency and neurodegeneration. *NeuroToxicology* **2010**, *31*, 509-517.
[79] M. Kipp, T. Clarner, J. Dang, S. Copray, C. Beyer, The cuprizone animal model: new insights into an old story. *Acta Neuropathologica* **2009**, *118*, 723-736.
[80] P. Maña, S. A. Fordham, M. A. Staykova, M. Correcha, D. Silva, D. O. Willenborg, D. Liñares, Demyelination caused by the copper chelator cuprizone halts T cell mediated autoimmune neuroinflammation. *Journal of Neuroimmunology* **2009**, *210*, 13-21.
[81] L. Liu, A. Belkadi, L. Darnall, T. Hu, C. Drescher, A. C. Cotleur, D. Padovani-Claudio, T. He, K. Choi, T. E. Lane, R. H. Miller, R. M. Ransohoff, CXCR2-positive neutrophils are essential for cuprizone-induced demyelination: relevance to multiple sclerosis. *Nat Neurosci* **2010**, *13*, 319-326.
[82] V. K. Tuohy, M. Yu, B. Weinstock-Guttman, R. P. Kinkel, Diversity and plasticity of self recognition during the development of multiple sclerosis. *The Journal of Clinical Investigation* **1997**, *99*, 1682-1690.
[83] K. W. Wucherpfennig, J. L. Strominger, MOLECULAR MIMICRY IN T-CELL-MEDIATED AUTOIMMUNITY - VIRAL PEPTIDES ACTIVATE HUMAN T-CELL CLONES SPECIFIC FOR MYELIN BASIC-PROTEIN. *Cell* **1995**, *80*, 695-705.
[84] K. W. Wucherpfennig, Mechanisms for the induction of autoimmunity by infectious agents. *The Journal of Clinical Investigation* **2001**, *108*, 1097-1104.
[85] R. S. Fujinami, M. B. A. Oldstone, AMINO-ACID HOMOLOGY BETWEEN THE ENCEPHALITOGENIC SITE OF MYELIN BASIC-PROTEIN AND VIRUS - MECHANISM FOR AUTOIMMUNITY. *Science* **1985**, *230*, 1043-1045.
[86] Y. S. Mao, C. Z. Lu, X. Wang, B. G. Xiao, Induction of experimental autoimmune encephalomyelitis in Lewis rats by a viral peptide with limited homology to myelin basic protein. *Experimental Neurology* **2007**, *206*, 231-239.
[87] K. I. Voumvourakis, D. K. Kitsos, S. Tsiodras, G. Petrikkos, E. Stamboulis, Human Herpesvirus 6 Infection as a Trigger of Multiple Sclerosis. *Mayo Clinic Proceedings* **2010**, *85*, 1023-1030.
[88] M. V. Tejada-Simon, Y. C. Q. Zang, J. Hong, V. M. Rivera, J. W. Z. Zhang, Cross-reactivity with myelin basic protein and human herpesvirus-6 in multiple sclerosis. *Annals of Neurology* **2003**, *53*, 189-197.
[89] M. V. Tejada-Simon, Y. C. Q. Zang, J. Hong, V. M. Rivera, J. M. Killian, J. W. Z. Zhang, Detection of viral DNA and immune responses to the human herpesvirus 6 101-kilodalton virion protein in patients with multiple sclerosis and in controls. *Journal of Virology* **2002**, *76*, 6147-6154.
[90] J. Ahlqvist, J. Fotheringham, N. Akhyani, K. Yao, A. Fogdell-Hahn, S. Jacobson, Differential tropism of human herpesvirus 6 (HHV-6) variants and induction of latency by HHV-6A in oligodendrocytes. *Journal of Neurovirology* **2005**, *11*, 384-394.
[91] N. Akhyani, R. Berti, M. B. Brennan, S. S. Soldan, J. M. Eaton, H. F. McFarland, S. Jacobson, Tissue distribution and variant characterization of human herpesvirus (HHV)-6: Increased prevalence of HHV-6A in patients with multiple sclerosis. *Journal of Infectious Diseases* **2000**, *182*, 1321-1325.
[92] R. Alvarez-Lafuente, A. Martinez, M. Garcia-Montojo, A. Mas, V. De Las Heras, M. I. Dominguez-Mozo, C. M. del Carmen, M. Lopez-Cavanillas, M. Bartolome, E. G. de la

Concha, E. Urcelay, R. Arroyo, MHC2TA rs4774C and HHV-6A active replication in multiple sclerosis patients. *European Journal of Neurology* **2010**, *17*, 129-135.
[93] S. S. Soldan, T. P. Leist, K. N. Juhng, H. F. McFarland, S. Jacobson, Increased lymphoproliferative response to human herpesvirus type 6A variant in multiple sclerosis patients. *Annals of Neurology* **2000**, *47*, 306-313.
[94] G. Harauz, V. Ladizhansky, J. M. Boggs, Structural Polymorphism and Multifunctionality of Myelin Basic Protein. *Biochemistry* **2009**, *48*, 8094-8104.
[95] J. M. Boggs, Myelin basic protein: a multifunctional protein. *Cellular and Molecular Life Sciences* **2006**, *63*, 1945-1961.
[96] A. Roach, K. Boylan, S. Horvath, S. B. Prusiner, L. E. Hood, Characterization of cloned cDNA representing rat myelin basic protein: Absence of expression in brain of shiverer mutant mice. *Cell* **1983**, *34*, 799-806.
[97] M. S. Windrem, M. C. Nunes, W. K. Rashbaum, T. H. Schwartz, R. A. Goodman, G. McKhann, N. S. Roy, S. A. Goldman, Fetal and adult human oligodendrocyte progenitor cell isolates myelinate the congenitally dysmyelinated brain. *Nat Med* **2004**, *10*, 93-97.
[98] G. Harauz, N. Ishiyama, C. M. D. Hill, I. R. Bates, D. S. Libich, C. Farès, Myelin basic protein--diverse conformational states of an intrinsically unstructured protein and its roles in myelin assembly and multiple sclerosis. *Micron* **2004**, *35*, 503-542.
[99] G. D. Fasman, *Circular dichroism and the conformational analysis of biomolecules*, Plenum Press, New York, **1996**.
[100] D. S. Libich, G. Harauz, Solution NMR and CD spectroscopy of an intrinsically disordered, peripheral membrane protein: evaluation of aqueous and membrane-mimetic solvent conditions for studying the conformational adaptability of the 18.5 kDa isoform of myelin basic protein (MBP). *European Biophysics Journal with Biophysics Letters* **2008**, *37*, 1015-1029.
[101] T. Bund, J. M. Boggs, G. Harauz, N. Hellmann, D. Hinderberger, Copper Uptake Induces Self-Assembly of 18.5 kDa Myelin Basic Protein (MBP). *Biophysical Journal* **2010**, *99*, 3020-3028.
[102] D. R. Beniac, M. D. Luckevich, G. J. Czarnota, T. A. Tompkins, R. A. Ridsdale, F. P. Ottensmeyer, M. A. Moscarello, G. Harauz, Three-dimensional Structure of Myelin Basic Protein. *Journal of Biological Chemistry* **1997**, *272*, 4261-4268.
[103] E. R. Vossenaar, A. J. W. Zendman, W. J. van Venrooij, G. J. M. Pruijn, PAD, a growing family of citrullinating enzymes: genes, features and involvement in disease. *Bioessays* **2003**, *25*, 1106-1118.
[104] M. A. Moscarello, F. G. Mastronardi, D. D. Wood, The role of citrullinated proteins suggests a novel mechanism in the pathogenesis of multiple sclerosis. *Neurochemical Research* **2007**, *32*, 251-256.
[105] A. A. Musse, Z. Li, C. A. Ackerley, D. Bienzle, H. Lei, R. Poma, G. Harauz, M. A. Moscarello, F. G. Mastronardi, Peptidylarginine deiminase 2 (PAD2) overexpression in transgenic mice leads to myelin loss in the central nervous system. *Disease Models & Mechanisms* **2008**, *1*, 229-240.
[106] L. B. Pritzker, S. Joshi, J. J. Gowan, G. Harauz, M. A. Moscarello, Deimination of myelin basic protein. 1. Effect of deimination of arginyl residues of myelin basic protein on its structure and susceptibility to digestion by cathepsin D. *Biochemistry* **2000**, *39*, 5374-5381.

[107] L. B. Pritzker, S. Joshi, G. Harauz, M. A. Moscarello, Deimination of myelin basic protein. 2. Effect of methylation of MBP on its deimination by peptidylarginine deiminase. *Biochemistry* **2000**, *39*, 5382-5388.
[108] S. G. Amur, G. Shanker, J. M. Cochran, H. S. Ved, R. A. Pieringer, Correlation between inhibition of myelin basic protein (arginine) methyltransferase by sinefungoin and lack of compact myelin formation in cultures of cerebral cells from embryonic mice. *Journal of Neuroscience Research* **1986**, *16*, 367-376.
[109] D. Hirschberg, O. Radmark, H. Jornvall, T. Bergman, Thr94 in bovine myelin basic protein is a second phosphorylation site for 42-kDa mitogen-activated protein kinase (ERK2). *J Protein Chem* **2003**, *22*, 177-181.
[110] R. J. Davis, The mitogen-activated protein kinase signal transduction pathway. *J Biol Chem* **1993**, *268*, 14553-14556.
[111] L. J. Pike, Rafts defined: a report on the Keystone Symposium on Lipid Rafts and Cell Function. *Journal of Lipid Research* **2006**, *47*, 1597-1598.
[112] L. S. DeBruin, G. Harauz, White matter rafting - Membrane microdomains in myelin. *Neurochemical Research* **2007**, *32*, 213-228.
[113] S. Hossain, G. Fragoso, W. E. Mushynski, G. Almazan, Regulation of peripheral myelination by Src-like kinases. *Experimental Neurology* **2010**, *226*, 47-57.
[114] J. M. Boggs, G. Rangaraj, W. Gao, Y.-M. Heng, Effect of Phosphorylation of Myelin Basic Protein By MAPK on its Interactions with Actin and Actin Binding to a Lipid Membrane in Vitro†. *Biochemistry* **2005**, *45*, 391-401.
[115] J. M. Boggs, G. Rangaraj, Y.-M. Heng, Y. Liu, G. Harauz, Myelin basic protein binds microtubules to a membrane surface and to actin filaments in vitro: Effect of phosphorylation and deimination. *Biochimica et Biophysica Acta* **2011**, *1808*, 761-773.
[116] K. P. Lu, G. Finn, T. H. Lee, L. K. Nicholson, Prolyl cis-trans isomerization as a molecular timer. *Nat Chem Biol* **2007**, *3*, 619-629.
[117] M. A. Kelly, B. W. Chellgren, A. L. Rucker, J. M. Troutman, M. G. Fried, A. F. Miller, T. P. Creamer, Host-guest study of left-handed polyproline II helix formation. *Biochemistry* **2001**, *40*, 14376-14383.
[118] B. K. Kay, M. P. Williamson, M. Sudol, The importance of being proline: the interaction of proline-rich motifs in signaling proteins with their cognate domains. *The FASEB Journal* **2000**, *14*, 231-241.
[119] E. Polverini, G. Rangaraj, D. S. Libich, J. M. Boggs, G. Harauz, Binding of the Proline-Rich Segment of Myelin Basic Protein to SH3 Domains: Spectroscopic, Microarray, and Modeling Studies of Ligand Conformation and Effects of Posttranslational Modifications†. *Biochemistry* **2007**, *47*, 267-282.
[120] T. Pawson, PROTEIN MODULES AND SIGNALING NETWORKS. *Nature* **1995**, *373*, 573-580.
[121] K. Kami, R. Takeya, H. Sumimoto, D. Kohda, Diverse recognition of non-PxxP peptide ligands by the SH3 domains from p67phox, Grb2 and Pex13p. *EMBO J* **2002**, *21*, 4268-4276.
[122] M. Harkiolaki, M. Lewitzky, R. J. C. Gilbert, E. Jones, R. P. Bourette, G. Mouchiroud, H. Sondermann, I. Moarefi, S. M. Feller, Structural basis for SH3 domain-mediated high-affinity binding between Mona/Gads and SLP-76. *EMBO J* **2003**, *22*, 2571-2582.
[123] L. Homchaudhuri, E. Polverini, W. Gao, G. Harauz, J. M. Boggs, Influence of Membrane Surface Charge and Post-Translational Modifications to Myelin Basic Protein on Its

Ability To Tether the Fyn-SH3 Domain to a Membrane in Vitro. *Biochemistry* **2009**, *48*, 2385-2393.
[124] K. Biffiger, S. Bartsch, D. Montag, A. Aguzzi, M. Schachner, U. Bartsch, Severe hypomyelination of the murine CNS in the absence of myelin-associated glycoprotein and Fyn tyrosine kinase. *Journal of Neuroscience* **2000**, *20*, 7430-7437.
[125] H. Umemori, S. Sato, T. Yagi, S. Aizawa, T. Yamamoto, INITIAL EVENTS OF MYELINATION INVOLVE FYN TYROSINE KINASE SIGNALING. *Nature* **1994**, *367*, 572-576.
[126] A. Belkadi, P. LoPresti, Truncated Tau with the Fyn-binding domain and without the microtubule-binding domain hinders the myelinating capacity of an oligodendrocyte cell line. *Journal of Neurochemistry* **2008**, *107*, 351-360.
[127] C. Klein, E. M. Kramer, A. M. Cardine, B. Schraven, R. Brandt, J. Trotter, Process outgrowth of oligodendrocytes is promoted by interaction of Fyn kinase with the cytoskeletal protein Tau. *Journal of Neuroscience* **2002**, *22*, 698-707.
[128] http://www.cryst.bbk.ac.uk/pps97/assignments/projects/szabo/pphelix.htm. Accessed April 7th, 2011.
[129] E. F. Pettersen, T. D. Goddard, C. C. Huang, G. S. Couch, D. M. Greenblatt, E. C. Meng, T. E. Ferrin, UCSF Chimera—A visualization system for exploratory research and analysis. *Journal of Computational Chemistry* **2004**, *25*, 1605-1612.
[130] R. White, C. Gonsior, E. M. Kramer-Albers, N. Stohr, S. Huttelmaier, J. Trotter, Activation of oligodendroglial Fyn kinase enhances translation of mRNAs transported in hnRNP A2-dependent RNA granules. *Journal of Cell Biology* **2008**, *181*, 579-586.
[131] H. Umemori, Y. Kadowaki, K. Hirosawa, Y. Yoshida, K. Hironaka, H. Okano, T. Yamamoto, Stimulation of myelin basic protein gene transcription by Fyn tyrosine kinase for myelination. *Journal of Neuroscience* **1999**, *19*, 1393-1397.
[132] B. M. Sullivan, L. Coscoy, The U24 Protein from Human Herpesvirus 6 and 7 Affects Endocytic Recycling. *Journal of Virology* **2010**, *84*, 1265-1275.
[133] A. Roy, A. Kucukural, Y. Zhang, I-TASSER: a unified platform for automated protein structure and function prediction. *Nature Protocols* **2010**, *5*, 725-738.
[134] S. Z. Salahuddin, D. V. Ablashi, P. D. Markham, S. F. Josephs, S. Sturzenegger, M. Kaplan, G. Halligan, P. Biberfeld, F. Wongstaal, B. Kramarsky, R. C. Gallo, ISOLATION OF A NEW VIRUS, HBLV, IN PATIENTS WITH LYMPHOPROLIFERATIVE DISORDERS. *Science* **1986**, *234*, 596-601.
[135] G. Dominguez, T. R. Dambaugh, F. R. Stamey, S. Dewhurst, N. Inoue, P. E. Pellett, Human Herpesvirus 6B Genome Sequence: Coding Content and Comparison with Human Herpesvirus 6A. *Journal of Virology* **1999**, *73*, 8040-8052.
[136] D. Ablashi, H. Agut, Z. Berneman, G. Campadelli-Fiume, D. Carrigan, L. Ceccerini-Nelli, B. Chandran, S. Chou, H. Collandre, R. Cone, T. Dambaugh, S. Dewhurst, D. DiLuca, L. Foa-Tomasi, B. Fleckenstein, N. Frenkel, R. Gallo, U. Gompels, C. Hall, M. Jones, G. Lawrence, M. Martin, L. Montagnier, F. Neipel, J. Nicholas, P. Pellett, A. Razzaque, G. Torrelli, B. Thomson, S. Salahuddin, L. Wyatt, K. Yamanishi, Human herpesvirus-6 strain groups: a nomenclature. *Archives of Virology* **1993**, *129*, 363-366.
[137] U. A. Gompels, J. Nicholas, G. Lawrence, M. Jones, B. J. Thomson, M. E. D. Martin, S. Efstathiou, M. Craxton, H. A. Macaulay, The DNA Sequence of Human Herpesvirus-6: Structure, Coding Content, and Genome Evolution. *Virology* **1995**, *209*, 29-51.

[138] D. H. Dockrell, Human herpesvirus 6: molecular biology and clinical features. *Journal of Medical Microbiology* **2003**, *52*, 5-18.
[139] D. K. Braun, G. Dominguez, P. E. Pellett, Human herpesvirus 6. *Clinical Microbiology Reviews* **1997**, *10*, 521-&.
[140] L. Flamand, A. L. Komaroff, J. H. Arbuckle, P. G. Medveczky, D. V. Ablashi, Review, Part 1: Human Herpesvirus-6-Basic Biology, Diagnostic Testing, and Antiviral Efficacy. *Journal of Medical Virology* **2010**, *82*, 1560-1568.
[141] K. Yao, J. R. Crawford, A. L. Komaroff, D. V. Ablashi, S. Jacobson, Review Part 2: Human Herpesvirus-6 in Central Nervous System Diseases. *Journal of Medical Virology* **2010**, *82*, 1669-1678.
[142] N. M. Regush, *The virus within : a coming epidemic*, Dutton, New York, **2000**.
[143] M. L. Opsahl, P. G. E. Kennedy, Early and late HHV-6 gene transcripts in multiple sclerosis lesions and normal appearing white matter. *Brain* **2005**, *128*, 516-527.
[144] R. S. Fujinami, M. G. von Herrath, U. Christen, J. L. Whitton, Molecular mimicry, bystander activation, or viral persistence: Infections and autoimmune disease. *Clinical Microbiology Reviews* **2006**, *19*, 80-+.
[145] J. H. Arbuckle, M. M. Medveczky, J. Luka, S. H. Hadley, A. Luegmayr, D. Ablashi, T. C. Lund, J. Tolar, K. De Meirleir, J. G. Montoya, A. L. Komaroff, P. F. Ambros, P. G. Medveczky, The latent human herpesvirus-6A genome specifically integrates in telomeres of human chromosomes in vivo and in vitro. *Proceedings of the National Academy of Sciences of the United States of America* **2010**, *107*, 5563-5568.
[146] T. Mori, K. Tanaka-Taya, H. Satoh, Y. Aisa, R. Yamazaki, J. Kato, Y. Ikeda, S. Okamoto, Transmission of chromosomally integrated human herpesvirsus 6 (HHV-6) variant A from a parent to children leading to misdiagnosis of active HHV-6 infection. *Transplant Infectious Disease* **2009**, *11*, 503-506.
[147] L. De Bolle, L. Naesens, E. De Clercq, Update on Human Herpesvirus 6 Biology, Clinical Features, and Therapy. *Clin. Microbiol. Rev.* **2005**, *18*, 217-245.
[148] L. Potenza, M. Luppi, P. Barozzi, G. Rossi, S. Cocchi, M. Codeluppi, M. Pecorari, M. Masetti, F. Di Benedetto, W. Gennari, M. Portolani, G. E. Gerunda, T. Lazzarotto, M. P. Landini, T. F. Schulz, G. Torelli, G. Guaraldi, HHV-6A in Syncytial Giant-Cell Hepatitis. *New England Journal of Medicine* **2008**, *359*, 593-602.
[149] A. Fogdell-Hahn, S. S. Soldan, S. Shue, N. Akhyani, H. Refai, J. Ahlqvist, S. Jacobson, Co-purification of soluble membrane cofactor protein (CD46) and human herpesvirus 6 variant A genome in serum from multiple sclerosis patients. *Virus Research* **2005**, *110*, 57-63.
[150] H. Kong, Q. Baerbig, L. Duncan, N. Shepel, M. Mayne, Human herpesvirus type 6 indirectly enhances oligodendrocyte cell death. *Journal of Neurovirology* **2003**, *9*, 539-550.
[151] M. Swanberg, O. Lidman, L. Padyukov, P. Eriksson, E. Akesson, M. Jagodic, A. Lobell, M. Khademi, O. Borjesson, C. M. Lindgren, P. Lundman, A. J. Brookes, J. Kere, H. Luthman, L. Alfredsson, J. Hillert, L. Klareskog, A. Hamsten, F. Piehl, T. Olsson, MHC2TA is associated with differential MHC molecule expression and susceptibility to rheumatoid arthritis, multiple sclerosis and myocardial infarction. *Nat Genet* **2005**, *37*, 486-494.
[152] A. Martínez, R. Álvarez-Lafuente, A. Mas, M. Bartolomé, M. García-Montojo, V. de las Heras, E. G. de la Concha, R. Arroyo, E. Urcelay, Environment-gene interaction in

multiple sclerosis: Human herpesvirus 6 and MHC2TA. *Human Immunology* **2007**, *68*, 685-689.
[153] Y. Asano, T. Yoshikawa, S. Suga, I. Kobayashi, T. Nakashima, T. Yazaki, Y. Kajita, T. Ozaki, CLINICAL-FEATURES OF INFANTS WITH PRIMARY HUMAN HERPESVIRUS 6 INFECTION (EXANTHEM-SUBITUM, ROSEOLA INFANTUM). *Pediatrics* **1994**, *93*, 104-108.
[154] K. Yao, N. Akhyani, D. Donati, N. Sengamalay, J. Fotheringham, E. Ghedin, M. Bishop, J. Barrett, F. Kashanchi, S. Jacobson, Detection of HHV-6B in post-mortem central nervous system tissue of a post-bone marrow transplant recipient: a multi-virus array analysis. *Journal of Clinical Virology* **2006**, *37*, S57-S62.
[155] D. Donati, N. Akhyani, A. Fogdell-Hahn, C. Cermelli, R. Cassiani-Ingoni, A. Vortmeyer, J. D. Heiss, P. Cogen, W. D. Gaillard, S. Sato, W. H. Theodore, S. Jacobson, Detection of human herpesvirus-6 in mesial temporal lobe epilepsy surgical brain resections. *Neurology* **2003**, *61*, 1405-1411.
[156] J. Fotheringham, D. Donati, N. Akhyani, A. Fogdell-Hahn, A. Vortmeyer, J. D. Heiss, E. Williams, S. Weinstein, D. A. Bruce, W. D. Gaillard, S. Sato, W. H. Theodore, S. Jacobson, Association of human herpesvirus-6B with mesial temporal lobe epilepsy. *Plos Medicine* **2007**, *4*, 848-857.
[157] P. Zou, Y. Isegawa, K. Nakano, M. Haque, Y. Horiguchi, K. Yamanishi, Human herpesvirus 6 open reading frame U83 encodes a functional chemokine. *Journal of Virology* **1999**, *73*, 5926-5933.
[158] Y. Isegawa, Z. Ping, K. Nakano, N. Sugimoto, K. Yamanishi, Human herpesvirus 6 open reading frame U12 encodes a functional beta-chemokine receptor. *Journal of Virology* **1998**, *72*, 6104-6112.
[159] C. P. Fitzsimons, U. A. Gompels, D. Verzijl, H. F. Vischer, C. Mattick, R. Leurs, M. J. Smit, Chemokine-directed trafficking of receptor stimulus to different G proteins: Selective inducible and constitutive signaling by human herpesvirus 6-encoded chemokine receptor U51. *Molecular Pharmacology* **2006**, *69*, 888-898.
[160] J. Jaworska, A. Gravel, K. Fink, N. Grandvaux, L. Flamand, Inhibition of Transcription of the Beta Interferon Gene by the Human Herpesvirus 6 Immediate-Early 1 Protein. *Journal of Virology* **2007**, *81*, 5737-5748.
[161] N. L. Glosson, A. W. Hudson, Human herpesvirus-6A and -6B encode viral immunoevasins that downregulate class I MHC molecules. *Virology* **2007**, *365*, 125-135.
[162] P. J. Bjorkman, M. A. Saper, B. Samraoui, W. S. Bennett, J. L. Strominger, D. C. Wiley, The foreign antigen binding site and T cell recognition regions of class I histocompatibility antigens. *Nature* **1987**, *329*, 512-518.
[163] M. M. Davis, P. J. Bjorkman, T-cell antigen receptor genes and T-cell recognition. *Nature* **1988**, *334*, 395-402.
[164] K. Yao, M. Mandel, N. Akyani, K. Maynard, N. Sengamalay, J. Fotheringham, E. Ghedin, F. Kashanchi, S. Jacobson, Differential HHV-6A gene expression in T cells and primary human astrocytes based on multi-virus array analysis. *Glia* **2006**, *53*, 789-798.
[165] B. M. Sullivan, L. Coscoy, Downregulation of the T-Cell receptor complex and impairment of T-Cell activation by human herpesvirus 6 U24 protein. *Journal of Virology* **2008**, *82*, 602-608.
[166] M. Zerial, H. McBride, Rab proteins as membrane organizers. *Nat Rev Mol Cell Biol* **2001**, *2*, 107-117.

[167] C. Bucci, R. G. Parton, I. H. Mather, H. Stunnenberg, K. Simons, B. Hoflack, M. Zerial, The small GTPase rab5 functions as a regulatory factor in the early endocytic pathway. *Cell* **1992**, *70*, 715-728.
[168] P. Lusso, M. Malnati, A. De Maria, C. Balotta, S. DeRocco, P. Markham, R. Gallo, Productive infection of CD4+ and CD8+ mature human T cell populations and clones by human herpesvirus 6. Transcriptional down-regulation of CD3. *The Journal of Immunology* **1991**, *147*, 685-691.
[169] P. Lusso, P. D. Markham, E. Tschachler, F. di Marzo Veronese, S. Z. Salahuddin, D. V. Ablashi, S. Pahwa, K. Krohn, R. C. Gallo, In vitro cellular tropism of human B-lymphotropic virus (human herpesvirus-6). *The Journal of Experimental Medicine* **1988**, *167*, 1659-1670.
[170] M. Comar, P. D'Agaro, D. Horejsh, M. Galvan, S. Fiorentini, M. Andolina, A. Caruso, D. Di Luca, C. Campello, Long-lasting CD3(+) T-cell deficiency after cord blood stem cell transplantation in a human herpesvirus 6-infected child. *Journal of Clinical Microbiology* **2005**, *43*, 2002-2003.
[171] J. C. Grivel, F. Santoro, S. Chen, G. Faga, M. S. Malnati, Y. Ito, L. Margolis, P. Lusso, Pathogenic effects of human herpesvirus 6 in human lymphoid tissue ex vivo. *Journal of Virology* **2003**, *77*, 8280-8289.
[172] C. L. Miller, J. H. Lee, E. Kieff, A. L. Burkhardt, J. B. Bolen, R. Longnecker, EPSTEIN-BARR-VIRUS PROTEIN LMP2A REGULATES REACTIVATION FROM LATENCY BY NEGATIVELY REGULATING TYROSINE KINASES INVOLVED IN SIG-MEDIATED SIGNAL-TRANSDUCTION. *Infectious Agents and Disease-Reviews Issues and Commentary* **1994**, *3*, 128-136.
[173] B.-S. Lee, X. Alvarez, S. Ishido, A. A. Lackner, J. U. Jung, Inhibition of Intracellular Transport of B Cell Antigen Receptor Complexes by Kaposi's Sarcoma–Associated Herpesvirus K1. *The Journal of Experimental Medicine* **2000**, *192*, 11-22.
[174] J. Park, B. S. Lee, J. K. Choi, R. E. Means, J. Choe, J. U. Jung, Herpesviral protein targets a cellular WD repeat endosomal protein to downregulate T lymphocyte receptor expression. *Immunity* **2002**, *17*, 221-233.
[175] K.-K. Han, A. Martinage, Possible relationship between coding recognition amino acid sequence motif or residue(s) and post-translational chemical modification of proteins. *International Journal of Biochemistry* **1992**, *24*, 1349-1363.
[176] http://www.cbs.dtu.dk/services/TMHMM-2.0/. Accessed Feb. 9, 2011.
[177] U. Kutay, E. Hartmann, T. A. Rapoport, A class of membrane proteins with a C-terminal anchor. *Trends in Cell Biology* **1993**, *3*, 72-75.
[178] N. Borgese, S. Brambillasca, S. Colombo, How tails guide tail-anchored proteins to their destinations. *Current Opinion in Cell Biology* **2007**, *19*, 368-375.
[179] R. N. Harty, M. E. Brown, G. Wang, H. Jon, F. P. Hayes, A PPxY Motif within the VP40 Protein of Ebola Virus Interacts Physically and Functionally with a Ubiquitin Ligase: Implications for Filovirus Budding. *Proceedings of the National Academy of Sciences of the United States of America* **2000**, *97*, 13871-13876.
[180] K. F. Harvey, A. Dinudom, D. I. Cook, S. Kumar, The Nedd4-like protein KIAA0439 is a potential regulator of the epithelial sodium channel. *Journal of Biological Chemistry* **2001**, *276*, 8597-8601.
[181] R. J. Ingham, G. Gish, T. Pawson, The Nedd4 family of E3 ubiquitin ligases: functional diversity within a common modular architecture. *Oncogene* **2004**, *23*, 1972-1984.

[182] O. Staub, S. Dho, P. C. Henry, J. Correa, T. Ishikawa, J. McGlade, D. Rotin, WW domains of Nedd4 bind to the proline-rich PY motifs in the epithelial Na+ channel deleted in Liddle's syndrome. *Embo Journal* **1996**, *15*, 2371-2380.
[183] H. K. Shi, C. Asher, A. Chigaev, Y. Yung, E. Reuveny, R. Seger, H. Garty, Interactions of beta and gamma ENaC with Nedd4 can be facilitated by an ERK-mediated phosphorylation. *Journal of Biological Chemistry* **2002**, *277*, 13539-13547.
[184] J. Eichberg, S. Iyer, Phosphorylation of myelin proteins: Recent advances. *Neurochemical Research* **1996**, *21*, 527-535.
[185] A. R. Tait, S. K. Straus, Phosphorylation of U24 from Human Herpes Virus type 6 (HHV-6) and its potential role in mimicking myelin basic protein (MBP) in multiple sclerosis. *Febs Letters* **2008**, *582*, 2685-2688.
[186] C. Rabu, V. Schmid, B. Schwappach, S. High, Biogenesis of tail-anchored proteins: the beginning for the end? *J Cell Sci* **2009**, *122*, 3605-3612.
[187] V. Favaloro, M. Spasic, B. Schwappach, B. Dobberstein, Distinct targeting pathways for the membrane insertion of tail-anchored (TA) proteins. *Journal of Cell Science* **2008**, *121*, 1832-1840.
[188] V. Favaloro, F. Vilardi, R. Schlecht, M. P. Mayer, B. Dobberstein, Asna1/TRC40-mediated membrane insertion of tail-anchored proteins. *Journal of Cell Science* **2010**, *123*, 1522-1530.
[189] M. Mariappan, X. Li, S. Stefanovic, A. Sharma, A. Mateja, R. J. Keenan, R. S. Hegde, A ribosome-associating factor chaperones tail-anchored membrane proteins. *Nature* **2010**, *466*, 1120-1124.
[190] M. Schuldiner, J. Metz, V. Schmid, V. Denic, M. Rakwalska, H. D. Schmitt, B. Schwappach, J. S. Weissman, The GET Complex Mediates Insertion of Tail-Anchored Proteins into the ER Membrane. *Cell* **2008**, *134*, 634-645.
[191] A. Mateja, A. Szlachcic, M. E. Downing, M. Dobosz, M. Mariappan, R. S. Hegde, R. J. Keenan, The structural basis of tail-anchored membrane protein recognition by Get3. *Nature* **2009**, *461*, 361-U358.
[192] G. Bozkurt, G. Stjepanovic, F. Vilardi, S. Amlacher, K. Wild, G. Bange, V. Favaloro, K. Rippe, E. Hurt, B. Dobberstein, I. Sinning, Structural insights into tail-anchored protein binding and membrane insertion by Get3. *Proceedings of the National Academy of Sciences* **2009**, *106*, 21131-21136.
[193] D. Horst, V. Favaloro, F. Vilardi, H. C. van Leeuwen, M. A. Garstka, A. D. Hislop, C. Rabu, E. Kremmer, A. B. Rickinson, S. High, B. Dobberstein, M. E. Ressing, E. J. H. J. Wiertz, EBV Protein BNLF2a Exploits Host Tail-Anchored Protein Integration Machinery To Inhibit TAP. *The Journal of Immunology* **2011**, *186*, 3594-3605.
[194] C. Winterstein, J. Trotter, E.-M. Kramer-Albers, Distinct endocytic recycling of myelin proteins promotes oligodendroglial membrane remodeling. *J Cell Sci* **2008**, *121*, 834-842.
[195] E. Arnaud, J. Zenker, A.-S. de Preux Charles, C. Stendel, A. Roos, J.-J. Médard, N. Tricaud, H. Kleine, B. Luscher, J. Weis, U. Suter, J. Senderek, R. Chrast, SH3TC2/KIAA1985 protein is required for proper myelination and the integrity of the node of Ranvier in the peripheral nervous system. *Proceedings of the National Academy of Sciences* **2009**, *106*, 17528-17533.
[196] C. Stendel, A. Roos, H. Kleine, E. Arnaud, M. Ozcelik, P. N. M. Sidiropoulos, J. Zenker, F. Schupfer, U. Lehmann, R. M. Sobota, D. W. Litchfield, B. Luscher, R. Chrast, U.

Suter, J. Senderek, SH3TC2, a protein mutant in Charcot-Marie-Tooth neuropathy, links peripheral nerve myelination to endosomal recycling. *Brain* **2010**, *133*, 2462-2474.
[197] C. R. Midgett, D. R. Madden, Breaking the bottleneck: eukaryotic membrane protein expression for high-resolution structural studies. *J Struct Biol* **2007**, *160*, 265-274.
[198] B. M. Sullivan, L. Coscoy, The U24 protein from human herpesvirus 6 and 7 affects endocytic recycling. *J Virol* **2010**, *84*, 1265-1275.
[199] D. B. Smith, K. S. Johnson, Single-step purification of polypeptides expressed in Escherichia coli as fusions with glutathione S-transferase. *Gene* **1988**, *67*, 31-40.
[200] C. V. Maina, P. D. Riggs, A. G. Grandea, 3rd, B. E. Slatko, L. S. Moran, J. A. Tagliamonte, L. A. McReynolds, C. D. Guan, An Escherichia coli vector to express and purify foreign proteins by fusion to and separation from maltose-binding protein. *Gene* **1988**, *74*, 365-373.
[201] R. Janknecht, G. de Martynoff, J. Lou, R. A. Hipskind, A. Nordheim, H. G. Stunnenberg, Rapid and efficient purification of native histidine-tagged protein expressed by recombinant vaccinia virus. *Proc Natl Acad Sci U S A* **1991**, *88*, 8972-8976.
[202] S. Wagner, M. L. Bader, D. Drew, J. W. de Gier, Rationalizing membrane protein overexpression. *Trends Biotechnol* **2006**, *24*, 364-371.
[203] R. B. Kapust, D. S. Waugh, Escherichia coli maltose-binding protein is uncommonly effective at promoting the solubility of polypeptides to which it is fused. *Protein Sci* **1999**, *8*, 1668-1674.
[204] K. D. Pryor, B. Leiting, High-level expression of soluble protein in Escherichia coli using a His6-tag and maltose-binding-protein double-affinity fusion system. *Protein Expr Purif* **1997**, *10*, 309-319.
[205] S. Nallamsetty, B. P. Austin, K. J. Penrose, D. S. Waugh, Gateway vectors for the production of combinatorially-tagged His6-MBP fusion proteins in the cytoplasm and periplasm of Escherichia coli. *Protein Sci* **2005**, *14*, 2964-2971.
[206] A. Korepanova, J. D. Moore, H. B. Nguyen, Y. Hua, T. A. Cross, F. Gao, Expression of membrane proteins from Mycobacterium tuberculosis in Escherichia coli as fusions with maltose binding protein. *Protein Expr Purif* **2007**, *53*, 24-30.
[207] S. Ramachandran, H. Lu, U. Prabhu, A. E. Ruoho, Purification and characterization of the guinea pig sigma-1 receptor functionally expressed in Escherichia coli. *Protein Expr Purif* **2007**, *51*, 283-292.
[208] J. Lian, S. Ding, J. Cai, D. Zhang, Z. Xu, X. Wang, Improving aquaporin Z expression in Escherichia coli by fusion partners and subsequent condition optimization. *Appl Microbiol Biotechnol* **2009**, *82*, 463-470.
[209] H. Kadokura, F. Katzen, J. Beckwith, Protein disulfide bond formation in prokaryotes. *Annu Rev Biochem* **2003**, *72*, 111-135.
[210] P. H. Bessette, F. Aslund, J. Beckwith, G. Georgiou, Efficient folding of proteins with multiple disulfide bonds in the Escherichia coli cytoplasm. *Proc Natl Acad Sci U S A* **1999**, *96*, 13703-13708.
[211] F. Hatahet, V. D. Nguyen, K. E. Salo, L. W. Ruddock, Disruption of reducing pathways is not essential for efficient disulfide bond formation in the cytoplasm of E. coli. *Microb Cell Fact* **2010**, *9*, 67.
[212] V. D. Nguyen, F. Hatahet, K. E. Salo, E. Enlund, C. Zhang, L. W. Ruddock, Pre-expression of a sulfhydryl oxidase significantly increases the yields of eukaryotic

disulfide bond containing proteins expressed in the cytoplasm of E.coli. *Microb Cell Fact* **2011**, *10*, 1.
[213] A. G. Planson, J. I. Guijarro, M. E. Goldberg, A. F. Chaffotte, Assistance of maltose binding protein to the in vivo folding of the disulfide-rich C-terminal fragment from Plasmodium falciparum merozoite surface protein 1 expressed in Escherichia coli. *Biochemistry* **2003**, *42*, 13202-13211.
[214] B. Miroux, J. E. Walker, Over-production of proteins in Escherichia coli: mutant hosts that allow synthesis of some membrane proteins and globular proteins at high levels. *J Mol Biol* **1996**, *260*, 289-298.
[215] S. Wagner, M. M. Klepsch, S. Schlegel, A. Appel, R. Draheim, M. Tarry, M. Hogbom, K. J. van Wijk, D. J. Slotboom, J. O. Persson, J. W. de Gier, Tuning Escherichia coli for membrane protein overexpression. *Proc Natl Acad Sci U S A* **2008**, *105*, 14371-14376.
[216] K. Maskos, M. Huber-Wunderlich, R. Glockshuber, DsbA and DsbC-catalyzed oxidative folding of proteins with complex disulfide bridge patterns in vitro and in vivo. *J Mol Biol* **2003**, *325*, 495-513.
[217] N. Sreerama, R. W. Woody, On the analysis of membrane protein circular dichroism spectra. *Protein Sci* **2004**, *13*, 100-112.
[218] A. R. Tait, S. K. Straus, Phosphorylation of U24 from Human Herpes Virus type 6 (HHV-6) and its potential role in mimicking myelin basic protein (MBP) in multiple sclerosis. *FEBS Lett* **2008**, *582*, 2685-2688.
[219] B. A. Wallace, J. G. Lees, A. J. Orry, A. Lobley, R. W. Janes, Analyses of circular dichroism spectra of membrane proteins. *Protein Sci* **2003**, *12*, 875-884.
[220] S. Khrapunov, H. Cheng, S. Hegde, J. Blanchard, M. Brenowitz, Solution structure and refolding of the Mycobacterium tuberculosis pentapeptide repeat protein MfpA. *J Biol Chem* **2008**, *283*, 36290-36299.
[221] E. Jacoby, R. Bouhelal, M. Gerspacher, K. Seuwen, The 7 TM G-protein-coupled receptor target family. *ChemMedChem* **2006**, *1*, 761-782.
[222] A. J. Rader, G. Anderson, B. Isin, H. G. Khorana, I. Bahar, J. Klein-Seetharaman, Identification of core amino acids stabilizing rhodopsin. *Proc Natl Acad Sci U S A* **2004**, *101*, 7246-7251.
[223] J. Tucker, R. Grisshammer, Purification of a rat neurotensin receptor expressed in Escherichia coli. *Biochem J* **1996**, *317 (Pt 3)*, 891-899.
[224] R. Grisshammer, J. Tucker, Quantitative evaluation of neurotensin receptor purification by immobilized metal affinity chromatography. *Protein Expr Purif* **1997**, *11*, 53-60.
[225] Y. Shibata, J. F. White, M. J. Serrano-Vega, F. Magnani, A. L. Aloia, R. Grisshammer, C. G. Tate, Thermostabilization of the Neurotensin Receptor NTS1. *J Mol Biol* **2009**.
[226] A. A. Pioszak, H. E. Xu, Molecular recognition of parathyroid hormone by its G protein-coupled receptor. *Proc Natl Acad Sci U S A* **2008**, *105*, 5034-5039.
[227] C. G. Tate, Overexpression of mammalian integral membrane proteins for structural studies. *FEBS Lett* **2001**, *504*, 94-98.
[228] T. P. Roosild, J. Greenwald, M. Vega, S. Castronovo, R. Riek, S. Choe, NMR structure of Mistic, a membrane-integrating protein for membrane protein expression. *Science* **2005**, *307*, 1317-1321.
[229] J. Panula-Perala, J. Siurkus, A. Vasala, R. Wilmanowski, M. G. Casteleijn, P. Neubauer, Enzyme controlled glucose auto-delivery for high cell density cultivations in microplates and shake flasks. *Microb Cell Fact* **2008**, *7*, 31.

[230] E. Massey-Gendel, A. Zhao, G. Boulting, H. Y. Kim, M. A. Balamotis, L. M. Seligman, R. K. Nakamoto, J. U. Bowie, Genetic selection system for improving recombinant membrane protein expression in E. coli. *Protein Sci* **2009**, *18*, 372-383.
[231] G. Skretas, G. Georgiou, Genetic analysis of G protein-coupled receptor expression in Escherichia coli: inhibitory role of DnaJ on the membrane integration of the human central cannabinoid receptor. *Biotechnol Bioeng* **2009**, *102*, 357-367.
[232] A. J. Link, G. Skretas, E. M. Strauch, N. S. Chari, G. Georgiou, Efficient production of membrane-integrated and detergent-soluble G protein-coupled receptors in Escherichia coli. *Protein Sci* **2008**, *17*, 1857-1863.
[233] Y. Kim, Z. Paroush, K. Nairz, E. Hafen, G. Jimenez, S. Y. Shvartsman, Substrate-dependent control of MAPK phosphorylation in vivo. *Molecular Systems Biology* **2011**, *7*.
[234] A. J. Steck, S. H. Appel, Phosphorylation of myelin basic protein. *J Biol Chem* **1974**, *249*, 5416-5420.
[235] K. C. DesJardins, P. Morell, Phosphate groups modifying myelin basic proteins are metabolically labile; methyl groups are stable. *J Cell Biol* **1983**, *97*, 438-446.
[236] C. M. Atkins, M. Yon, N. P. Groome, J. D. Sweatt, Regulation of myelin basic protein phosphorylation by mitogen-activated protein kinase during increased action potential firing in the hippocampus. *J Neurochem* **1999**, *73*, 1090-1097.
[237] J. M. Boggs, G. Rangaraj, W. Gao, Y. M. Heng, Effect of phosphorylation of myelin basic protein by MAPK on its interactions with actin and actin binding to a lipid membrane in vitro. *Biochemistry* **2006**, *45*, 391-401.
[238] J. J. Ramwani, R. M. Epand, M. A. Moscarello, Secondary structure of charge isomers of myelin basic protein before and after phosphorylation. *Biochemistry* **1989**, *28*, 6538-6543.
[239] A. K. Erickson, D. M. Payne, P. A. Martino, A. J. Rossomando, J. Shabanowitz, M. J. Weber, D. F. Hunt, T. W. Sturgill, Identification by mass spectrometry of threonine 97 in bovine myelin basic protein as a specific phosphorylation site for mitogen-activated protein kinase. *J Biol Chem* **1990**, *265*, 19728-19735.
[240] L. S. DeBruin, J. D. Haines, D. Bienzle, G. Harauz, Partitioning of myelin basic protein into membrane microdomains in a spontaneously demyelinating mouse model for multiple sclerosis. *Biochem Cell Biol* **2006**, *84*, 993-1005.
[241] L. S. DeBruin, J. D. Haines, L. A. Wellhauser, G. Radeva, V. Schonmann, D. Bienzle, G. Harauz, Developmental partitioning of myelin basic protein into membrane microdomains. *J Neurosci Res* **2005**, *80*, 211-225.
[242] M. Yon, C. A. Ackerley, F. G. Mastronardi, N. Groome, M. A. Moscarello, Identification of a mitogen-activated protein kinase site in human myelin basic protein in situ. *J Neuroimmunol* **1996**, *65*, 55-59.
[243] P. Medveczky, J. Antal, A. Patthy, K. Kekesi, G. Juhasz, L. Szilagyi, L. Graf, Myelin basic protein, an autoantigen in multiple sclerosis, is selectively processed by human trypsin 4. *FEBS Lett* **2006**, *580*, 545-552.
[244] G. L. Stoner, C. F. Ryschkewitsch, D. L. Walker, D. Soffer, H. D. Webster, Immunocytochemical search for JC papovavirus large T-antigen in multiple sclerosis brain tissue. *Acta Neuropathol* **1986**, *70*, 345-347.

[245] P. Ferrante, E. Omodeo-Zorini, R. Caldarelli-Stefano, M. Mediati, E. Fainardi, E. Granieri, D. Caputo, Detection of JC virus DNA in cerebrospinal fluid from multiple sclerosis patients. *Mult Scler* **1998**, *4*, 49-54.
[246] L. Del Valle, S. Delbue, J. Gordon, S. Enam, S. Croul, P. Ferrante, K. Khalili, Expression of JC virus T-antigen in a patient with MS and glioblastoma multiforme. *Neurology* **2002**, *58*, 895-900.
[247] M. Sospedra, R. Martin, Immunology of multiple sclerosis. *Annu Rev Immunol* **2005**, *23*, 683-747.
[248] A. Martinez, R. Alvarez-Lafuente, A. Mas, M. Bartolome, M. Garcia-Montojo, V. de Las Heras, E. G. de la Concha, R. Arroyo, E. Urcelay, Environment-gene interaction in multiple sclerosis: human herpesvirus 6 and MHC2TA. *Hum Immunol* **2007**, *68*, 685-689.
[249] K. W. Wucherpfennig, J. L. Strominger, Molecular mimicry in T cell-mediated autoimmunity: viral peptides activate human T cell clones specific for myelin basic protein. *Cell* **1995**, *80*, 695-705.
[250] M. V. Tejada-Simon, Y. C. Zang, J. Hong, V. M. Rivera, J. Z. Zhang, Cross-reactivity with myelin basic protein and human herpesvirus-6 in multiple sclerosis. *Ann Neurol* **2003**, *53*, 189-197.
[251] J. A. McKenzie, P. R. Strauss, A quantitative method for measuring protein phosphorylation. *Anal Biochem* **2003**, *313*, 9-16.
[252] M. L. Opsahl, P. G. Kennedy, Early and late HHV-6 gene transcripts in multiple sclerosis lesions and normal appearing white matter. *Brain* **2005**, *128*, 516-527.
[253] J. M. Boggs, Myelin basic protein: a multifunctional protein. *Cell Mol Life Sci* **2006**, *63*, 1945-1961.
[254] E. Polverini, G. Rangaraj, D. S. Libich, J. M. Boggs, G. Harauz, Binding of the proline-rich segment of myelin basic protein to SH3 domains: spectroscopic, microarray, and modeling studies of ligand conformation and effects of posttranslational modifications. *Biochemistry* **2008**, *47*, 267-282.
[255] F. J. Ekinci, T. B. Shea, Phosphorylation of tau alters its association with the plasma membrane. *Cell Mol Neurobiol* **2000**, *20*, 497-508.
[256] K. Yao, N. Akyani, D. Donati, N. Sengamalay, J. Fotheringham, E. Ghedin, M. Bishop, J. Barrett, F. Kashanchi, S. Jacobson, Detection of HHV-6B in post-mortem central nervous system tissue of a post-bone marrow transplant recipient: a multi-virus array analysis. *J Clin Virol* **2006**, *37 Suppl 1*, S57-62.
[257] K. Yao, M. Mandel, N. Akyani, K. Maynard, N. Sengamalay, J. Fotheringham, E. Ghedin, F. Kashanchi, S. Jacobson, Differential HHV-6A gene expression in T cells and primary human astrocytes based on multi-virus array analysis. *Glia* **2006**, *53*, 789-798.
[258] Y. Hu, I. Doudevski, D. Wood, M. Moscarello, C. Husted, C. Genain, J. A. Zasadzinski, J. Israelachvili, Synergistic interactions of lipids and myelin basic protein. *Proc Natl Acad Sci U S A* **2004**, *101*, 13466-13471.
[259] R. Mechelli, V. Annibali, G. Ristori, D. Vittori, G. Coarelli, M. Salvetti, Multiple sclerosis etiology: beyond genes and environment. *Expert Rev Clin Immunol* **2010**, *6*, 481-490.
[260] R. A. Marrie, Environmental risk factors in multiple sclerosis aetiology. *Lancet Neurol* **2004**, *3*, 709-718.
[261] C. Genain, CARANTECH, INC. (Mill Valley, CA, US) Unites States, **2006**, p. 26

[262] D. Schwartz, G. M. Church, Collection and motif-based prediction of phosphorylation sites in human viruses. *Sci Signal* **2010**, *3*, rs2.
[263] P. W. Yang, S. S. Chang, C. H. Tsai, Y. H. Chao, M. R. Chen, Effect of phosphorylation on the transactivation activity of Epstein-Barr virus BMRF1, a major target of the viral BGLF4 kinase. *J Gen Virol* **2008**, *89*, 884-895.
[264] M. Brahic, Multiple sclerosis and viruses. *Ann Neurol* **2010**, *68*, 6-8.
[265] K. Biffiger, S. Bartsch, D. Montag, A. Aguzzi, M. Schachner, U. Bartsch, Severe hypomyelination of the murine CNS in the absence of myelin-associated glycoprotein and fyn tyrosine kinase. *J Neurosci* **2000**, *20*, 7430-7437.
[266] S. Hossain, G. Fragoso, W. E. Mushynski, G. Almazan, Regulation of peripheral myelination by Src-like kinases. *Exp Neurol* **2010**, *226*, 47-57.
[267] C. Seiwa, M. Yamamoto, K. Tanaka, M. Fukutake, T. Ueki, S. Takeda, R. Sakai, A. Ishige, K. Watanabe, M. Akita, T. Yagi, H. Asou, Restoration of FcRgamma/Fyn signaling repairs central nervous system demyelination. *J Neurosci Res* **2007**, *85*, 954-966.
[268] J. Nakahara, K. Tan-Takeuchi, C. Seiwa, M. Gotoh, T. Kaifu, A. Ujike, M. Inui, T. Yagi, M. Ogawa, S. Aiso, T. Takai, H. Asou, Signaling via immunoglobulin Fc receptors induces oligodendrocyte precursor cell differentiation. *Dev Cell* **2003**, *4*, 841-852.
[269] C. Seiwa, I. Sugiyama, T. Yagi, T. Iguchi, H. Asou, Fyn tyrosine kinase participates in the compact myelin sheath formation in the central nervous system. *Neurosci Res* **2000**, *37*, 21-31.
[270] R. E. Brown, K. L. Jarvis, K. J. Hyland, Protein measurement using bicinchoninic acid: elimination of interfering substances. *Anal Biochem* **1989**, *180*, 136-139.
[271] L. F. Liebes, R. Zand, W. D. Phillips, Solution behavior, circular dichroism and 22 HMz PMR studies of the bovine myelin basic protein. *Biochim Biophys Acta* **1975**, *405*, 27-39.
[272] G. Munoz, S. H. Marshall, An alternative method for a fast separation of phosphotyrosine. *Anal Biochem* **1990**, *190*, 233-237.
[273] E.-M. Krämer-Albers, R. White, From axon–glial signalling to myelination: the integrating role of oligodendroglial Fyn kinase. *Cellular and Molecular Life Sciences* **2011**, 1-10.
[274] M. Simons, J. Trotter, Wrapping it up: the cell biology of myelination. *Current Opinion in Neurobiology* **2007**, *17*, 533-540.
[275] W. Baron, D. Hoekstra, On the biogenesis of myelin membranes: Sorting, trafficking and cell polarity. *FEBS Letters* **2010**, *584*, 1760-1770.
[276] S. E. Pfeiffer, A. E. Warrington, R. Bansal, The oligodendrocyte and its many cellular processes. *Trends in Cell Biology* **1993**, *3*, 191-197.
[277] B. R. Sperber, E. A. Boyle-Walsh, M. J. Engleka, P. Gadue, A. C. Peterson, P. L. Stein, S. S. Scherer, F. A. McMorris, A unique role for fyn in CNS myelination. *Journal of Neuroscience* **2001**, *21*, 2039-2047.
[278] D. J. Osterhout, A. Wolven, R. M. Wolf, M. D. Resh, M. V. Chao, Morphological differentiation of oligodendrocytes requires activation of Fyn tyrosine kinase. *Journal of Cell Biology* **1999**, *145*, 1209-1218.
[279] G. S. Martin, The hunting of the Src. *Nature Reviews Molecular Cell Biology* **2001**, *2*, 467-475.

[280] G. Lee, S. T. Newman, D. L. Gard, H. Band, G. Panchamoorthy, Tau interacts with src-family non-receptor tyrosine kinases. *Journal of Cell Science* **1998**, *111*, 3167-3177.
[281] R. Dixit, J. L. Ross, Y. E. Goldman, E. L. F. Holzbaur, Differential regulation of dynein and kinesin motor proteins by tau. *Science* **2008**, *319*, 1086-1089.
[282] H. Shelton, M. Harris, Hepatitis C virus NS5A protein binds the SH3 domain of the Fyn tyrosine kinase with high affinity: mutagenic analysis of residues within the SH3 domain that contribute to the interaction. *Virology Journal* **2008**, *5*, 24.
[283] D. A. Renzoni, D. J. R. Pugh, G. Siligardi, P. Das, C. J. Morton, C. Rossi, M. D. Waterfield, I. D. Campbell, J. E. Ladbury, Structural and Thermodynamic Characterization of the Interaction of the SH3 Domain from Fyn with the Proline-Rich Binding Site on the p85 Subunit of PI3-Kinase†. *Biochemistry* **1996**, *35*, 15646-15653.
[284] A. Velyvis, J. Vaynberg, Y. Yang, O. Vinogradova, Y. Zhang, C. Wu, J. Qin, Structural and functional insights into PINCH LIM4 domain-mediated integrin signaling. *Nat Struct Mol Biol* **2003**, *10*, 558-564.
[285] J. Vaynberg, T. Fukuda, K. Chen, O. Vinogradova, A. Velyvis, Y. Z. Tu, L. Ng, C. Y. Wu, J. Qin, Structure of an ultraweak protein-protein complex and its crucial role in regulation of cell morphology and motility. *Molecular Cell* **2005**, *17*, 513-523.
[286] J. P. Mackay, M. Sunde, J. A. Lowry, M. Crossley, J. M. Matthews, Protein interactions: is seeing believing? *Trends in Biochemical Sciences* **2007**, *32*, 530-531.
[287] B. Bochicchio, A. M. Tamburro, Polyproline II structure in proteins: Identification by chiroptical spectroscopies, stability, and functions. *Chirality* **2002**, *14*, 782-792.
[288] B. W. Chellgren, T. P. Creamer, Short sequences of non-proline residues can adopt the polyproline II helical conformation. *Biochemistry* **2004**, *43*, 5864-5869.
[289] T. K. Mal, S. J. Matthews, H. Kovacs, I. D. Campbell, J. Boyd, Some NMR experiments and a structure determination employing a {N-15,H-2} enriched protein. *Journal of Biomolecular Nmr* **1998**, *12*, 259-276.
[290] S. Arold, R. O'Brien, P. Franken, M.-P. Strub, F. Hoh, C. Dumas, J. E. Ladbury, RT Loop Flexibility Enhances the Specificity of Src Family SH3 Domains for HIV-1 Nef†,‡. *Biochemistry* **1998**, *37*, 14683-14691.
[291] B. M. Sullivan, L. Coscoy, Downregulation of the T-cell receptor complex and impairment of T-cell activation by human herpesvirus 6 u24 protein. *J Virol* **2008**, *82*, 602-608.
[292] M. Harris, K. Coates, Identification of cellular proteins that bind to the human immunodeficiency virus type 1 nef gene product in vitro: a role for myristylation. *J Gen Virol* **1993**, *74*, 1581-1589.
[293] J. H. Pan, C. B. Lai, W. R. P. Scott, S. K. Straus, Synthetic Fusion Peptides of Tick-Borne Encephalitis Virus as Models for Membrane Fusion. *Biochemistry* **2010**, *49*, 287-296.
[294] C. J. Morton, D. J. R. Pugh, E. L. J. Brown, J. D. Kahmann, D. A. C. Renzoni, I. D. Campbell, Solution structure and peptide binding of the SH3 domain from human Fyn. *Structure* **1996**, *4*, 705-714.
[295] H. Edelhoch, Spectroscopic Determination of Tryptophan and Tyrosine in Proteins*. *Biochemistry* **1967**, *6*, 1948-1954.
[296] C. N. Pace, F. Vajdos, L. Fee, G. Grimsley, T. Gray, HOW TO MEASURE AND PREDICT THE MOLAR ABSORPTION-COEFFICIENT OF A PROTEIN. *Protein Science* **1995**, *4*, 2411-2423.

[297] M. A. Friese, X. Montalban, N. Willcox, J. I. Bell, R. Martin, L. Fugger, The value of animal models for drug development in multiple sclerosis. *Brain* **2006**, *129*, 1940-1952.
[298] L. K. Tamm, B. Y. Liang, NMR of membrane proteins in solution. *Progress in Nuclear Magnetic Resonance Spectroscopy* **2006**, *48*, 201-210.
[299] K. G. Fleming, Riding the wave: structural and energetic principles of helical membrane proteins. *Current Opinion in Biotechnology* **2000**, *11*, 67-71.
[300] S. H. White, The progress of membrane protein structure determination. *Protein Science* **2004**, *13*, 1948-1949.
[301] S. White.http://blanco.biomol.uci.edu/Membrane_Proteins_xtal.html. April 10th, 2010.
[302] C. R. Sanders, F. Sonnichsen, Solution NMR of membrane proteins: practice and challenges. *Magnetic Resonance in Chemistry* **2006**, *44*, S24-S40.
[303] R. Page, J. Moore, H. Nguyen, M. Sharma, R. Chase, F. Gao, C. Mobley, C. Sanders, L. Ma, F. Sönnichsen, S. Lee, S. Howell, S. Opella, T. Cross, Comprehensive evaluation of solution nuclear magnetic resonance spectroscopy sample preparation for helical integral membrane proteins. *Journal of Structural and Functional Genomics* **2006**, *7*, 51-64.
[304] R. D. Krueger-Koplin, P. L. Sorgen, S. T. Krueger-Koplin, A. O. Rivera-Torres, S. M. Cahill, D. B. Hicks, L. Grinius, T. A. Krulwich, M. E. Girvin, An evaluation of detergents for NMR structural studies of membrane proteins. *Journal of Biomolecular Nmr* **2004**, *28*, 43-57.
[305] A. Bax, S. Grzesiek, METHODOLOGICAL ADVANCES IN PROTEIN NMR. *Accounts of Chemical Research* **1993**, *26*, 131-138.
[306] J. A. Määttä, J.-P. Erälinna, M. Röyttä, A. A. Salmi, A. E. Hinkkanen, Physical state of the neuroantigen in adjuvant emulsions determines encephalitogenic status in the BALB/c mouse. *Journal of Immunological Methods* **1996**, *190*, 133-141.
[307] E. Wallström, T. Olsson, in *Sourcebook of Models for Biomedical Research* (Ed.: P. M. Conn), Humana Press, **2008**, pp. 547-556.
[308] W. van Eden, J. P. A. Wagenaar-Hilbers, M. H. M. Wauben, *Adjuvant Arthritis in the Rat*, John Wiley & Sons, Inc., **2001**.
[309] A. Chattopadhyay, E. London, Fluorimetric determination of critical micelle concentration avoiding interference from detergent charge. *Analytical Biochemistry* **1984**, *139*, 408-412.
[310] A. Chattopadhyay, K. G. Harikumar, Dependence of critical micelle concentration of a zwitterionic detergent on ionic strength: Implications in receptor solubilization. *Febs Letters* **1996**, *391*, 199-202.
[311] J. Tucker, R. Grisshammer, Purification of a rat neurotensin receptor expressed in Escherichia coli. *Biochemical Journal* **1996**, *317*, 891-899.
[312] Z. Y. Wang, H. Suzuki, M. Kobayashi, T. Nozawa, Solution structure of the Rhodobacter sphaeroides PufX membrane protein: Implications for the quinone exchange and protein-protein interactions. *Biochemistry* **2007**, *46*, 3635-3642.
[313] L. Guilhaudis, A. Jacobs, M. Caffrey, Solution structure of the HIV gp120 C5 Domain. *European Journal of Biochemistry* **2002**, *269*, 4860-4867.
[314] H. Young, V. Roongta, T. J. Daly, K. H. Mayo, NMR structure and dynamics of monomeric neutrophil-activating peptide 2. *Biochemical Journal* **1999**, *338*, 591-598.
[315] J. F. Ellena, B. Y. Liang, M. Wiktor, A. Stein, D. S. Cafiso, R. Jahn, L. K. Tamm, Dynamic structure of lipid-bound synaptobrevin suggests a nucleation-propagation

mechanism for trans-SNARE complex formation. *Proceedings of the National Academy of Sciences of the United States of America* **2009**, *106*, 20306-20311.
[316] D. Long, D. W. Yang, Buffer Interference with Protein Dynamics: A Case Study on Human Liver Fatty Acid Binding Protein. *Biophysical Journal* **2009**, *96*, 1482-1488.
[317] M. E. Call, J. R. Schnell, C. Q. Xu, R. A. Lutz, J. J. Chou, K. W. Wucherpfennig, The structure of the zeta zeta transmembrane dimer reveals features essential for its assembly with the T cell receptor. *Cell* **2006**, *127*, 355-368.
[318] S. A. Goncharuk, A. A. Shulga, Y. S. Ermolyuk, P. K. Kuzmichev, V. A. Sobol, E. V. Bocharov, V. V. Chupin, A. S. Arseniev, M. P. Kirpichnikov, Bacterial synthesis, purification, and solubilization of membrane protein KCNE3, a regulator of voltage-gated potassium channels. *Biochemistry-Moscow* **2009**, *74*, 1344-1349.
[319] P. Romero, Z. Obradovic, X. Li, E. C. Garner, C. J. Brown, A. K. Dunker, Sequence complexity of disordered protein. *Proteins: Structure, Function, and Bioinformatics* **2001**, *42*, 38-48.
[320] C. J. Oldfield, E. L. Ulrich, Y. Cheng, A. K. Dunker, J. L. Markley, Addressing the intrinsic disorder bottleneck in structural proteomics. *Proteins: Structure, Function, and Bioinformatics* **2005**, *59*, 444-453.
[321] P. E. Wright, H. J. Dyson, Intrinsically unstructured proteins: re-assessing the protein structure-function paradigm. *Journal of Molecular Biology* **1999**, *293*, 321-331.
[322] G. A. Hashim, D. D. Wood, M. A. Moscarello, Myelin lipophilin-induced demyelinating disease of the central nervous system. *Neurochemical Research* **1980**, *5*, 1137-1145.
[323] P. J. Plant, J. Correa, N. Goldenberg, J. Bain, J. Batt, The inositol phosphatase MTMR4 is a novel target of the ubiquitin ligase Nedd4. *Biochem J* **2009**, *419*, 57-63.

Appendix A: Additional Data for U24 Proteins/Peptides

A.1 SDS-PAGE and MALDI-TOF-MS Analysis of MBP-6×His-U24 Degradation Product

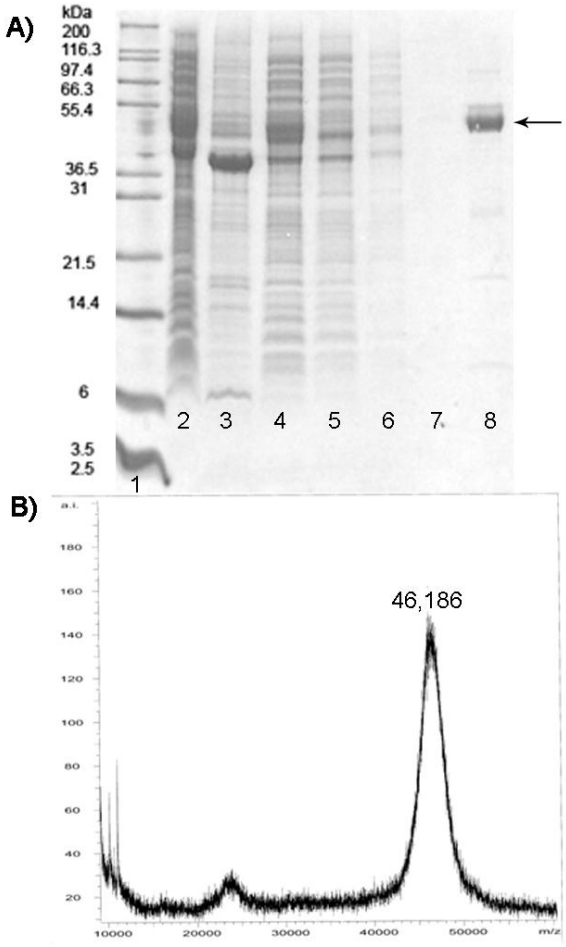

Analysis of isolated, degraded MPB-6×His-U24. Protein was purified from cells of C41(DE3) grown in M9 media that had expressed pMAL-c2x-U24 at 37°C (see Chapter 2 Materials and Methods). Essentially, cells were lysed by French press in 20 mM K phosphate, 0.5 M NaCl, pH 7.4 centrifuged 90 minutes at 25,000 ×*g* and the supernatant loaded on a 5 ml Ni^{2+} column to be then washed with the same buffer. Protein was eluted with buffer containing 500 mM imidazole. A) SDS-PAGE of purification fractions: lane 1) molecular weight markers; 2) cell lysate; 3) pellet after centrifugation; 4) supernatant; 5) wash 1 (50 mL); 6) wash 2 (50 mL); 7) wash 3 (50 mL); 8) isolated degradation product (25 mL). Arrow points to the isolated protein that was then submitted for B) MALDI-TOF MS analysis. Expected mass of the full-length MBP-6×His-U24 fusion is in the range of ~ 54.3 kDa.

A.2 MALDI-TOF Analysis of Isolated NΔ9-U24

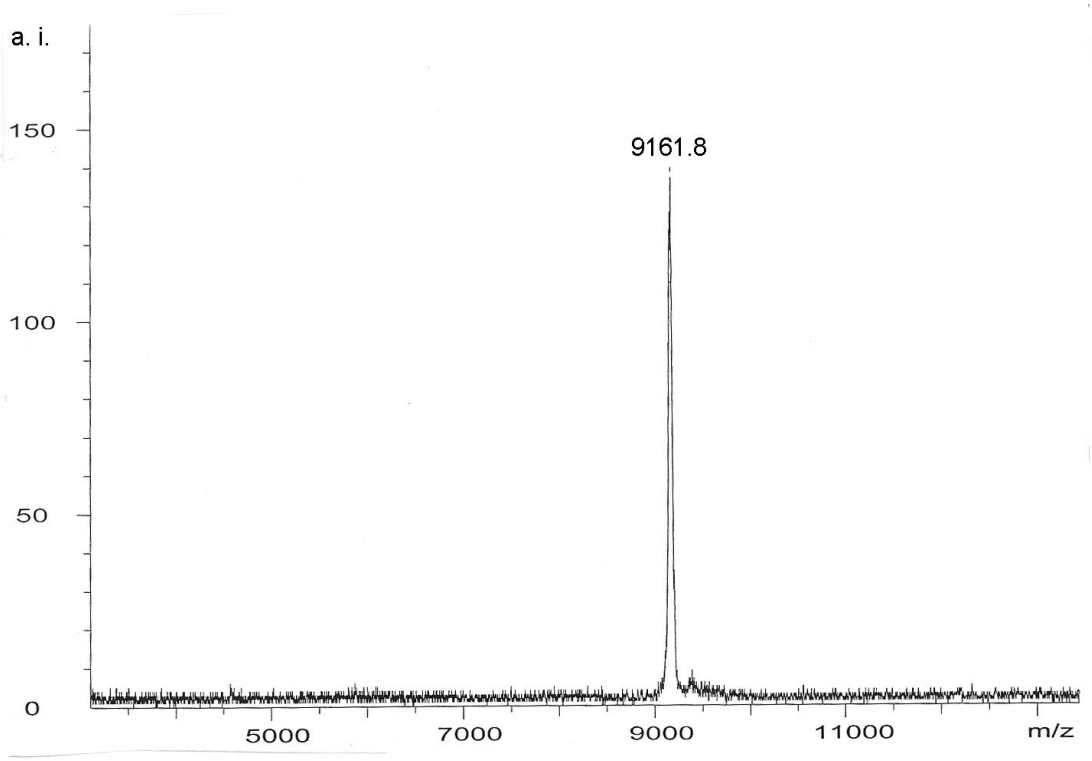

MALDI-TOF MS mass analysis of the NΔ9-U24 protein described in Chapter 4, analyzed as described in the Materials and Methods section of Chapter 3. NΔ9-U24 is a U24 deletion mutant missing the 9 N-terminus amino acids, MDPRTPPPS; the new N-terminal sequence begins with GSYSEVL (GS is present after thrombin cleavage from the MBP-6×His dual tag). Experimental mass is 9158.8, theoretical is 9161.8 Da.

A.3 HPLC Elution Profile and MALDI-TOF Analysis of the Synthetic U24 Peptide

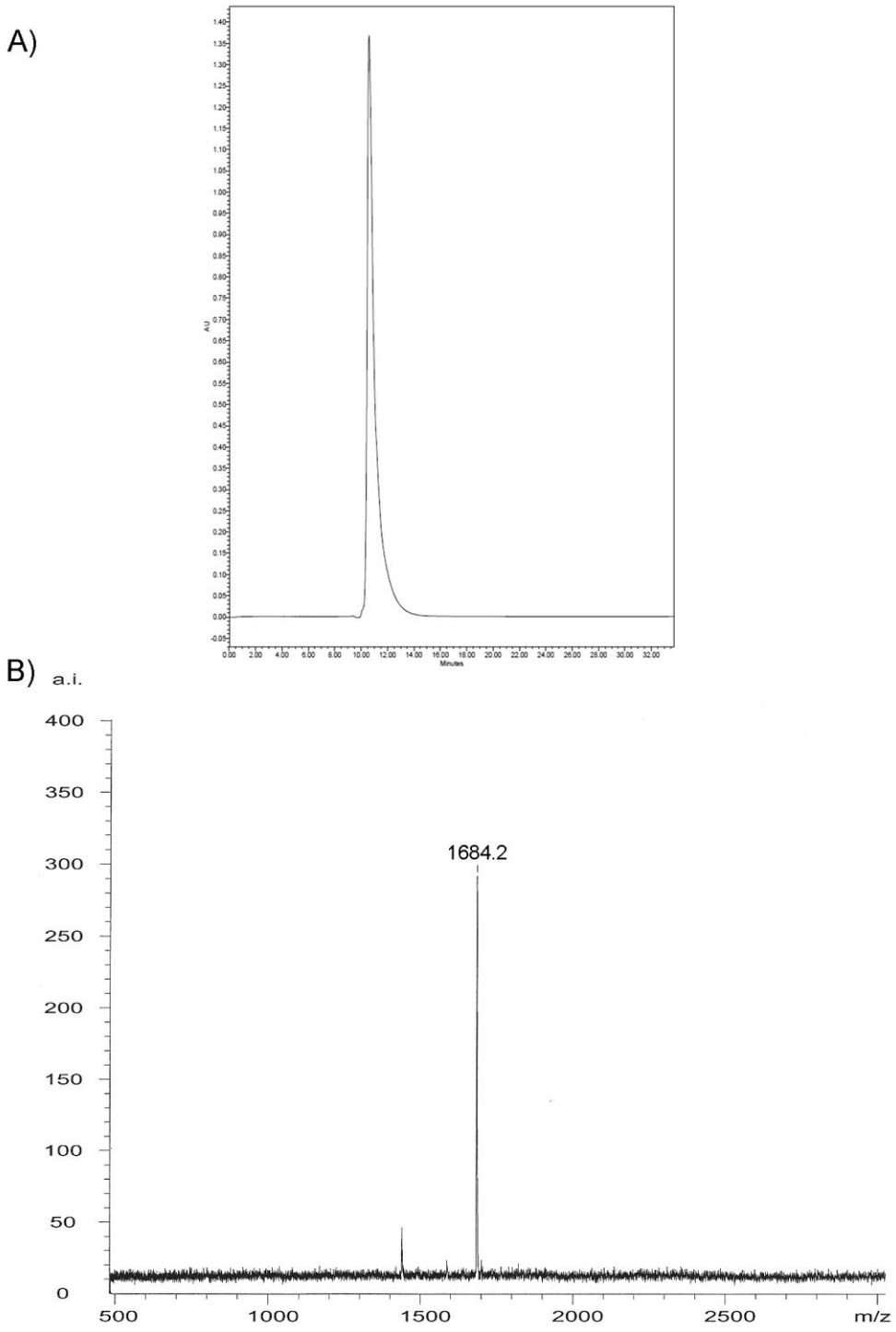

Synthetic 15 mer peptide of the N-terminus of U24, having the sequence MDPPRTPPPSYSEVL (described in Chapter 4). A) HPLC trace of isolated peptide and B) MALDI-TOF MS mass identification. Experimental mass is 1684.2 Da, theoretical is 1685.9 Da.